Membrane characterization for linear and nonlinear systems: upstream and downstream methods

By

Neveen Alqasas

Thesis submitted to the
Faculty of Graduate and Post-Doctoral Studies
in partial fulfillment of the requirements
for the Doctorate in Philosophy in Chemical Engineering.

Department of Chemical and Biological Engineering
Faculty of Engineering
University of Ottawa

Abstract

Gas separation with polymer membranes are becoming one of the mainstream separation techniques for a myriad of industrial applications. Membrane technologies are recognized as a viable and economical unit operation compared to more conventional separation processes. The design and material selection of membrane separation processes depends highly on the transport properties of separated gas molecules within the membrane material. Therefore, to use efficient methods for gas membrane characterization is paramount for the proper design of membrane separation processes. A membrane can be typically characterized by three main properties: permeability, solubility and diffusivity. The permeability of a membrane is the product of its diffusivity and solubility, therefore obtaining two of the three parameters is sufficient to fully characterize a membrane. The time-lag method is one of the oldest and most used gas membrane characterization methods. However, it suffers from various limitations that make the method not applicable for many types of membranes.

The focus in this study was to develop new gas membrane characterization techniques that are based on extracting the membrane properties from the upstream gas pressure measurements rather than only from the downstream pressure measurements. It is believed that characterizing the membrane based on the upstream pressure measurements would be highly useful in characterizing barrier materials which are usually difficult to characterize using the conventional time-lag method. Moreover, glassy polymers which are widely used in industry exhibit behavior associated with nonlinear sorption isotherms and, therefore, the conventional time-lag method is incapable of obtaining an accurate estimation of glassy polymer properties. As a result, sorption experiments to generate a sorption isotherm are usually required in addition to permeation experiments to fully characterize glassy polymer membranes.

To quantify the errors associated with the conventional time-lag assumptions and to fundamentally comprehend the impact of nonlinearities on the time-lag method, a comprehensive numerical investigation has been undertaken using the finite difference method. The investigation has clearly put in evidence the effect of the various Langmuir parameters on the accuracy of the time lag and on the time required to achieve steady state. This investigation also

allowed assessing the errors associated with the usual assumptions made on the boundary conditions in determining the time lag.

In this study, three novel gas membrane characterization methods were developed and proposed. Two of the proposed methods are concerned with the characterization of membranes that can be represented with a linear sorption isotherm. These two methods are entirely based on the upstream pressure measurements. The third membrane characterization method that is proposed is based on the dynamic monitoring of both upstream and downstream pressure measurements and is applicable to systems that exhibit a nonlinear isotherm sorption behavior. The three proposed methods are promising and further experimental validation is recommended to determine their full range of applicability.

Résumé

Les membranes polymériques pour la séparation des gaz sont de plus en plus utilisées comme technique de séparation pour une myriade d'applications industrielles. Les systèmes membranaires sont reconnus comme des opérations unitaires viables et économiques par rapport aux autres procédés de séparation plus conventionnels. La conception et la sélection des matériaux pour les procédés de séparation par membranes dépendent grandement des propriétés de transport des molécules de gaz à l'intérieur de la matrice de la membrane. Par conséquent, la disponibilité de méthodes efficaces pour la caractérisation des membranes est primordiale pour permettre la conception de procédés de séparation par membranes. Une membrane est généralement caractérisée par trois principales propriétés: la perméabilité, la solubilité et la diffusivité. La perméabilité d'une membrane est le produit de la diffusivité et de la solubilité. Ainsi, l'obtention de deux des trois paramètres est suffisante pour caractériser une membrane. La méthode de décalage temporel est une des méthodes de caractérisation des membranes la plus ancienne et la plus utilisée. Cependant, elle souffre de diverses contraintes qui la rendent non applicable pour la caractérisation de nombreux types de membranes.

L'objectif de cette étude était de développer de nouvelles techniques de caractérisation des membranes pour la séparation des gaz basées sur l'extraction des propriétés de la membrane à partir des mesures de pression gazeuse en amont et non pas seulement à partir des mesures de pression en aval de la membrane. Il y a lieu de croire que la caractérisation de la membrane sur la base des mesures de pression en amont serait très utile dans la caractérisation des matériaux barrières qui sont généralement difficiles à caractériser en utilisant la méthode conventionnelle de décalage temporel. En outre, les polymères vitreux qui sont largement utilisés dans l'industrie montrent un comportement découlant des isothermes de sorption non-linéaires et, par conséquent, la méthode de décalage temporel classique est incapable d'obtenir une estimation précise des propriétés de ces polymères vitreux. Pour contourner ce problème, des expériences servant à déterminer l’isotherme de sorption sont généralement requises en plus des expériences de perméation afin de pleinement caractériser les membranes polymériques vitreuses.

Pour quantifier les erreurs associées aux hypothèses classiques de la méthode de décalage temporel et pour mieux comprendre l'impact de la non-linéarité sur la méthode de décalage

temporel, une étude numérique a été menée en utilisant la méthode des différences finies. Cette étude numérique a clairement mis en évidence l'effet des différents paramètres de l'isotherme de Langmuir sur la précision de la valeur du décalage temporel et sur le temps nécessaire pour atteindre l'état d'équilibre. Cette étude a également permis d'évaluer les erreurs associées aux hypothèses habituelles faites sur les conditions aux limites dans la détermination de la valeur du décalage temporel.

Dans cette étude, trois nouvelles méthodes de caractérisation de la membrane pour la séparation des gaz ont été développées et analysées. Deux des méthodes proposées ont trait à la caractérisation des membranes qui peuvent être représentées à l'aide d'une isotherme de sorption linéaire. Ces deux méthodes sont entièrement basées sur les mesures de pression en amont de la membrane. La troisième méthode de caractérisation des membranes est basée sur l'observation de la variation dynamique des pressions en amont et en aval de la membrane. Cette dernière méthode est applicable pour des systèmes qui peuvent être caractérisés par une isotherme de sorption non linéaire. Les trois méthodes proposées possèdent un grand potentiel et, par conséquent, doivent être soumises à une validation expérimentale rigoureuse pour déterminer pleinement leur gamme d'applicabilité.

Acknowledgment

This work would have never been possible without the continuous support and guidance from my two supervisors, Dr. Jules Thibault and Dr. Boguslaw Kruczek, who have been patient, encouraging and believing in my potential throughout the past four years. I would like to express my warm gratitude and thanks for all their efforts to help me through this work, guide me and being there whenever I needed them.

I would also like to thank the University of Ottawa for the admission scholarship and the National Science and Engineering Research (NSERC) for the financial support for this project.

I would like to express my sincere thanks to all my colleagues at the University of Ottawa and all my friends for their continuous support and encouragement. They have made my stay at the University of Ottawa very pleasant.

Last and not least, my warmest appreciation goes to every member in my family, my three sisters, my brother, and my mother who have been continuously supporting me and believing in my ability to accomplish the work that I have performed in this thesis. Without their love and trust, this was work would not have been possible

I would like to dedicate the work in this dissertation to my mother, Lamis and my deceased father Suhail, who would have been so proud of me if he was still with us today.

وَأَعْلَنَ في الْكَوْنِ أَنَّ الطُّمُوحَ لَهِيبُ الْحَيَاةِ وَرُوحُ الظَّفَر

إِذَا طَمَحَتْ لِلْحَيَاةِ النُّفُوسُ فَلا بُدَّ أَنْ يَسْتَجِيبَ الْقَدَرْ

للشاعر : أبو القاسم الشابي

"Announce to Universe that ambition is the flame of life and the soul of victory

If souls aspire to life, destiny will respond"

Statement of contributions of collaborators

I hereby declare that I am the sole author of this thesis and that no part of this work has been submitted or accepted for any other degree.

Dr. Jules Thibault and Dr. Boguslaw Kruczek supervised this thesis. Both supervisors provided continual guidance throughout this work and made editorial comments and corrections to the written work presented. Miss Haoyu Wu has co-authored the paper on numerical methods (Chapter 4); part of this work was done conjunctly when she was doing her undergraduate thesis and M.Eng project in the Department of Chemical Engineering at the University of Ottawa.

The responsibilities of the author, Neveen Al-Qasas, in order to fulfill the requirements of this thesis were as follows:

1- Develop a new gas membrane characterization technique that is based on the upstream pressure measurements.
2- Use the numerical finite difference method to do a comprehensive investigation on the accuracy of the downstream and upstream time-lag methods and gain a better understanding of the limitations and constraints of the traditional time-lag methods.
3- Solve for the analytical concentration profile of a laminated two-membrane system.
4- Determine the optimal numerical finite difference scheme using a known benchmark analytical solution to provide accurate numerical simulations for both explicit and implicit schemes.
5- To produce a written thesis in partial fulfillment of the requirements for obtaining a PhD degree in Applied Science.

Contents

List of Figures

List of Tables

Chapter 1

Introduction

1.1 Introduction

The rate of growth of gas membrane separations has been phenomenal in the last 30 years. Progress in this field was made possible because of the development of new materials and new membrane fabrications methods. The use of membrane for gas separation in industry has gained popularity due to its simplicity compared to other separation processes known in industry. Separation using membrane technology is usually more efficient in terms of energy consumption, therefore resulting in lower capital and operating costs. Membrane processes occupies a low plant footprint, have low maintenance cost, are easy to install and operate, are mechanically simple and are easy to scale up. Membrane technologies have been used in various industries, such as the separation of H_2 from refinery off gases, ammonia purge gas and syngas, CO_2 removal from natural gas including the enhanced oil recovery application, acid gas separation, and air separation for N_2 production. The separation mechanism of membranes varies according to the structure of the membrane material. The different possible mechanisms include, solution-diffusion, facilitated transport, Knudsen diffusion, surface diffusion and molecular sieving [1]. Most industrial membranes are made of polymeric materials. Designing a membrane separation process for industrial applications requires understanding the diffusion mechanism taking place inside the membrane. Nonporous polymeric materials are widely used as membrane materials and the most common transport phenomenon in nonporous polymeric membranes is the solution-diffusion mechanism. The mechanism of transport according to the solution-diffusion model occurs in three steps: 1) the gas molecules at the upstream side of the membrane dissolve in the membrane material proportionally to the solubility (S) of the gas in the membrane material, 2) the gas molecules diffuse through the membrane driven by a concentration gradient with a diffusion rate that is specific to each gas molecule and proportional to the diffusivity (D) of each gas molecule within the matrix of the polymeric material, 3) desorption of the gas molecules from the membrane material to the gas phase at the downstream side of the membrane. Separation occurs between the different molecules present in the upstream gas due to the difference in the amount of the different gases dissolving in the membrane and to the rate at

which the various molecules diffuse within the membrane material [2]. The productivity of the membrane is defined by the membrane's permeability (P) which is defined in Eq. (1.1).

$$P = DS \tag{1.1}$$

where the diffusivity D is the kinetic parameter and the solubility S is the thermodynamic parameter. Each species present in the upstream gas phase has specific values of diffusivity and solubility.

The transport of molecules inside the polymeric materials occurs as a result of a random molecular motion of individual molecules. The driving force behind the transport process which involves the two kinetic (P and D) and one sorption parameter(S), is the concentration difference between the two phases separated by the membrane [3]. The transport of molecules occurs to equalize the concentration difference or the chemical potential of the penetrant in the phases separated by the membrane. The steady state transport process is described by Fick's first law of diffusion shown in Eq. (2)

$$J = -D\left(\frac{\partial C}{\partial x}\right) \tag{1.2}$$

Fick's law of diffusion states that the flux, J, in the direction of transport is proportional to the concentration gradient ($\partial C/\partial x$), and the proportionality constant is the diffusion coefficient D. Under transient state, the Fick's second law of diffusion is applicable and is described in Eq. (1.3)

$$\frac{\partial C}{\partial t} = D\left(\frac{\partial C^2}{\partial x^2}\right) \tag{1.3}$$

The application of Eqs (1.1) and (1.2) implies the ideal case where the diffusion coefficient is independent of distance, time and concentration [4].

Polymeric membranes can be divided in to two types: glassy polymers and rubbery polymers. The internal structure of these two types of membrane is different; hence they exhibit different transport behaviours. The transport properties of polymeric materials depend on the free volume within the polymer and on the segmental mobility of the polymer chains. The mobility of the polymer chains depends on the degree of crosslinking, the extent of unsaturation, degree of crystallinity and nature of substituents. Rubbery polymers have a large segmental mobility and a large amount of free volume between polymeric chains while glassy polymers are known to be

hard and brittle moiety with restricted chain mobility [4]. A polymer is considered a glassy polymer when it is below its glass transition temperature (T_g), while it is a rubbery polymer when it is above this glass transition temperature. The interstitial volume dependence on temperature is crucial in defining the difference between the rubbery and glassy state of an amorphous polymer [5]. The sorption behaviour in a glassy polymer is different to that for the rubbery polymer. In rubbery polymers, the sorption follows Henry's law of dissolution Eq. (1.4) (linear model); while for glassy polymers two adsorption mechanisms present, the Henry's dissolution and Langmuir hole filling Eq. (1.5).

$$C = Sp \tag{1.4}$$

$$C = Sp + C_H^{'} \frac{bp}{1+bp} \tag{1.5}$$

where C'_H is the hole saturation constant, b is the hole affinity constant, and p is the operating pressure. The model in Eq. (1.5) is known as the dual-mode sorption model. The dual-mode sorption model in glassy polymers has been examined and validated by many workers [6-9].

Whether the membrane is glassy or rubbery, its transport properties must be known to allow designing a gas separation process. The main transport properties that characterize the membrane are its solubility, diffusivity and permeability. For glassy polymers, where the sorption behaviour follows the dual-mode sorption model Eq. (1.5), the Langmuir parameters C'_H and b are also required in addition the three main transport properties,. The rate of permeation across a membrane at a given point for species i is governed by the following relation:

$$N_i = \frac{P_i}{L} A \Delta p_i \tag{1.6}$$

where p_i is the partial pressure of species i in the mixture, P_i is its permeability, A is the membrane area, and L is the membrane thickness. One of the main design parameters for membrane separation is the membrane area. The capital cost of the membrane process is mainly determined by the permeation area required to achieve a certain separation. The membrane process design depends on the overall objective of the separation, i.e. the desired product is the retentate and/or the permeate stream. Therefore, product purity and recovery are major factors in designing the process [1]. Based on Eq. (1.6), the rate of permeation N_i increases with an increase in the membrane permeability for species i. The permeability is usually considered constant for a certain species. As a result, a higher permeability leads to a smaller membrane area

to achieve a certain level of productivity. Underestimating the permeability will result in an overdesign of the membrane separation process and a higher capital cost. On the other hand, if the permeability is overestimated, it will not be possible to achieve the desired product quality and recovery. Therefore, an essential step in designing membrane separation processes is to efficiently characterize the transport properties of the species to be separated using the selected membrane.

There are several gas membrane characterization method used to determine the transport properties of a membrane [10-12]. However, the most commonly used technique is the time-lag method that originates from the work of Daynes in 1920 [13] and was brought to its full prominence three decades later by Barrer [14-15]. The time-lag method depends on monitoring the downstream pressure increase and observing the slope of the pressure-time curve as the pseudo-steady state is reached. In principle, time-lag method could also be based on monitoring of the upstream pressure decay, but this is rarely practiced because of technical limitations [12]. Typically, the three transport coefficients are determined in a single dynamic gas permeation experiment, often referred to as a time-lag experiment. A membrane, which is initially degassed, is exposed to a step increase in feed pressure while the time-dependent gas permeation across the membrane is determined from the rate of pressure increase or pressure decay in a fixed compartment volume either at the downstream side or upstream side of the membrane, respectively. The permeability is determined from the slope of the linear portion of the pressure versus time graph; extrapolation of that linear portion to the time axis gives the downstream time lag (θ_d) Eq. (1.7) if the downstream pressure is monitored and the upstream time lag (θ_{up}) Eq. (1.8) if the upstream pressure is monitored.

$$\theta_d = \frac{L^2}{6D} \tag{1.7}$$

$$\theta_{up} = -\frac{L^2}{3D} \tag{1.8}$$

Both upstream and downstream time lags are a function of the membrane diffusivity D and its thickness L. Due to the simplicity of the time-lag permeation experiment, for decades the time lag method was used to obtain the transport properties of gas membranes regardless of the type of the membrane being used. The time-lag method was derived mathematically based on two

main assumptions; one related to the boundary conditions and the second is related to the type of isotherm that the gas molecules exhibit with the membrane material. The assumed boundary conditions consider that the concentration downstream of the membrane is always zero and the upstream pressure is always constant. In a real experiment, even if large compartment volumes are used, the downstream pressure is never zero and the upstream pressure is never constant. In addition, it is important to stress that if the upstream and downstream pressures remained at their initial value, the time-lag method could not be used as it relies on the pressure change as a function of time. Various studies have quantified the error resulting from the assumptions on boundary conditions [16-17]. The second assumption is that the time-lag method was derived considering the sorption behaviour of rubbery polymers only and did not take in to account the glassy polymer sorption behaviour, therefore always assuming a linear isotherm. However, most of membranes used in industry are glassy polymers which exhibit nonlinear adsorption isotherm. The diffusivity obtained using the time-lag method to characterize membranes following the dual-mode sorption model is not the actual diffusivity; it is the apparent diffusivity that is not a constant parameter but varies with the operating pressure. Other models [18-21] that describe the transport of molecules in glassy polymers had been examined in the literature. The complete immobilization model assumes that the molecules in Langmuir's sites are immobilized and in instantaneous equilibrium with the gas molecules in Henry's region [22; 8; 18]. On the other hand, when the gas molecules adsorbed at Langmuir's sites are not totally immobilized and contribute to diffusion, the resulting model is the partial immobilization model [19-20; 23-25]. The presence of reversible reaction between the two populations of gas molecules has also been investigated suggesting a non-instantaneous equilibrium model [26-29]. The time-lag method also requires achieving steady state which makes it impractical to be used to characterize barrier materials for which reaching steady state may be extremely long. Accordingly, the time-lag method suffers from various problems related to the unrealistic boundary conditions, the assumption of the presence of a linear isotherm only and the requirements of reaching steady state. Despite all the previous mentioned drawbacks, the time-lag method is still practically the only method used to characterize gas membranes.

The time-lag measurements can be based on either upstream pressure or downstream pressure measurements. However, the downstream time-lag method is used more frequently in practice compared to the upstream time-lag method. Nevertheless, it is believed that when

characterization is based on the upstream pressure measurements, the problem associated with the downstream boundary conditions can be avoided since the downstream compartment can be evacuated continuously. Also, another advantage of using the upstream pressure measurements is the ability to characterize barrier materials. If the membrane parameters can be extracted from the initial variation in the upstream pressure measurements, then there is no need to wait for the molecules to exit to the downstream side.

The need of a new and robust characterization method that is based either on upstream or downstream pressure measurements for gas permeation experiment that overcomes the main drawbacks of the time-lag method is essential and it is the main objective of this work. In the current study, new methods for characterizing polymeric membranes are proposed. The new methods are proposed for linear and nonlinear systems that follow the complete immobilization model with instantaneous equilibrium. For a linear system, the focus is on extracting the membrane properties from the upstream pressure measurements only and keeping the downstream under vacuum therefore not violating the downstream boundary condition. On the other hand, for characterizing nonlinear isotherms, the possibility of combining the upstream and downstream pressure measurements is discussed and a new method that is capable of extracting the kinetic and sorption parameters of the membrane under realistic boundary conditions is proposed.

1.2 Thesis structure

The results of this investigation are mainly presented in five main chapters, each covering a specific topic. Chapters 2 and 3 present two different characterization methods for a linear system. Both methods rely on the upstream pressure measurements only. Chapter 2 represents a new characterization method for barrier materials that is based on laminating the membrane under study with a lower resistance layer. A complete analytical solution of the two-membrane system was used to establish a novel characterization technique that is based on upstream pressure measurements only. Chapter 3 uses the analytical solution of the slab membrane behaving as a semi- infinite solid and the one for a slab membrane to extract the membrane properties by monitoring the deviation from the semi-infinite behaviour that occurs later in the experiment. For both methods, the downstream side of the membrane is always evacuated such that the downstream boundary condition is always satisfied.

The next three chapters of this thesis present a comprehensive review on the effect of nonlinearity of the isotherm in the accuracy of the results obtained from the conventional time-lag method and on the time of establishing the pseudo steady state. The investigation is performed using the finite difference numerical modeling. Therefore, Chapter 4 presents a comprehensive numerical investigation concerned with the selection of the optimal finite difference scheme for solving the Fick's diffusion equation that leads to the accurate determination of the membrane time lag. Based on the results obtained in Chapter 4, Chapter 5 presents the effect of the degree of nonlinearity of the isotherm on the downstream time-lag method and on the time of achieving steady state. In Chapter 6, results of the downstream and upstream time lag investigation leads to the proposal of a novel characterization technique for a nonlinear system that is based on the combination of the upstream and downstream time lag measurements under realistic boundary conditions of a permeation experiment. Finally Chapter 7 presents a summary of the major outcomes, conclusions, and future recommendations.

1.3 References

[1] R. D. Noble, S. S. Alexander, Membrane Separations Technology Principles and Applications, Science Direct, Amsterdam; New York: Elsevier, 1995, Chapter 11

[2] J. G. Wijmans, R. W. Baker, The Solution-Diffusion Model: a Review, Journal of Membrane Science, 107 (1995), 1-21.

[3] M. Chainey, In: Cheremisinoff NP, Composites and Speciality Applications, Hand book of Polymer Science and Technology, Vol 4, New York: Marcel Dekker, 1989, p499

[4] S. C. George, S. Thomas, Transport Phenomena through Polymeric Systems, Progress Polymer Science, 26 (2001), 985-1017.

[5] R. Tant, G. L. Wilkes, An Overview of the Non-equilibrium Behavior of Polymer Glasses, Polymer Engineering and Science, 21(1981), 874-895.

[6] P. Meares, The diffusion of Gases through Polyvinyl Acetate, Journal of American Chemical Society, 76 (1954), 3415-3422.

[7] A. S. Michaels, W.R. Vieth, J. A. Barrie, Diffusion of Gases in Polyethylene Terephthalate, Journal of applied Physics, 34 (1963), 13-20.

[8] W. R. Vieth, C. S. Frangoulis, J. A. Rionda, Kinetics of sorption of Methane in Glassy polystyrene, Journal of Colloid and interface science, 22 (1966), 454-491.

[9] D. R. Kemp, D. R. Paul, Gas Sorption in Polymer Membranes Containing Adsorptive Fillers, Journal of Polymer Science: Polymer Physics Edition, 21 (1974), 485-500.

[10] W.A. Rogers, R.S., Buritz, D., Alpert, "Diffusion coefficient, solubility, and permeability for helium in glass", J. Appl. Phys. 257 (1954) 868-875.

[11] R.M. Felder, "Estimation of Gas transport Coefficients from Differential permeation, integral permeation and Sorption rate", Journal of Membrane Science. 3 (1978) 15-27.

[12] M. Al-Ismaily, "A novel method of characterizing polymer membrane using upstream gas permeation tests", Master thesis, University of Ottawa, 2011.

[13] H. A. Daynes, The Process of Diffusion through a Rubber Membrane, R. Soc. Proc. A97 (1920), 286-307.

[14] R.M., Barrer, Permeation, Diffusion and Solution of Gases, Trans. Faraday Soc., 35 (1939), 628-64.

[15] R. M. Barrer, Stationary and Non-Stationary States of Flow of Hydrogen in Palladium and Iron, Trans. Faraday. Soc., 36 (1940),1235-1248.

[16] R. C. L. Jenkins, P. M. Nelson, L Spirer, Calculations of the Transient Diffusion of Gas through a Solid Membrane in to A Finite Outflow Volume, Transactions of the Faraday Society, 66 (1970), 1391-1401.

[17] P. Taveira, A. Mendes, C. Costa, On the determination of diffusivity and sorption coefficients using different time-lag models, Journal of Membrane Science, 221 (2003), 123-133.

[18] D. R. Paul, Effect of Immobilizing Adsorption on the diffusion time-lag, Journal of membrane science: Part A-2, 7(1969), 1811-1818.

[19] J. H. Petropoulos, Quantitative analysis of gaseous diffusion in glassy polymers, Part A-2, 8 (1970), 1797-1701.

[20] W. J. Koros, D. R. Paul, A. A. Rocha, Carbon Dioxide Sorption and Transport in Polycaronate, Journal of Polymer Science: Polymer Physics Edition, 14 (1976), 687-702.

[21] M. A. Islam, H. Buschatz, Gas permeation through a glassy polymer membrane: chemical potential gradient or dual mobility mode?, Chemical Engineering Science, 57 (2002), 2089-2099.

[22] W. R. Vieth, K. J. Sladek, A model for diffusion in a glassy polymer, Journal of colloid Science, 20 (1965), 1014-1033.

[23] D.R. Paul, W. J. Koros, Effect of partially immobilizing sorption on permeability and the diffusion time-lag, Journal of Polymer science: Polymer physics edition, 14(1976), 675-685.

[24] W. J. Koros, A. H. Chan, D. R. Paul, Sorption and transport of various gases in polycarbonate, Journal of Membrane Science, 2 (1977), 165-190.

[25] W. J. Koros, D. R. Paul, Transient and Steady-State Permeation in Poly(ethylene Terephthalate) above and below the glass transition, Journal of Polymer Science, Polymer Physics Edition, 16 (1978), 2171-2187.

[26] J. A. Tshudy, C. V. Frankenberg, A model Incorporating Reversible Immobilization for Sorption and Diffusion in Glassy Polymers, Journal of Polymer Science: Polymer Physics Edition, 11 (1973), 2027-2037.

[27] E. Favre, N. Morliere, D. Roizard, Experimental Evidence and Implications of an Imperfect Upstream Pressure Step for the time-lag Technique, Journal of Membrane Science, 207 (2002), 59–72.

[28] Y.K. Zhang, N. M. Kocherginsky, Time lag for Transmembrane Transport without Interface Equilibrium, Journal of Membrane Science, 225 (2003), 105-114.

[29] J. Guo, T. A. Barbari, A Dual Mode, Local Equilibrium Relaxation Model for Small Molecule Diffusion in a Glassy Polymer, Macromolecules, 41 (2008), 238-245.

Chapter 2

Analysis of Gas Transport in Laminated Semi-Infinite Solid: Novel Method for Complete Membrane Characterization during Highly Transient State

Neveen Al-Qasas, Jules Thibault and Boguslaw Kruczek*

University of Ottawa, Department of Chemical and Biological Engineering

161 Louis Pasteur, Ottawa, Ontario, Canada K1N 6N5

Abstract

Gas transport in a two-layer membrane system, subjected to a step increase in feed pressure, is modelled under highly transient state in which the Layer 2 behaves as a semi-infinite solid. The system of governing partial deferential equations is solved using Laplace transforms, and the solution is used to obtain the expression for the pressure decay in the upstream volume. Accordingly, the pressure decay at short and long times is directly proportional to the square root of time, where the early and late slopes are dependent on the properties (i.e., diffusivity and solubility) of the materials of Layer 1 and Layer 2, respectively. Knowing the properties of the material of Layer 2, the material of Layer 1 can be fully characterized based on the early slope and the rate at which this early slope changes once the penetrant enters Layer 2. Since the thickness of Layer 1 in the two-layer system can be orders of magnitude smaller than that of a stand-alone membrane, the approach presented in this paper may allow characterizing barrier materials, which otherwise could not be characterized in a reasonable timeframe by traditional integral, permeation and sorption techniques. In addition, the new method may be used for characterization of the selective layer in thin film composite membranes.

Keywords: Membrane characterization; Two-layer membrane system; Transient diffusion; Pressure decay; Laplace transforms

Publication status: Journal of Membrane Science, 460 (2014) 25–33.

2.1 Introduction

The knowledge of transport properties, i.e. permeability (P), diffusivity (D) and solubility (S) of small molecules in a membrane facilitates the systematic selection of membranes and prediction of their performances in actual applications. In addition, it enables the investigation of structure-property relationships in the process of developing of new membrane materials. It is commonly assumed that species transport in polymeric membrane follows the solution-diffusion mechanism in which:

$$P = D \cdot S \tag{2.1}$$

In general, the methods for the determination of transport properties can be divided into three groups: 1) integral permeation, 2) differential permeation, and 3) sorption methods [1]. The time-lag method, which originates from the work of Daynes [2], is by far the most common integral permeation method and, at the same time, the most widely used for membrane characterization. In the time-lag method, the cumulative amount of a penetrant passes through a membrane as a result of a step change in feed pressure is determined as a function of time. The change in pressure downstream from the membrane in the downstream receiver is directly related to the gas flux emerging from the membrane. At steady state, the gas flux and thus the rate of pressure increase become constant. Extrapolating the linear portion of the pressure increase to the time axis allows the determination of the downstream time lag (θ_d), which in the simplest case is related to D through:

$$\theta_d = \frac{L^2}{6D} \tag{2.2}$$

where, L is the membrane thickness. Alternatively, if the pressure decay in the upstream receiver was also monitored, extrapolating the linear portion of the pressure decay to the time axis would yield the upstream time lag (θ_u), which is given by:

$$\theta_u = -\frac{L^2}{3D} \tag{2.3}$$

The permeability is directly proportional to the steady state slope of the pressure decay in the upstream receiver and the pressure increase in the downstream receiver. Then, knowing D and P, the solubility is determined from Eq. (1).

The time lags given by Eq. (2.3) and Eq. (2.4) are often referred to as the adsorption time lags, because they result from an increase in feed pressure, and thus adsorption of penetrant by a

membrane. Alternatively, time lags can be obtained using a membrane, which is initially in equilibrium with a gas, in case of which the experiment is initiated by a step decrease in feed pressure. The resulting downstream and upstream time lags are referred to as the desorption time lags [3-5]. The desorption time lag experiments are more challenging than the adsorption time lag experiments. However, the combination of the two is very useful when characterizing membranes with concentration-dependent diffusion coefficient [6].

Using adsorption integral permeation experiment, Rogers et al. [7] proposed a method for estimating the membrane properties at early times corresponding to Fourier numbers, $Fo < 0.15$ $\left(Fo = Dt/L^2\right)$, at which the expression for the rate of pressure increase in the downstream volume dp/dt can be written as:

$$\ln\left[\left(\frac{dp}{dt}\right)\sqrt{t}\right] = \ln\left[\frac{2ARTSp_o}{V_d}\sqrt{\frac{D}{\pi}}\right] - \frac{L^2}{4Dt} \tag{2.4}$$

where, A is the membrane area, V_d is the volume of the downstream reservoir, p_o is the pressure in the upstream receiver after its pressurization, T is the absolute temperature, and R is the universal gas constant. Plotting the left hand side of Eq. (2.4) versus $1/t$ should yield a straight line with a slope equal to $-L^2/4D$, from which D can be evaluated. After D has been determined, S can be calculated by solving Eq. (2.4).

Another variation of the integral permeation method based on the approximation of Rogers et al. was recently proposed by Al-Ismaily et al. [8], who re-derived Eq. (2.4) to a more convenient form:

$$\ln\left[\frac{p}{\sqrt{t}}\right] = \ln\left[\frac{4ARTSp_o}{V_d}\sqrt{\frac{D}{\pi}}\right] - \frac{L^2}{4Dt} \tag{2.5}$$

The determination of D from Eq. (2.5) does not require numerical differentiation of the experimental pressure increase, which is necessary when using Eq. (2.4), and which may introduce significant noise to the data. Moreover, instead of determining S from the intercept of Eq. (2.5), which requires extrapolation to $1/t = 0$, i.e. to infinitely long times at which Eq. (2.5) is not applicable, Al-Ismaily et al. focused on the determination of permeability P from the transient flux entering the membrane that was evaluated from the pressure decay in the upstream reservoir [8].

In differential permeation methods, the permeation rate through a membrane, following a step change in the driving force, is measured directly as a function of time [9]. The diffusivity can be determined from the half time ($t_{1/2}$):

$$D = \frac{L^2}{7.199 t_{1/2}} \tag{2.6}$$

The half time is the time at which the relative permeation rate reaches the value of 0.5, i.e.

$$Q_{rel}(t) = \frac{Q(t) - Q_1}{Q_2 - Q_1} = 0.5 \tag{2.7}$$

where Q_1 and Q_2 are the initial and final steady state permeation rates through the membrane. If initially there was no pressure difference across the membrane, $Q_1 = 0$ in Eq. (2.7).

The early times solution proposed by Rogers et al. [7] is also applicable to differential permeation methods. More specifically, the rate of pressure increase, dp/dt, in Eq. (2.4) is replaced by the time-dependent permeation rate through the membrane, $Q(t)$. Plotting $\ln\left[Q(t)\sqrt{t}\right]$ versus $1/t$ should yield a straight line with a slope equal to $-L^2/4D$, from which D can be evaluated. The permeability is determined from either the initial or the final steady state permeation rate.

Integration of $Q(t)$ over time provides the basis for a moment method [10]. More specifically, the quantity τ_p obtained from:

$$\tau_p = \int_0^\infty \left(1 - \frac{Q(t)}{Q_2}\right) dt \tag{2.8}$$

is equal to the time lag (θ_u) that would be measured in an integral permeation experiment at the same temperature and boundary conditions. Consequently, after estimating τ_p, D can be estimated from Eq. (2), while P can be evaluated from the new steady state permeation rate Q_2.

Sorption methods rely on the accurate monitoring of the mass of penetrant, $M(t)$, absorbed by the medium being characterized, following a step change in the concentration of the penetrant in the fluid that is in contact with the medium. In the simplest case, the fluid phase is a pure gaseous penetrant. The quantity $M(t)$ can be estimated by monitoring the increase in the mass of the medium using a microbalance, or by monitoring the total pressure of the gas phase. Unlike the integral and differential permeation methods, the penetrant in sorption methods does not

leave the medium. Consequently, after long times, a new equilibrium (M_∞), rather than steady state transport, is established.

All techniques that are used for the differential permeation methods are also applicable for the sorption methods. Defining a half time ($t_{1/2}$) as the time required to absorb 50% of the penetrant that would be absorbed at the new equilibrium i.e., the time at which $M(t) = 0.5M_\infty$, the diffusivity in a slab membrane when the penetrant enters the membrane from both sides is given by [1]:

$$D = 0.04919\frac{L^2}{t_{1/2}} \tag{2.9}$$

Alternatively, at very short times, the plot of $M(t)/M_\infty$ versus $t^{1/2}$ is linear with the slope given by:

$$Slope = \frac{4}{L}\sqrt{\frac{D}{\pi}} \tag{2.10}$$

In terms of the sorption moment (τ_s), the diffusivity can be evaluated from:

$$D = \frac{L^2}{12\tau_s} \tag{2.11}$$

where:

$$\tau_s = \int_0^\infty \left(1 - \frac{M(t)}{M_\infty}\right) dt \tag{2.12}$$

The solubility in sorption methods is determined based on M_∞ at a given concentration of the penetrant in the fluid phase and the equilibrium pressure. Knowing D and S, the permeability is evaluated from Eq. (2.1).

Except for the methods based on the approximate solution of Rogers et al. [7] for early times, all the other methods require either attaining steady state transport or a new equilibrium, which in the case of barrier materials may take weeks or even months. On the other hand, the approximate solution of Rogers et al. [7], which is applicable only for permeation methods, is based on the penetrant exiting the membrane. At Fo = 0.05, the flux out of the membrane is just 3% of the steady state value, while at Fo = 0.15 (i.e. at the upper end at which the early time solution is applicable) it increases to 50% of the steady state value. In the case of barrier materials, for which the solution of Rogers et al. [7] would be most suitable, steady state fluxes are generally very small, making accurate measurements of transient fluxes out for the membrane practically impossible. On the other hand, at $Fo < 0.05$, at which a slab membrane

behaves as a semi-infinite solid, transient fluxes into the membrane are much greater than the steady state value making them easier to be monitored from the rate of pressure decay in the upstream receiver (Δp_u).

The pressure decay in the upstream receiver due to gas transport into a semi-infinite solid is given [11]:

$$\Delta p_u = p_o - p(t) = \frac{2ARTp_oS\sqrt{D}}{V_u\sqrt{\pi}}t^{1/2} \tag{2.13}$$

where V_u is the volume of the upstream reservoir while p_o and $p(t)$ refer to the pressures in the upstream reservoir immediately after and at time t after the step change in feed pressure, respectively. If either S, D or P were known, Eq. (2.13) along with Eq. (2.1) could be used to determine the unknown transport coefficients from the slope of the pressure decay versus $\sqrt{t}$. If none of the transport coefficients are known ahead of time, Eq. (2.13) has little value because it does not allow decoupling S from D.

The objective of this work is to investigate the possibility of mutually decoupling S and D of a material in the form of a thin film by combining it with another film made from a different material of known properties. Two cases are considered: (1) unknown material is Layer 1 in the two-layer system; (2) unknown material is Layer 2 in the two-layer system. To achieve this objective with short experiments, information under highly transient period before the penetrant emerges from Layer 2 of the two-layer system is used. Consequently, the characterization is to be performed based on monitoring the pressure decay in the upstream volume. There has been a significant body of research on diffusion in multi-layered membrane systems [12-14], but all the past efforts were focused on the systems in which steady state transport was allowed to be attained.

It should be emphasized that measurements of pressure decay at the high pressure side of the membrane, on which the analyses presented in this paper rely, are very challenging and rarely practiced today. On the other hand, an apparatus capable of this type of measurements was already developed and used in membrane characterizations more than 30 years ago [6,15]. Recently, we have also developed and successfully used a two-tank system capable of very accurate monitoring of pressure decay resulting from gas transport into a membrane [8]. This

system is currently being upgraded, and the details of the upgraded system will be disclosed in a future publication.

2.2 Mathematical description of the problem

Figure 2.1 presents a schematic representation of a two-layer system in a constant volume (CV) testing system. Layer 1 made from Material 1 and Layer 2 made from Material 2 have properties (diffusion coefficient, solubility and permeability) and thicknesses of D_1, S_1, P_1, L_1, and D_2, S_2, P_2, L_2, respectively. The upstream and downstream reservoirs have volumes V_u and V_d, respectively, and the pressure on both sides of the two-layer system (p_u and p_d) can be accurately monitored. Initially, both p_u and p_d are zero and consequently both layers are completely depleted from any gas species. The experiment is initiated by a step pressure increase in the upstream reservoir to p_o. Since the pressure decrease due to the gas transport into Layer 1 is much smaller than p_o, the pressure in the upstream reservoir remains approximately constant during the course of the experiment, $p_u(t) \approx p_o$. After pressurization of the upstream volume, the concentration profiles in Layers 1 and 2 develop according to Fick's second law.

$$\frac{\partial C_1}{\partial t} = D_1 \frac{\partial^2 C_1}{\partial x_1^2} \tag{2.14}$$

$$\frac{\partial C_2}{\partial t} = D_2 \frac{\partial^2 C_2}{\partial x_2^2} \tag{2.15}$$

The corresponding initial and boundary conditions for Layer 1 are given by:

$$IC: C_1(x_1, 0) = 0 \tag{2.16}$$

$$BC1: C_1(0, t) = p_o S_1 \tag{2.17}$$

$$BC2: -D_1 \left.\frac{\partial C_1}{\partial x_1}\right|_{x_1 = L_1} = -D_2 \left.\frac{\partial C_2}{\partial x_2}\right|_{x_2 = 0} \tag{2.18}$$

The initial condition for Layer 2 is identical to that given by Eq. (2.16):

$$IC: C_2(x_2, 0) = 0 \tag{2.19}$$

Layer 2 is also subjected to the second boundary condition of Layer 1, i.e. Eq. (2.18) is used to solve for the concentration at the interface within the Layer 1, but the same boundary condition cannot be used again for Layer 2. Instead, assuming equilibrium at the interface of the two

layers, the solubility coefficients of the two Materials are used to formulate the first boundary condition for Layer 2.

$$BC1: C_2(0,t) = \frac{S_2}{S_1} C_1(L_1,t) = f_1(t) \tag{2.20}$$

The second boundary condition for Layer 2 is given by:

$$BC2: C_2(L_2,t) = f_2(t) \tag{2.21}$$

Assuming that the resistance to gas transport in Layer 2 (L_2^2/D_2) is much greater than that in Layer 1 (L_1^2/D_1), Layer 2 will behave as a semi-infinite solid for some time after initiation of the gas permeation experiment, during which the second boundary condition ($BC2$) for Layer 2 will simplify to:

$$BC2: C_2(L_2,t) = f_2(t) \Rightarrow C_2(x_2 \to \infty, t) = 0 \tag{2.22}$$

It is important to note that by increasing the thickness of Layer 2, it is possible to increase the time during which Eq. (2.22) will be applicable.

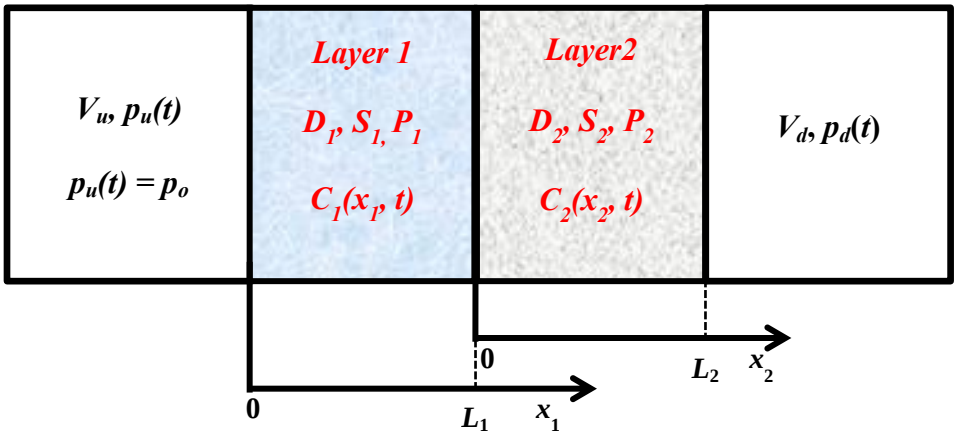

Figure 2.1: Schematic representation of the two-layer membrane system in a constant volume (CV) testing system.

2.3 Analytical solution of the concentration profiles for the two-membrane system

The system of the two partial differential equations (PDEs) described above is solved using Laplace transforms. First, the system of the PDEs along with the initial and boundary conditions are transformed into the Laplace domain, and the solution in the Laplace domain is obtained. This is followed by finding the corresponding inverse Laplace transforms to convert the solution

back to the time domain, i.e. to obtain $C_1(x_1,t)$ and $C_2(x_2,t)$. Finally, the application of the Fick's first law to $C_1(x_1,t)$, which is then evaluated at $x_1 = 0$ and integrated over time, allows obtaining the expression for the pressure decay in the upstream reservoir.

2.3.1 Solution in the Laplace domain

Application of the Laplace transforms to Eqs. (2.14) and (2.15) along with the corresponding initial conditions given by Eqs. (2.16) and (2.19) leads to:

$$\frac{d^2\bar{C}_1}{dx_1^{\,2}} - \frac{s}{D_1}\bar{C}_1 = 0 \tag{2.23}$$

$$\frac{d^2\bar{C}_2}{dx_2^{\,2}} - \frac{s}{D_2}\bar{C}_2 = 0 \tag{2.24}$$

where: $\bar{C}_i = \bar{C}_i(x_i,s) = \int_0^\infty e^{-st} C_i(x_i,t)dt$.

The general solutions of Eqs. (2.23) and (2.24) are:

$$\bar{C}_1 = A_1 \exp\left(-x_1\sqrt{s/D_1}\right) + B_1 \exp\left(x_1\sqrt{s/D_1}\right) \tag{2.25}$$

$$\bar{C}_2 = A_2 \exp\left(-x_2\sqrt{s/D_2}\right) + B_2 \exp\left(x_2\sqrt{s/D_2}\right) \tag{2.26}$$

The determination of constants A_1, B_1, A_2, and B_2 requires the Laplace transforms of the respective boundary conditions given by Eqs. (2.17), (2.18), (2.20), and (2.22), which are:

$$\bar{C}_1(x_1 = 0, s) = \frac{p_0 S_1}{s} \tag{2.27}$$

$$-D_1 \left.\frac{d\bar{C}_1}{dx_1}\right|_{x_1 = L_1} = -D_2 \left.\frac{d\bar{C}_2}{dx_2}\right|_{x_2 = 0} \tag{2.28}$$

$$\bar{C}_2(x_2 = 0, s) = \frac{S_2}{S_1}\bar{C}_1\left(x_1 = L_1, s\right) \tag{2.29}$$

$$\bar{C}_2(x_2 \to \infty, s) = 0 \tag{2.30}$$

It follows from Eqs. (2.26) and (2.30) that $B_2 = 0$, and thus Eq. (2.26) becomes:

$$\bar{C}_2 = A_2 \exp\left(-x_2\sqrt{s/D_2}\right) \tag{2.31}$$

Substituting Eq. (2.25) into Eq. (2.27) leads to:

$$A_1 + B_1 = \frac{p_0 S_1}{s} \tag{2.32}$$

Substituting Eqs. (2.25) and (2.31) into Eq. (2.28) gives:

$$D_1 A_1 \sqrt{\frac{s}{D_1}} \exp\left(-L_1\sqrt{s/D_1}\right) - D_1 B_1 \sqrt{\frac{s}{D_1}} \exp\left(L_1\sqrt{s/D_1}\right) = D_2 A_2 \sqrt{\frac{s}{D_2}} \tag{2.33}$$

Finally, substituting Eqs. (2.25) and (2.31) into Eq. (2.29) results in the third independent equation:

$$A_2 - \frac{S_2}{S_1}\left[A_1 \exp\left(-L_1\sqrt{s/D_1}\right) + B_1 \exp\left(L_1\sqrt{s/D_1}\right)\right] = 0 \tag{2.34}$$

Solving simultaneously Eqs. (2.32) – (2.34), i.e. a system of three equations and three unknowns (A_1, A_2 and B_1), gives the following expressions for the constants:

$$A_1 = \left(\frac{p_0 S_1}{s}\right)\left\{\frac{\exp\left(L_1\sqrt{s/D_1}\right)\left[\sqrt{sD_1} + \frac{S_2}{S_1}\sqrt{sD_2}\right]}{\exp\left(L_1\sqrt{s/D_1}\right)\left(\sqrt{sD_1} + \frac{S_2}{S_1}\sqrt{sD_2}\right) + \exp\left(-L_1\sqrt{s/D_1}\right)\left(\sqrt{sD_1} - \frac{S_2}{S_1}\sqrt{sD_2}\right)}\right\} \tag{2.35}$$

$$B_1 = \left(\frac{p_0 S_1}{s}\right)\left\{\frac{\exp\left(-L_1\sqrt{s/D_1}\right)\left[\sqrt{sD_1} - \frac{S_2}{S_1}\sqrt{sD_2}\right]}{\exp\left(L_1\sqrt{s/D_1}\right)\left(\sqrt{sD_1} + \frac{S_2}{S_1}\sqrt{sD_2}\right) + \exp\left(-L_1\sqrt{s/D_1}\right)\left(\sqrt{sD_1} - \frac{S_2}{S_1}\sqrt{sD_2}\right)}\right\} \tag{2.36}$$

$$A_2 = \left(\frac{p_0 S_2}{s}\right)\left[\frac{2\sqrt{D_1}}{\exp\left(L_1\sqrt{s/D_1}\right)\left(\sqrt{D_1} + \frac{S_2}{S_1}\sqrt{D_2}\right) + \exp\left(-L_1\sqrt{s/D_1}\right)\left(\sqrt{D_1} - \frac{S_2}{S_1}\sqrt{D_2}\right)}\right] \tag{2.37}$$

Substituting Eqs. (2.35) and (2.36) into Eq. (2.25) and Eq. (2.37) along with $B_2 = 0$ into Eq. (2.26) leads to the final solutions in the Laplace domain:

$$\bar{C}_1 = \left(\frac{p_0 S_1}{s}\right)\frac{\left\{\eta \exp\left[\sqrt{s/D_1}\left(L_1 - x_1\right)\right] + \psi \exp\left[\sqrt{s/D_1}\left(x_1 - L_1\right)\right]\right\}}{\left[\eta \exp\left(\sqrt{s/D_1}L_1\right) + \psi \exp\left(-\sqrt{s/D_1}L_1\right)\right]} \tag{2.38}$$

$$\bar{C}_2 = \left(\frac{p_0 S_2}{s}\right)\frac{2S_1\sqrt{D_1}\exp\left(-x_2\sqrt{s/D_2}\right)}{\left[\eta \exp\left(\sqrt{s/D_1}L_1\right) + \psi \exp\left(-\sqrt{s/D_1}L_1\right)\right]} \tag{2.39}$$

where:

$$\eta = \left(S_1\sqrt{D_1} + S_2\sqrt{D_2} \right) \tag{2.40}$$

$$\psi = \left(S_1\sqrt{D_1} - S_2\sqrt{D_2} \right) \tag{2.41}$$

2.3.2 Solution in the time domain

To obtain the concentration responses in Membranes 1 and 2, i.e. $C_1(t)$ and $C_2(t)$, requires finding the inverse Laplace transforms of Eqs. (2.38) and (2.39). We will focus first on Eq. (2.38), which can be rearranged to the following form:

$$\bar{C}_1 = \left(\frac{p_0 S_1}{s} \right) \frac{\left\{ \exp\left(-x_1\sqrt{s/D_1} \right) + Y \exp\left[\sqrt{s/D_1}\left(x_1 - 2L_1 \right) \right] \right\}}{\left[1 + Y \exp\left(-2L_1\sqrt{s/D_1} \right) \right]} \tag{2.42}$$

where,

$$Y = \frac{\psi}{\eta} = \frac{S_1\sqrt{D_1} - S_2\sqrt{D_2}}{S_1\sqrt{D_1} + S_2\sqrt{D_2}} \tag{2.43}$$

Also, it follows from Eq. (2.43) that: $-1 < Y < 1$.

Recognizing that:

$$\frac{1}{\left[1 + Y \exp\left(-2L_1\sqrt{s/D_1} \right) \right]} = \sum_{n=0}^{\infty} (-1)^n Y^n \exp\left(\frac{-2nL_1}{\sqrt{D_1}} \sqrt{s} \right) \tag{2.44}$$

Eq. (2.42) is rewritten as:

$$\bar{C}_1 = \frac{p_0 S_1}{s} \sum_{n=0}^{\infty} (-1)^n Y^n \exp\left(\frac{-2nL_1}{\sqrt{D_1}} \sqrt{s} \right) \left\{ \exp\left(-x_1\sqrt{s/D_1} \right) + Y \exp\left[\sqrt{s/D_1}\left(x_1 - 2L_1 \right) \right] \right\} \tag{2.45}$$

Furthermore, the above equation can be rearranged to:

$$\bar{C}_1 = \bar{f} \cdot \bar{g} + \bar{f} \cdot \bar{h} \tag{2.46}$$

where:

$$\bar{f} = \frac{p_0 S_1}{s} \tag{2.47}$$

$$\bar{g} = \sum_{n=0}^{\infty} (-1)^n Y^n \exp\left(-\sqrt{s} \left[\frac{2nL_1 + x_1}{\sqrt{D_1}} \right] \right) \tag{2.48}$$

$$\bar{h} = \sum_{n=0}^{\infty} (-1)^n Y^{n+1} \exp\left(-\sqrt{s} \left[\frac{2L_1(n+1) - x_1}{\sqrt{D_1}} \right] \right) \tag{2.49}$$

Using the properties of Laplace transforms,

$$C_1 = L^{-1}\left\{\bar{C}_1\right\} = L^{-1}\left\{\bar{f} \cdot \bar{g}\right\} + L^{-1}\left\{\bar{f} \cdot \bar{h}\right\} \tag{2.50}$$

According to the convolution theorem:

$$L^{-1}\left\{\bar{f} \cdot \bar{g}\right\} = F * G = \int_0^t F(t-\tau) \cdot G(\tau) d\tau \tag{2.51}$$

where *F* and *G* are the inverse Laplace transform of $\bar{f}$ and $\bar{g}$, respectively. The inverse Laplace transforms of the functions defined by Eqs. (2.47) - (2.49) are widely available [16] and are given by:

$$L^{-1}\left\{\bar{f}\right\} = F = p_0 S_1 \tag{2.52}$$

$$L^{-1}\left\{\bar{g}\right\} = G = \sum_{n=0}^{\infty} (-1)^n Y^n \left(\frac{2nL_1 + x_1}{2\sqrt{D_1 \pi}} \right) \exp\left(-\frac{(2nL_1 + x_1)^2}{4D_1 t} \right) \frac{1}{t^{3/2}} \tag{2.53}$$

$$L^{-1}\left\{\bar{h}\right\} = H = \sum_{n=0}^{\infty} (-1)^n Y^{n+1} \left(\frac{2L_1(n+1) - x_1}{2\sqrt{D_1 \pi}} \right) \exp\left(-\frac{(2L_1(n+1) - x_1)^2}{4D_1 t} \right) \frac{1}{t^{3/2}} \tag{2.54}$$

Application of the convolution theorem to the products on the right hand side of Eq. (2.46) along with the inverse Laplace transforms provided above leads to:

$$L^{-1}\left\{\bar{f} \cdot \bar{g}\right\} = \int_0^t p_0 S_1 \sum_{n=0}^{\infty} (-1)^n Y^n \frac{(2nL_1 + x_1)}{2\sqrt{D_1 \pi}} \exp\left(-\frac{(2nL_1 + x_1)^2}{4D_1 \tau} \right) \frac{1}{\tau^{3/2}} d\tau \tag{2.55}$$

$$L^{-1}\left\{\bar{f} \cdot \bar{h}\right\} = \int_0^t p_0 S_1 \sum_{n=0}^{\infty} (-1)^n Y^{n+1} \left(\frac{2(n+1)L_1 - x_1}{2\sqrt{D_1 \pi}} \right) \exp\left(-\frac{\left[2L_1(n+1) - x_1\right]^2}{4D_1 \tau} \right) \frac{1}{\tau^{3/2}} d\tau \tag{2.56}$$

Performing the above integrations and substituting the resulting expressions into Eq. (2.50) leads, after rearrangements, to the final expression for the concentration response in Membrane 1:

$$C_1 = p_0 S_1 \left[\sum_{n=0}^{\infty} (-1)^n Y^n erfc\left(\frac{(2nL_1 + x_1)}{2\sqrt{D_1 t}} \right) + \sum_{n=0}^{\infty} (-1)^n Y^{n+1} erfc\left(\frac{(2L_1(n+1) - x_1)}{2\sqrt{D_1}\sqrt{t}} \right) \right] \tag{2.57}$$

A similar approach is also used to obtain the concentration response in Membrane 2. Dividing the numerator and denominator of Eq. (2.39) by $\eta \exp\left(\sqrt{s/D_1} L_1\right)$ leads to:

$$\bar{C}_2(s) = 2Z \frac{p_0 S_2}{s} \frac{\exp\left(-\sqrt{s}\left(x_2/\sqrt{D_2} + L_1/\sqrt{D_1}\right)\right)}{\left[1 + Y \exp\left(-2L_1\sqrt{s/D_1}\right)\right]} \tag{2.58}$$

where,

$$Z = \frac{S_1\sqrt{D_1}}{\eta} = \frac{S_1\sqrt{D_1}}{\left(S_1\sqrt{D_1} + S_2\sqrt{D_2}\right)} \tag{2.59}$$

Recognizing that:

$$\frac{1}{\left[1 + Y \exp\left(-2L_1\sqrt{s/D_1}\right)\right]} = \sum_{n=0}^{\infty} (-1)^n Y^n \exp\left(-2nL_1\sqrt{\frac{s}{D_1}}\right) \tag{2.60}$$

Eq. (2.58) is rewritten as:

$$\bar{C}_2 = 2Z \frac{p_0 S_2}{s} \exp\left[-\sqrt{s}\left(\frac{x_2}{\sqrt{D_2}} + \frac{L_1}{\sqrt{D_1}}\right)\right] \sum_{n=0}^{\infty} (-1)^n Y^n \exp\left(\frac{-2nL_1}{\sqrt{D_1}}\sqrt{s}\right) \tag{2.61}$$

The inverse Laplace transform of Eq. (2.61) can be obtained by using the procedure applied to Eq. (2.45), which involves the application of the convolution theorem, or directly by making use of Wolfram Alpha [17]. The final expression for the concentration response in Membrane 2 is then given by:

$$C_2 = L^{-1}\left\{\bar{C}_2\right\} = 2Zp_0 S_2 \sum_{n=0}^{\infty} (-1)^n Y^n erfc\left(\frac{\sqrt{D_1}x_2 + \sqrt{D_2}L_1(1+2n)}{2\sqrt{D_1 D_2 t}} \right) \tag{2.62}$$

It can be shown that Eq. (2.57) satisfies the initial and boundary conditions given by Eqs. (2.16) – (2.18); similarly, Eq. (2.62) satisfies its initial and boundary conditions given by Eqs. (2.19), (2.20) and (2.22).

2.3.3 Pressure decay in the upstream reservoir

At early times, the gas transport is in transient state, which means that the gas flux in the two-layer system depends on the position within the system. Consequently, the pressure decay in the upstream volume must be evaluated based on the gas flux entering Layer 1.

In general, the gas flux anywhere within the two-layer system is determined by applying Fick's first law:

$$J_i = -D_i \frac{\partial C_i}{\partial x_i} \tag{2.63}$$

Differentiating Eq. (2.23) with respect to x_1 and substitution into Eq. (2.63), in which $D_i = D_1$, leads to:

$$J_1 = \frac{\sqrt{D_1}\, p_o S_1}{\sqrt{t\pi}} \left(\sum_{n=0}^{\infty} (-1)^n Y^n \exp\left[-\frac{(2nL_1 + x_1)^2}{4D_1 t} \right] - \sum_{n=0}^{\infty} (-1)^n Y^{n+1} \exp\left\{ -\frac{\left[2L_1 (n+1) - x_1 \right]^2}{4D_1 t} \right\} \right) \tag{2.64}$$

Setting $x_1 = 0$ in Eq. (2.64) gives the expression for the gas flux entering Layer 1 as a function of time:

$$J_1(0,t) = \frac{\sqrt{D_1}\, p_o S_1}{\sqrt{t\pi}} \left\{ \sum_{n=0}^{\infty} (-1)^n Y^n \exp\left(-\frac{n^2 L_1^2}{D_1 t} \right) - \sum_{n=0}^{\infty} (-1)^n Y^{n+1} \exp\left[-\frac{L_1^2 (n+1)^2}{D_1 t} \right] \right\} \tag{2.65}$$

Knowing the gas flux entering Layer 1, the pressure decay in the upstream reservoir can now be evaluated from:

$$\Delta p_u(t) = p_o - p_u(t) = \frac{ART}{V_u} \int_0^t J(0,t)\, dt \tag{2.66}$$

Substituting Eq. (2.65) into Eq. (2.66) and integrating the resulting equation leads to the final expression for the pressure decay in the upstream reservoir:

$$\Delta p_u(t) = \frac{2ARTp_o S_1 L_1}{V_u} \sum_{n=0}^{\infty} (-1)^n Y^n \left\{ \begin{array}{l} \sqrt{\frac{Fo}{\pi}} \left[\exp\left(-\frac{n^2}{Fo} \right) - Y \exp\left(-\frac{(n+1)^2}{Fo} \right) \right] + \left[Y(n+1) - n \right] + \\ \left[n\, erf\left(\frac{n}{\sqrt{Fo}} \right) - Y(n+1)\, erf\left(\frac{(n+1)}{\sqrt{Fo}} \right) \right] \end{array} \right\} \quad (2.67)$$

where *Fo* is the Fourier number based on the first layer:

$$Fo = \frac{D_1 t}{L_1^2} \quad (2.68)$$

2.3.4 Limiting cases of the pressure decay in the upstream volume

Eq. (2.67) is an alternating infinite series consisting of three terms: the second term is independent of time whereas the first and third terms are two time-dependent terms. The first term involves two exponential functions of the negative inverse of the Fourier number. The third consists of two Gaussian error functions containing the inverse of the square root of the Fourier number. Despite its complex appearance, Eq. (2.67) simplifies significantly in two limiting cases: at short times, i.e. when $Fo \rightarrow 0$, and at long times, i.e., when $Fo \rightarrow \infty$. To derive the respective expressions for the pressure decay for these two limiting cases, one needs to focus first on the time-independent term.

According to Eq. (2.43), the *Y*-term must be greater than -1 but less than 1. If $S_1\sqrt{D_1} > S_2\sqrt{D_2}$, then Y is positive whereas if $S_1\sqrt{D_1} < S_2\sqrt{D_2}$, then Y is negative. Consequently, the infinite series involving the time-independent term has the following limits:

$$\text{for } -1 < Y < 1: \sum_{n=0}^{\infty} (-1)^n Y^n \left[Y(n+1) - n \right] = \frac{2Y}{(1+Y)^2} = \frac{S_1^2 D_1 - S_2^2 D_2}{2S_1^2 D_1} \quad (2.69)$$

One can also recognize that:

$$\lim(Fo \rightarrow 0) \left\{ \sum_{n=0}^{\infty} (-1)^n Y^n \left[\exp\left(-\frac{n^2}{Fo} \right) - Y \exp\left(-\frac{(n+1)^2}{Fo} \right) \right] \right\} = 1 \quad (2.70)$$

and that:

$$\lim(Fo \rightarrow 0) \left\{ \sum_{n=0}^{\infty} (-1)^n Y^n \left[n\, erf\left(\frac{n}{\sqrt{Fo}} \right) - Y(n+1)\, erf\left(\frac{(n+1)}{\sqrt{Fo}} \right) \right] \right\} = -\frac{2Y}{(1+Y)^2} \quad (2.71)$$

The equivalent expressions for the summation terms presented in Eq. (2.69) and Eq. (2.71), were obtained using the computational platform Wolfram Alpha [17] and verified numerically to be indeed equivalent. Therefore, at short times, Eq. (2.67) simplifies to:

$$\Delta p_u(t) = \frac{2ARTp_o S_1\sqrt{D_1}}{V_u\sqrt{\pi}}\sqrt{t} \tag{2.72}$$

It is important to note that Eq. (2.72) is identical to Eq. (2.13), which could be expected because at early times before gas molecules reach the interface between Layer 1 and Layer 2 the two-layer system will behave as a semi-infinite solid with the properties of material in Layer 1. Consequently, the early pressure decay will be directly proportional to $\sqrt{t}$, with the early slope ($Slope_1$) is equal to:

$$Slope_1 = \frac{2ARTp_o S_1\sqrt{D_1}}{V_u\sqrt{\pi}} \tag{2.73}$$

Considering the other limiting case, one can recognize that after very long times:

$$\lim\left(Fo\to\infty\right)\left\{\sum_{n=0}^{\infty}\left(-1\right)^n Y^n\left[\exp\left(-\frac{n^2}{Fo}\right)-Y\exp\left(-\frac{\left(n+1\right)^2}{Fo}\right)\right]\right\}=\frac{1-Y}{1+Y}=\frac{S_2\sqrt{D_2}}{S_1\sqrt{D_1}} \tag{2.74}$$

In addition:

$$\lim\left(Fo\to\infty\right)\left\{\sum_{n=0}^{\infty}\left(-1\right)^n Y^n\left[n\ erf\left(\frac{n}{\sqrt{Fo}}\right)-Y\left(n+1\right)erf\left(\frac{\left(n+1\right)}{\sqrt{Fo}}\right)\right]\right\}=0 \tag{2.75}$$

Substituting Eqs. (2.74), (2.75) and (2.69) into Eq. (2.67), leads after rearrangements to:

$$\Delta p_u(t) = \frac{2ARTp_o S_2\sqrt{D_2}}{V_u\sqrt{\pi}}\left[\sqrt{t}+\frac{L_1\sqrt{\pi}}{2S_1D_1S_2\sqrt{D_2}}\left(S_1^2D_1-S_2^2D_2\right)\right] \tag{2.76}$$

According to Eq. (2.76), the plot $\Delta p_u(t)$ versus $\sqrt{t}$ at very long times should also yield a straight line with a slope and intercept respectively given by the following equations:

$$Slope_2 = \frac{2ARTp_o S_2\sqrt{D_2}}{V_u\sqrt{\pi}} \tag{2.77}$$

$$Intercept = \frac{ARTp_o L_1}{V_u S_1 D_1}\left(S_1^2D_1-S_2^2D_2\right) \tag{2.78}$$

It is important to emphasize, that the expression for the slope given by Eq. (2.77), which will be referred to as a late slope, is similar to the expression for the early slope given by Eq. (2.73). The expression for the late slope is independent of the properties of the material of Layer 1. At that time, Layer 1 must be at pseudo steady-state, in which the concentration of penetrant varies linearly within Layer 1, with a slope that decreases with time.

2.4 Discussion

The major motivation of this research is to design a method for the determination of permeability, diffusivity and solubility of gases in solids based entirely on monitoring the pressure decay in the upstream volume during the highly transient state. Although the pressure decay at early times in a single layer system can be linearized with respect to $\sqrt{t}$, and the slope is proportional to $S\sqrt{D}$, the material of the layer cannot be fully characterized because the corresponding intercept is equal to zero. In other words, this approach does not allow decoupling *S* and *D*. To circumvent this problem, we have proposed to laminate the layer to be characterized with a layer of different but known properties and thickness. The details of the corresponding analytical solution were presented in the preceding section. It is important to emphasize that the obtained solution can be used in two possible scenarios, with the material to be characterized being in Layer 1, or in Layer 2.

Using Eq. (2.67), Figure 2.2 graphically illustrates the pressure decay response in these two cases. To generate Figure 2.2, the two-layer system consists of polyphenyelene oxide (PPO) and silicone rubber (SR). The properties of these two polymers for the transport of nitrogen are summarized in Table 1 [8,18]. In Figure 2.2a, Layer 1 is SR and Layer 2 is PPO while in Figure 2.2b Layer 1 is PPO and Layer 2 is SR. The corresponding *Y*-values defined by Eq. (2.43) are 0.63 in Figure 2.2a and -0.63 in Figure 2.2b. It is important to emphasize that when SR is used as Layer 1, its thickness is 100 μm, but when PPO is used as Layer 1 its thickness is 10 μm. The smaller thickness for the PPO layer was used because its diffusivity is three orders of magnitude smaller than the one for SR. The thickness of Layer 2 in the simulations shown in Figure 2.2 has to be sufficiently large to ensure that Layer 2 behaves as a semi-infinite solid during the entire simulation time.

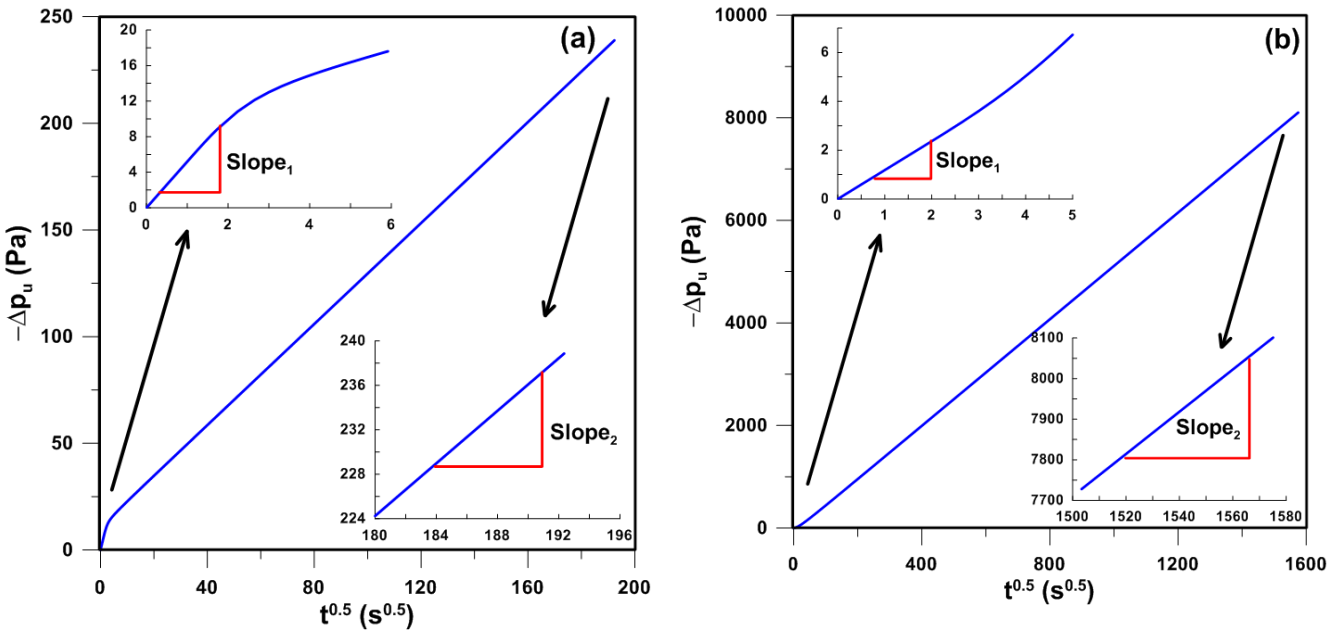

Figure 2.2: Pressure decay response in a two-layer system (PPO and SR polymers) based on Eq. (2.67) for a) Case I: Layer 1 is SR of thickness L_1 = 100 μm and Layer 2 is PPO; b) Case II: Layer 1 is PPO of thickness L_1 = 10 μm and Layer 2 is SR.

Table 2.1: Properties of the PPO [8] and SR [18] used for generation of Figs. 2.2a and 2.2b.

Membrane	D_i (m^2/s)	S_i (mol/m^3 Pa)	$S_i\sqrt{D_i}$ (mol/$s^{1/2}$ m^2 Pa)	L_i^* (μm)	Y_i^{**} (-)
SR [12]	$1.5\cdot10^{-9}$	$6.61\cdot10^{-5}$	$2.56\cdot10^{-9}$	100	0.63
PPO [4]	$4.52\cdot10^{-12}$	$2.74\cdot10^{-4}$	$5.83\cdot10^{-10}$	10	-0.63

* Thickness when used as Layer 1; when used as Layer 2, the thickness approaches to infinity to satisfy the requirement of semi-infinite solid

** *Y*-value when used as Layer 1

As shown in Figure 2.2, there are three regions in the pressure decay-response plots. At early times, the plot of $\Delta p_u(t)$ versus $\sqrt{t}$ is linear with the early slope given by Eq. (2.73). Then, in an intermediate region the slope changes (increases or decreases depending on the arrangement of the materials) until it reaches another constant value, the late slope given by Eq.

(2.77), at the beginning of the third region. It may appear from Figure 2.2 that the transition from the early to the late slope occurs rapidly. However, as it will be shown in subsequent analysis, the intermediate region stretches over a long period of time. For this reason, the abscissas in Figs. 2a and 2b extend to $\sqrt{t}$ = 200 $s^{0.5}$ and $\sqrt{t}$ = 1600 $s^{0.5}$, respectively.

2.4.1 Direct application of the pressure decay-response plots

The early and the late linear responses in Figure 2.2 provide three independent equations for: (1) the early slope - Eq. (2.73), (2) the late slope - Eq. (2.77), and (3) the intercept - Eq. (2.78). Knowing the properties of the low resistance Layer (S_i and D_i) along with the thickness of Layer 1 (L_1), there are only two unknowns, S_j and D_j, i.e. the properties of the high resistance layer, which can be either Layer 2 (Figure 2.2a) or Layer 1 (Fig 2.2b). The two arrangements of the materials are discussed next.

*Case I: Tested material is in Layer 2***.**

The first case, in which the properties of the material in Layer 2 are sought, appears to be attractive. This is because the time required to reach the late linear response would be minimized. In addition, due to its high resistance, the 2nd boundary condition for layer 2 given by Eq. (2.22) would be valid for a relatively long time, even when L_2 were not excessively large.

Out of the three independent equations, only the equations for the intercept and the late slope are useful in Case I, because the early slope is independent of the properties of the material in Layer 2. Knowing L_1, there are two equations, Eq. (2.77) and Eq. (2.78), and two unknowns, S_2 and D_2. Rearranging Eq. (2.77) to express S_2 in terms of D_2 leads to:

$$S_2 = \frac{Slope_2 \cdot V_u \sqrt{\pi}}{2ARTp_o \sqrt{D_2}} \tag{2.79}$$

Substituting Eq. (2.79) into Eq. (2.78) leads to cancellation of D_2. This is because S_2 and D_2 in the expressions for the late slope and the intercept are coupled in a similar way, $S_2^{2n} D_2^n$, where n = 0.5 in Eq. (2.77) and n = 1 in Eq. (2.78). In other words, despite the fact that adding Layer 1 to Layer 2 results in a non-zero intercept of the pressure decay versus $\sqrt{t}$, the properties of the material in Layer 2 cannot be determined before the gas emerges from Layer 2.

Case II: Tested material is in Layer 1.

The second case, in which the thickness of Layer 1 is known, but its properties are unknown, is not as attractive from a practical point of view as the first case. This is because to ensure the validity of the 2nd boundary condition for Layer 2 and thus to observe the late linear response during the course of the experiment, L_1 would need to be very small while L_2 very large. On the other hand, if the late linear response were observed, the properties of the material in Layer 2 would not be required for the complete characterization of the material in Layer 1.

In the second case, the expression for the early slope, Eq. (2.73), can be rearranged to a form similar to that given by Eq. (2.79), in which S_1 is expressed in terms of D_1 and the early slope. Then, substituting the resulting expression into Eq. (2.78) leads, after rearrangements, to:

$$D_1 = \left[\frac{2K^2 L_1}{Intercept \cdot Slope_1 \cdot \sqrt{\pi}} \left(\frac{\pi \cdot Slope_1^2}{K^2} - S_2^2 D_2 \right) \right]^2 \tag{2.80}$$

where:

$$K = \frac{ARTp_o}{V_u} \tag{2.81}$$

The product $S_2^2 D_2$ can be expressed in terms of the late slope, which allows rewriting Eq. (2.80) in the following form:

$$D_1 = \left[\frac{L_1 \sqrt{\pi}}{2 \cdot Intercept \cdot Slope_1} \left(4 \cdot Slope_1^2 - Slope_2^2 \right) \right]^2 \tag{2.82}$$

Knowing D_1 and $Slope_1$, one can evaluate S_1 from Eq. (2.73), and then P_1 from Eq. (2.1).

It is important to note that in the second case there is no advantage of knowing the properties of the material in Layer 2 ahead of time. This is because in addition to $Slope_2$, the evaluation of D_1 from Eq. (2.82) also requires the value of *Intercept*. In turn, *Intercept* is obtained by extending the late linear pressure decay response to zero time. In other words, application of Eq. (2.82) for evaluation of D_1 requires observing $Slope_2$ experimentally even when its numerical value is known ahead of time.

2.4.2 The concept of relative slope

From the discussion so far it is evident that out of the two possible cases, the properties of a barrier material can be determined only when it is arranged as Layer 1 in the two-layer system.

On the other hand, this arrangement requires observing $Slope_2$ experimentally, which may not be possible in practice. To circumvent this problem, we shall focus on the second region in Figure 2.2, in which the slope changes from $Slope_1$ to $Slope_2$, and introduce a new term, which will be referred to as a relative slope:

$$Slope_{\mathrm{Rel}} = \frac{Slope_{\mathrm{Ins}} - Slope_1}{Slope_2 - Slope_1} \tag{2.83}$$

where, $Slope_{\mathrm{Ins}}$ is the instantaneous slope which can be evaluated from the plot of the experimental $\Delta p_u(t)$ versus $\sqrt{t}$. In other words, the apparent slope can be evaluated at any time after initiation of the experiment. At early times, the instantaneous slope will be constant and equal to $Slope_1$ while at late times it will approach the value of $Slope_2$. Therefore, the relative slope varies from 0 to 1.

Knowing the properties of the material in Layer 2, one does not need to observe experimentally $Slope_2$, because it can be evaluated from Eq. (2.77). If the properties of the material in Layer 2 were unknown, one could easily determine $Slope_2$ in a parallel experiment involving only the material in Layer 2.

We shall now derive the analytical expression for the relative slope. Dividing Eq. (2.67) by $\sqrt{t}$ leads, after rearrangements, to:

$$\Delta p_u(t) = \frac{2ARTp_oS_1\sqrt{D_1}}{V_u\sqrt{\pi}} \sum_{n=0}^{\infty} (-1)^n Y^n \left\{ \begin{array}{l} \left[\exp\left(-\dfrac{n^2}{Fo}\right) - Y\exp\left(-\dfrac{(n+1)^2}{Fo}\right) \right] + \\ \dfrac{1}{\sqrt{Fo}}\left[Y(n+1) - n \right] + \\ \dfrac{1}{\sqrt{Fo}}\left[n\, erf\left(\dfrac{n}{\sqrt{Fo}}\right) - Y(n+1)\, erf\left(\dfrac{(n+1)}{\sqrt{Fo}}\right) \right] \end{array} \right\} \tag{2.84}$$

Substituting Eqs. (2.73), (2.77) and (2.84) into Eq. (2.83), and applying the relationships given by Eqs. (2.43) and (2.69) leads to:

$$Slope_{\mathrm{Rel}} = \frac{\begin{array}{l}\sum_{n=0}^{\infty}(-1)^n Y^n\left[\exp\left(-\frac{n^2}{Fo}\right)-Y\exp\left(-\frac{(n+1)^2}{Fo}\right)\right]+\\ \frac{1}{\sqrt{Fo}}\sum_{n=0}^{\infty}(-1)^n Y^n\left[n\,erf\left(\frac{n}{\sqrt{Fo}}\right)-Y(n+1)erf\left(\frac{(n+1)}{\sqrt{Fo}}\right)\right]\\ +\frac{2Y}{(1+Y)^2\sqrt{Fo}}-1\end{array}}{\left(-\frac{2Y}{1+Y}\right)} \qquad (2.85)$$

According to Eq. (2.85), $Slope_{\mathrm{Rel}}$ depends only on Y and Fo. Knowing the $S_2\sqrt{D_2}$ product from a parallel experiment involving only Layer 2, and using the experimental $Slope_1$, the value of Y can be evaluated. In turn, knowing Y and the experimental $Slope_{\mathrm{Rel}}$, Fo can be determined from Eq. (2.85). Knowing the time at which $Slope_{\mathrm{Rel}}$ was evaluated and L_1, D_1 can be calculated from Eq. (2.68). Then, knowing D_1, S_1 can be determined from Eq. (2.73). Finally, the permeability of the material in Layer 1 is simply the product of D_1 and S_1.

As already stated, in the approach described above, one does not need to wait until the pressure decay becomes a linear function of $\sqrt{t}$ at late times. Moreover, this approach provides self-checking of the experimentally determined D_1, which for a Fickian system should be the same, regardless of the time at which it was determined. Once gas molecules start to emerge from Layer 2, the model will no longer be valid, which will be manifested by overestimating the actual D_1. In other words, once the estimated value of D_1 will start to increase with time, it will be an indication that gas molecules are emerging from Layer 2 into the downstream reservoir.

The concept of the relative slope also allows evaluating the time required to reach the late linear response, which corresponds to the relative slope approaching to unity. Figure 2.3 presents the plot of Eq. (2.85) for the two cases described earlier (Case I for Y = 0.63 and Case II for Y = - 0.63). Eq. (2.85) was simulated and ran to reach a relative slope value that is equal to 0.992. This implies that the apparent slope is already within 99% of the analytical value of $Slope_2$. For the case of Y = 0.63, the relative slope reached 99% of the final slope value at around Fo = 5550, while for the case of Y = - 0.63, the same relative slope value is reached at a much longer Fourier number that is around 111 000. The difference in the required Fo to reach a specific value of the relative slope explains different scales of the abscissas in Figs. 2a and 2b. At the same time, it is

important to emphasize that because of a log-scale of abscissa in Figure 2.3, the changes in the relative slope at the linear abscissa would not be as dramatic as those seen in Figure 2.3, in particular at large Fourier numbers.

Unlike Figure 2.2, which was generated for the specific properties of materials in Layers 1 and 2 in two possible arrangements, the resulting *Y*-values of 0.63 and -0.63, respectively, that were used in construction of Figure 2.3, can be obtained for infinite combinations of the properties of the two materials. Thus the plots of the relative slope as a function of *Fo* for different *Y*-values allow to draw some important general conclusions. The first such conclusion is that *Fo* number required to characterize the material in Layer 1 is significantly longer when $S_1\sqrt{D_1} < S_2\sqrt{D_2}$ (negative *Y*-value) compared to the case when $S_1\sqrt{D_1} > S_2\sqrt{D_2}$ (positive *Y*-value).

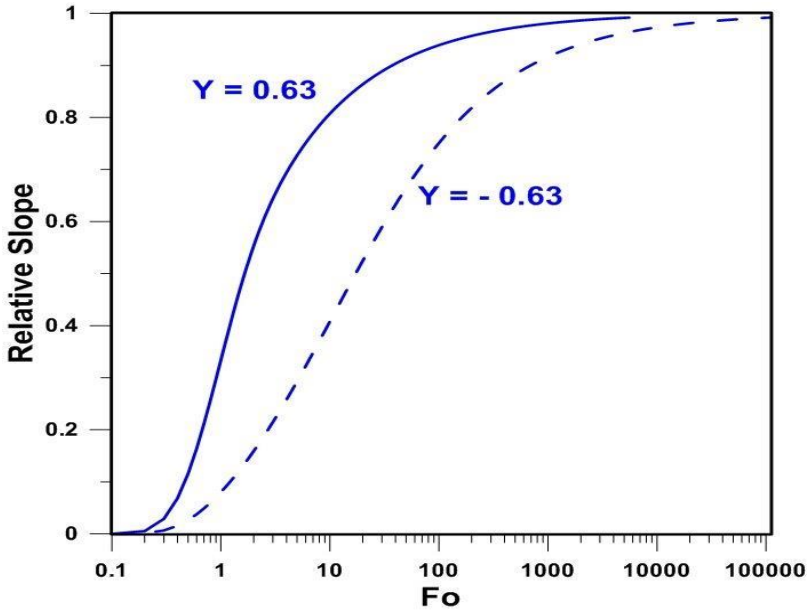

Figure 2.3: Relative slope versus *Fo* for values of *Y* = 0.63 and *Y* = -0.63.

To better understand the effect of *Y*-value on the time required to reach a specific relative slope, Figure 2.4 presents the plot of $Slope_{Rel}$ as a function of *Fo* for a wide range of *Y* values from -0.9 to 0.9. Figure 2.4a focuses on positive *Y* values, while Figure 2.4b focuses on negative *Y* values. The latter cases are of more practical interest, because they cover the case for the characterization of barrier materials, which might be difficult to characterize using the traditional techniques that rely on reaching steady state permeation. As a reference, Figure 2.4 includes *Y* =

0.63 and Y = -0.63 used in Figure 2.3. The simulations in Figure 2.4 are carried out until $Slope_{Rel}$ reaches the value of 0.97.

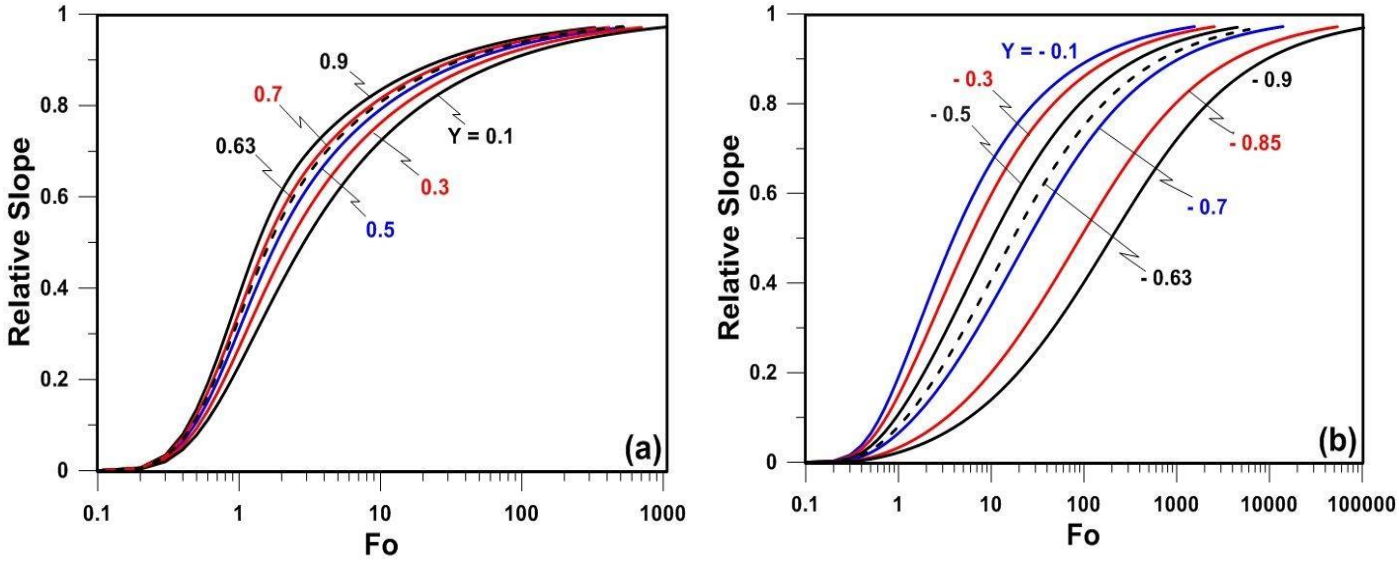

Figure 2.4: Graphical representation of Eq. (2.49) for the prediction of the relative slope based on *Fo* number for a) positive *Y* values, and b) negative *Y* values.

It can be noticed in Figure 2.4 that as *Y* increases (from -0.9 to -0.1 in Figure 2.4b, and from 0.1 to 0.9 in Figure 2.4a) the time to reach a specific relative slope decreases. However, the physical meaning of increasing *Y* value is different for the positive and negative values. Recalling Eq. (2.43), positive *Y* increases when $S_1\sqrt{D_1} - S_2\sqrt{D_2}$ increases, i.e. when the properties of the two membranes differ further apart. On the other hand, negative *Y* increases when $S_1\sqrt{D_1} - S_2\sqrt{D_2}$ decreases, i.e. when the properties of the two membranes are closer to each other. In one limiting case, when $S_1\sqrt{D_1} = S_2\sqrt{D_2}$ (i.e., *Y* = 0), the relative slope is undefined because the denominator of Eq. (2.83) becomes zero. In the other limit, when *Y* = 1 or -1, one layer in the two-layer system is an absolute barrier, i.e., the diffusion coefficient in the material of that layer is zero. The concept of the relative slope is not applicable for that limit either.

As already stated, the concept of the relative slope allows determination of the properties of the material in Layer 1 based on a single experimental $Slope_{Rel}$ when its value is greater than zero. In practice however, it would be desired to record $Slope_{Rel}$ at multiple times to ensure the

validity of the model. In the case of negative Y values, which is our main interest, and which is exemplified by Case II in Figure 2.2b, the rate of pressure decay increases once gas molecules start entering Layer 2. It should be emphasized however, that this increase is observed only because the abscissa in Figure 2.2 represents $\sqrt{t}$ rather than t. In the latter case, i.e. in a linear time domain, the rate pressure decay continuously decreases until steady state permeation is reached. In turn, the greater the rate of pressure decay in the time domain, the more reliable the rate of pressure decay in the square root of time domain will be. Therefore, it is of critical importance that non-zero relative slopes (e.g. $Slope_{Rel} = 0.1$) be reached as soon as possible after the initiation of the gas permeation test. According to Figure 2.4b, when $Y = -0.9$, $Slope_{Rel} = 0.1$ is reached at $Fo \approx 6$, but for $Y = -0.1$ the same relative slope is reached at $Fo \approx 0.6$. It is therefore important to have Y less negative. When the properties of a barrier material in Layer 1 are fixed, this can be achieved by using Layer 2 made of a material having high resistance to gas transport.

In the reference case of PPO in Layer 1 and SR in Layer 2, for which $Y = -0.63$, $D_1 = 4.52 \cdot 10^{-12}$ m^2/s is more than two orders of magnitude smaller than $D_2 = 1.5 \cdot 10^{-9}$ m^2/s. Conversely, if unknown material had a diffusion coefficient in the order 10^{-15} m^2/s or lower, one could use PPO as material in Layer 2, which would lead to Y value comparable to that in the reference case. As shown in Figure 2.4b, for $Y = -0.63$, $Slope_{Rel} = 0.1$ is reached at $Fo \approx 1$.
The actual time to reach $Slope_{Rel} = 0.1$ depends on the diffusion coefficient and the thickness of layer 1. For $L_1 = 10$ μm and $D_1 = 10^{-15}$ m^2/s, $Fo = 1$ corresponds to $t = 10^5$ s, which is not practical. On the other hand, with $L_1 = 0.1$ μm and the same D_1, $Fo = 1$ corresponds to $t = 10$ s. In other words, it would roughly require only 10 s to fully characterize a membrane with such a low diffusivity, if it was supported by a PPO layer.

Considering a conventional time-lag method, the Fourier number required to reach steady state permeation and thus to fully characterize a membrane is also in the order of unity, which is comparable to our reference case for which $Y = -0.63$. A question arises, what is the advantage of the proposed new method compared to the conventional time-lag method? A free standing membrane used in the conventional time-lag method should be at least 10 μm thick to ensure its proper handling. On the other hand, in the proposed method, the tested material in Layer 1 is supported by Layer 2, which allows minimizing the thickness of Layer 1, and L_1 in the order of 0.1 μm is not unreasonable. A spin technique allows preparing membranes with uniform thickness for wide range thicknesses including in the sub-micron range [19].

The proposed method may also be very useful for the characterization composite membranes, in which the skin layer represents Layer 1 while the support would be Layer 2. Conversely, if the properties of the skin layer are known, the proposed method may be used for the estimation of the effective thickness of the selective skin layer with the assumption that the transport mechanism in both layers is governed by the solution-diffusion model.

The importance of exact analytical solutions for a given transport in multi-layer systems at transient state is not limited to characterization of barrier materials. The mathematical analysis described in this paper might be applicable in other mass [20,21] and heat transfer [22] applications.

2.5. Conclusions

The objective of this work was to develop a method for complete characterization of gas transport coefficients in a membrane based on the upstream pressure decay measurements under highly transient period of a conventional time-lag test. Right after initiation of the test, the product of the solubility (S) and diffusivity (D) coefficients, expressed in a form $S\sqrt{D}$, is readily available from the slope of the upstream pressure decay versus square root of time plot. However, to decouple the two coefficients it is necessary for the penetrant to start emerging from the other side of the membrane. In the proposed method, the penetrant emerging from tested membrane enters a support layer made from another material of known properties.

A concentration profile in two-layer membrane system, under highly transient part of a conventional time lag test during which the support layer behaves as semi-infinite solid, was determined. An analytical solution of the governing system of partial differential equations was obtained using Laplace transforms, and the obtained solution was used to determine the pressure decay resulting from gas transport into the two-layer system. The pressure decay equation in the square root of time domain was shown to have two linear parts, with the two slopes exclusively depending on the properties of the materials in Layer 1 and Layer 2, respectively. Using the two slopes as limiting values, the concept of a relative slope was introduced. Moreover, it was proved that the relative slope depends only on Fourier number of the material of Layer 1 and the combination of two slopes, which can be easily determined experimentally. Consequently, the new method allows complete characterization of the tested membrane based of experimentally determined relative slope right after the penetrant crosses the interface between the two layers.

The major advantage of the two-layer system is that the thickness of the test layer can be minimized. Compared to a free standing membrane in conventional time lag method, the thickness of the test layer in the two layer system can be two orders of magnitude smaller. This translates to the reduction of tests time by a factor of 10^4. This may allow characterizing high barrier materials that could not be characterized by the current state of the art methods. In addition, the new method may be used for direct characterization of practical multi-layer membranes such as integrally skinned and thin film composite asymmetric membranes.

2.6. Nomenclature

A Cross sectional membrane area, m^2

C_i Gas concentration, mol/m^3.

D_i Diffusivity coefficient of penetrant *i* in membrane, m^2/s

Fo Fourier number, dimensionless

J Gas flux, mol/m^2 s

K Constant defined by Eq. (2.81), $N^2/mol\ m^2$

L_i Thickness of membrane/Layer *i*, m

M Mass of penetrant, g

M_∞ Mass of penetrant after reaching equilibrium, g

p Pressure, Pa

p_d Downstream pressure, Pa

p_o Feed pressure, Pa

P_i Permeability of coefficient of penetrant *i* in membrane, mol/m s Pa

p_u Upstream pressure, Pa

Q Permeation rate, mol/s

Q_{rel} Relative permeation rate, dimensionless

R Universal gas constant, Pa m^3/ mol K

S_i Solubility coefficient of penetrant *i* in membrane, mol/Pa m^3

t Time, s

$t_{1/2}$ Half time, s

T Temperature, K

x Distance, m

V_d Downstream volume, m^3

V_u Upstream volume, m^3

Y Constant defined by Eq. (2.43), dimensionless

Z Constant defined by Eq. (2.59), dimensionless

Δp_u Pressure decay, Pa

η Constant defined by Eq. (2.40), $mol/m^2\,Pa\,s^{1/2}$

ψ Constant defined by Eq. (2.41), $mol/m^2\,Pa\,s^{1/2}$

θ_d Downstream time lag, s

θ_u Upstream time lag, s

τ_p Permeation moment, s

τ_s Sorption moment, s

2.7. Acknowledgement

The authors gratefully acknowledge the financial support for this project provided by the Natural Science and Engineering Research Council of Canada.

2.8. References

[1] R.M. Felder, "Estimation of Gas transport Coefficients from Differential permeation, integral permeation and Sorption rate", J. Membrane Sci. 3 (1978) 15-27.

[2] H.A. Daynes, The process of diffusion through a rubber membrane, Proc. R. Soc. London Ser. A 97 (685) (1920) 286–307

[3] I. Fatt, "A modified diffusion time lag", J. Phys. Chem. 66 (1962) 760-62.

[4] J.H. Petropoulos, P.P. Roussis, "Study of Non Fickian Diffusion Anomalies through Time Lags. I. Some Time Dependent Anomalies", J. Phys. Chem. 47 (1967) 1491-96.

[5] D.R. Paul, "Determination of penetrant solubility from transient permeation measurements: J. Polym. Sci. Part A-1 7 (1969) 2031-35.

[6] R. Ash, R.M. Barrer, H.T. Chio, V.A.J. J Edge, "Apparatus and method for measuring sorption and desorption time lags in transport through membranes", J. Phys. E: Sci. Instrum. 11 (1978) 262-64.

[7] W.A. Rogers, R.S., Buritz, D., Alpert, "Diffusion coefficient, solubility, and permeability for helium in glass", J. Appl. Phys. 257 (1954) 868-875.

[8] M. Al-Ismaily, J.G., Wijmans, B., Kruczek, "A shortcut method for faster determination of permeability coefficient from time lag experiments", J. Membrane Sci., 234-424 (2012), 165-174.

[9] K.D. Ziegel, H. K. Frensdorff, D.E. Blair, " Measurement of Hydrogen Isotope Transport in Poly-(Vinyl Flouride) films by the permeation-rate method", J. Polym. Sci, A-2, 7 (1969) 809-819.

[10] R.M. Felder, R.D. Spence, J.K. Ferrell," A Method for the Dynamic Measurement of Diffusivities of Gases in Polymers" J. Appl. Polym. Sci., 19 (1975) 3193.

[11] M. Al-Ismaily, "A novel method of characterizing polymer membrane using upstream gas permeation tests", Master thesis, University of Ottawa, 2011.

[12] R. Ash, R.M. Barrer, D.G. Palmer, "Diffusion in multiple laminates", Brit. J. Appl. Phys. 16 (1965) 873-84.

[13] R.A. Siegel, "Algebraic, Differential, and integral relations for membranes in series and other multilaminar media: permeabilities, solute consumption, lag times, and mean first passage times", J. Phys. Chem. 95 (1991) 2556-65.

[14] S. Carranza, D.R. Paul, R.T. Bonnecaze, Multilayer reactive barrier materials, J. Membrane Sci. 399– 400 (2012) 73– 85.

[15] P.P. Roussis, K. Tsimillist, C. Savvakis, S. Amarantos, N. Kanellopoulos, J.H. Petropoulos, "On the measurement of desorption-permeation time lags", J. Phys. E: Sci. Instrum. 13 (1980) 403-05.

[16] A. D. Poularikas, "The Handbook for Formulas and Tables for signal processing", CRC Press LLC, Boca Raton, Fla, (1999), Chapter 2: Laplace Transform

[17] Wolfram alpha: http://www.wolframalpha.com/

[18] H. Zhang, A., Cloud, "The permeability characteristics of Silicon Rubber", SAMPE Fall Technical Conference, Global advances in materials and process engineering, (2006), Dallas, TX.

[19] S. Lashkari, B. Kruczek, “Effect of resistance to gas accumulation in multi-tank receivers on membrane characterization by the time lag method. Analytical approach for optimization of the receiver”, J. Membrane Sci. 360 (2010) 442-453.

[20] G.L. Graff, R.E. Williford, P.E. Burrows, “Mechanisms of vapor permeation through multilayer barrier films: Lag time versus equilibrium permeation”, J. Appl. Phys. 96(4) (2004) 1840-49.

[21] J.L. Osborne, I.C. Sanchez, D.R. Paul, “An asymptotic analysis of drug delivery from transdermal patches”, J. Membrane Sci. 442, (2013) 27-30.

[22] R.I. Hickson, S.I. Barry, G.N. Mercer, “Critical times in multilayer diffusion. Part 1: Exact solutions”, Inter. J. Heat and Mass Trans. 52(25-26) (2009) 5776-83.

Chapter 3

Membrane Characterization Based on the Upstream Pressure Decay in a Dynamic Gas Permeation Test

N. Al-Qasas, J. Thibault, B. Kruczek

University of Ottawa, Department of Chemical and Biological Engineering

161 Louis Pasteur, Ottawa, Ontario, Canada K1N 6N5

Abstract

The time-lag method is believed to be the most usable method for extracting the membrane properties via a simple dynamic permeation experiment; however this method suffers from major drawbacks that limit its use for some materials and under certain conditions. One of the major drawbacks of the time-lag method is that it relies on monitoring the pressure rise downstream from the membrane due to gas permeation, whereas the method is derived by assuming that the pressure downstream from the membrane is maintained at zero during the entire permeation experiment. To rectify this problem, it is proposed to characterize the membrane based on the pressure decay upstream from the membrane during a conventional time-lag experiment, while continuously evacuating the downstream side of the membrane. This modification allows for a better adherence to the boundary conditions on which the time-lag method relies. Right after initiation of the gas permeation experiment, the membrane behaves as a semi-infinite solid, and the rate of pressure decay is directly proportional to the square root of time. Once the permeating gases emerge downstream from the membrane, the membrane no longer behaves as a semi-infinite solid and the pressure decay becomes a non-linear function of the square root of time. In the proposed new method, the membrane properties are extracted based on the deviation of the recorded pressure decay from the semi-infinite behavior in the square root of the time domain. In this paper, we present the mathematical bases of the new method along with preliminary experimental results. The latter indicate that diffusivity, solubility and permeability of nitrogen in polyphenylene oxide (PPO) membrane used in this study are very close to the literature values.

Keywords: Membrane characterization, Semi-infinite solid, permeation experiments, upstream measurements.

Publication status: Journal of Fluid flow, Heat and Mass Transfer, 1 (2014), 57-64.

3.1 Introduction

The most common method for membrane characterization is the time-lag method that originates from the work of Daynes (1920). The time-lag method has been used since due to its simplicity. It relies on the temporal variation of the pressure in the downstream reservoir. The pressure changes downstream from the membrane are directly related to the gas flux emerging from the membrane. In turn, the gas flux anywhere within the membrane is governed by Fick's first law. The thin membrane is used as a separator between two chambers with known volumes. Both volumes are initially evacuated to remove any present species; the experiment starts by applying a step pressure increase in the upstream chamber and the resulting pressure rise in the downstream chamber is then monitored as a function of time. As the permeation rate reaches steady state, an extrapolation of the linear portion of the pressure rise curve to the time coordinate yields the time lag. The time lag is a function of the membrane thickness and gas diffusivity in the membrane. Therefore, measuring the downstream time lag experimentally and knowing the membrane thickness allows evaluating the diffusion coefficient in the membrane. The slope of the linear portion of the pressure rise curve is directly proportional to the permeability coefficient (*P*), and thus P can also be evaluated. Therefore, knowing *P* and *D*, the solubility *S* can be obtained from the ratio of *P* and *D*. The time-lag method is derived using the Fick's second law of diffusion:

$$\frac{\partial C}{\partial t} = D\frac{\partial^2 C}{\partial x^2} \tag{3.1}$$

The above differential equation is solved under the following boundary conditions:

$$\begin{aligned} &IC: C(x,0) = 0; \\ &BCs: C(0,t) = C_0 \; ; C(L,t) = C_L = 0 \end{aligned} \tag{3.2}$$

Therefore, since the conventional time-lag method relies on monitoring the rate of pressure increase in the downstream chamber, the second boundary condition is never valid. This

represents the major drawback of the conventional time-lag method. Although Eq. (3.1) can be solved under more realistic second boundary conditions and the solutions are available in the literature (Rutherford and Do, 1997) the corresponding expressions for the time lag become more complex and the method loses its mathematical simplicity. Despite the fact that the second boundary condition is never satisfied, it is a common practice to use the simplest form of the expression for the time lag that assumes $C(L,t) = 0$. Another drawback of the conventional time-lag method is that it requires reaching steady state permeation. Technically, because of gas accumulation in the downstream chamber, the actual steady state permeation cannot be attained. If the downstream chamber were continuously evacuated during the experiment, after the time corresponding to 3 time lags, the gas permeation would be within 1% of the steady state value. Consequently, it is often aimed to obtain the steady state slope from the data between 3 and 4 time lags. If the data is taken too early, the deviation from the steady state permeation is too large; on the other hand, waiting too long to take the data increases the influence of the buildup in the downstream chamber. Although in a properly designed experiment, the feed pressure is much greater than the downstream pressure resulting from gas permeation, there is a systematic error that is in many cases cannot be neglected (Jenkins et al., 1969).

The time-lag method also relies on the assumption that there is no resistance to gas accumulation downstream from the membrane. On the other hand, because of high vacuum, the transport of the gas molecules emerging from the membrane is governed by Knudsen diffusion, which implies that the measured time lag depends on the location of the pressure transducer downstream from the membrane (Kruczek et al., 2005). Moreover, although the resistance to gas transport in high vacuum is inversely proportional to the internal diameter of tubing, the presence of relatively large diameter accumulation chambers, which in themselves are resistance-free, greatly magnify the resistance effects in tubing that connect a membrane cell with the accumulation chambers (Kruczek et al., 2006; Laskari and Kruczek, 2010). In addition, the measurements of the time lag involves the contributions of many other system-related response times; therefore, in the case of highly diffusive and thin membranes, in which the time lag is small, the influence of system-related delays cannot be neglected (Nguyen et al., 1992; Nguyen et al., 1994; Villaluenga and Seoane, 2001). On the other hand, in the case of barrier materials characterized by very low diffusion coefficients, the actual time to reach quasi-steady state might

very long, which precludes application of the conventional time-lag method (Al-Ismaily et al., 2012).

To overcome drawbacks of a conventional time-lag method, a new method, which relies on monitoring of the pressure decay in the upstream chamber while the downstream side of the membrane is continuously evacuated, is proposed. This approach allows to comply with the second boundary condition during the entire permeation experiment, as well as to attain the actual steady state rather than quasi steady state permeation.

3.2 Mathematical description of the method

The main objective of this proposed method is to extract the transport properties of the membrane from the upstream pressure decay data rather than downstream pressure rise data. The mathematical bases of the new method are described next.

The solution of Eq. (3.1) subject to the initial and boundary conditions specified by Eq. (3.2) is given by:

$$C\left(x,t\right)=C_0\left(1-\frac{x}{L}\right)-2\frac{C_0}{\pi}\sum_{n=1}^{\infty}\ \frac{1}{n}\sin\left(\frac{n\pi x}{L}\right)\exp\left(-\frac{Dn^2\pi^2t}{L^2}\right) \tag{3.3}$$

Application of Fick's first law of diffusion to Eq. (3.3) and evaluating the resulting expression at $x = 0$ allows obtaining the equation for the gas flux entering the membrane as a function of time:

$$J\left(0,t\right)=\frac{DC_0}{L}+\frac{2DC_0}{L}\sum_{n=1}^{\infty}\ \exp\left(-\frac{Dn^2\pi^2t}{L^2}\right) \tag{3.4}$$

Integrating Eq. (3.4) over time and applying the ideal gas law leads to the expression for the pressure decay in the upstream chamber due to gas permeation into the membrane:

$$p_o-p\left(t\right)=\Delta p\left(0,t\right)=\frac{C_0ART}{V_u}\frac{D}{L}\left[t+\frac{L^2}{3D}-\frac{2L^2}{D\pi^2}\sum_{n=1}^{\infty}\ \frac{1}{n^2}\exp\left(-\frac{Dn^2\pi^2t}{L^2}\right)\right] \tag{3.5}$$

Where: p_o is the feed pressure, A is the membrane area, V_u is the upstream volume, R is the universal gas constant, and T is the absolute temperature. At relatively long times, the infinite series in Eq. (3.5) can be approximated by its first term and Eq. (3.5) simplifies to:

$$\Delta p\left(0,t\right)=\frac{C_0 ART}{V_u}\frac{D}{L}\left[t+\frac{L^2}{3D}-\frac{2L^2}{D\pi^2}\exp\left(-\frac{D\pi^2 t}{L^2}\right)\right] \tag{3.6}$$

In general, Eq. (3.6) is valid at Fourier number, *Fo* > 0.2, where $Fo=Dt/L^2$. On the other hand, at very short times (*Fo* < 0.05), i.e. before gas molecules emerge from the membrane, the membrane behaves as a semi-infinite solid and it can be shown that the pressure decay in the upstream chamber is a linear function of the square root of time:

$$\Delta p\left(0,t\right)=\frac{2ARTp_o S\sqrt{D}}{V_u\sqrt{\pi}}\sqrt{t} \tag{3.7}$$

Subtracting Eq. (3.7) from Eq. (3.6) leads, after rearrangements, to the following expression:

$$Diff_p\left(0,t\right)=\frac{ARTp_o S\sqrt{D}}{V_u L}\left[t\sqrt{D}+\frac{L^2}{3\sqrt{D}}-\frac{2L^2}{\sqrt{D}\pi^2}\exp\left(-\frac{D\pi^2 t}{L^2}\right)-\frac{2L\sqrt{t}}{\sqrt{\pi}}\right] \tag{3.8}$$

The above equation describes the deviation between the actual pressure decay due to gas permeation into a slab membrane from that which would occur if gas were permeating into a semi-infinite membrane. The deviation given by Eq. (3.8) is shown graphically as a function of the square root of time in Figure 3.1. It can be observed that experimentally meaningful deviations between Eq. (3.5) and Eq. (3.7) occur at *Fo* > 1, despite the fact that at *Fo* ≈ 0.05 gas molecules start to emerge from the membrane. At *Fo* > 1, the exponential term in Eq. (3.8) disappears and thus it simplifies to:

$$Diff_p\left(0,t\right)=\frac{ARTp_o S\sqrt{D}}{V_u L}\left[t\sqrt{D}+\frac{L^2}{3\sqrt{D}}-\frac{2L\sqrt{t}}{\sqrt{\pi}}\right] \tag{3.9}$$

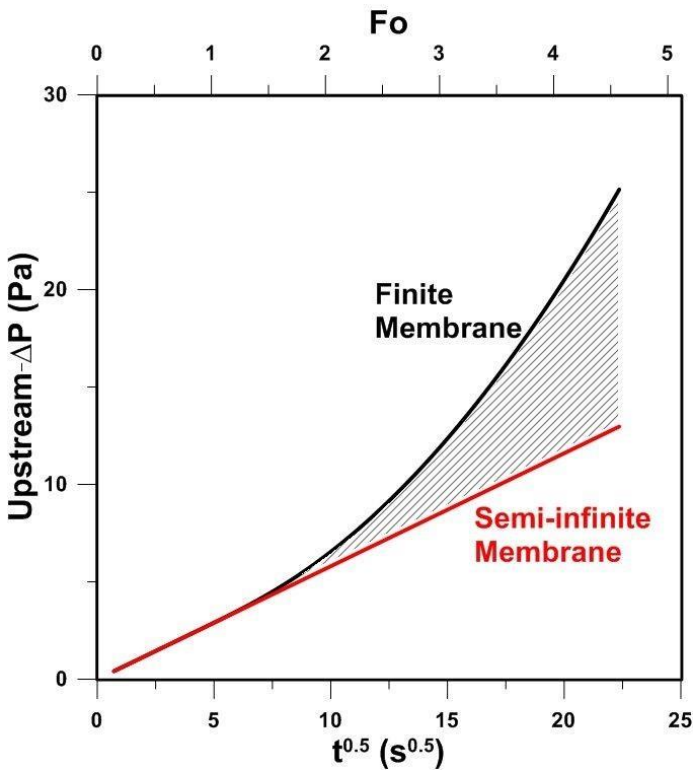

Figure 3.1: The deviation from the semi-infinite behaviour in the pressure decay of a membrane not behaving as a semi-infinite solid using the literature PPO properties (D = 4.52×10^{-12} m^2/s and S = 2.74×10^{-4} mol/m^3 Pa), T=298 K, membrane thickness L=23.5 µm.

There are two unknowns in Eq. (3.9), D and S. However, since Eq. (3.5) and Eq. (3.7) coincide at early times, the term $S\sqrt{D}$ can be evaluated from the early linear behavior in the square root of the time domain. Then, knowing $S\sqrt{D}$, the only unknown in Eq. (3.9) is D. In other words, by plotting the experimental pressure decay versus $\sqrt{t}$ and recording the deviation from the semi-infinite pressure decay, allows solving Eq. (9) for D. Once D is known, then S can be determined from the previously determined $S\sqrt{D}$. Finally, knowing D and S, the permeability coefficient (P) is simply the product of D and S.

It should be emphasized that once steady state permeation is attained, that is the pressure decay becomes a linear function of time; one could extract the membrane properties from the inflow time lag and the slope of the pressure decay curve in the time domain. However, because of limitations of the current experimental system, which will be discussed in the next section, this approach is not yet feasible.

3.3 Experimental procedures and results

The key aspect of the new characterization method relies on the very accurate monitoring of the pressure decay resulting from gas permeation into the membrane. Since the magnitude of this pressure decay must be orders of magnitude smaller than the feed pressure, commercially available absolute pressure transducers do not have a sufficient resolution to carry out this measurement. To solve this problem, the upstream part of a constant volume system used for membrane characterization in the conventional time-lag method was modified, as described previously by Al-Ismaily et al. (2012). Figure 3.2 shows a schematic diagram of the experimental setup. Briefly, the upstream section is split into a working volume and a reference volume. The two volumes, which are separated by a valve, are connected to a high accuracy differential pressure transducer (DPT, MKS model 226A.2TCDCDFB2A1) with a working range from -0.2 mmHg to 0.2 mmHg (±27 Pa). During the actual gas permeation experiment, the working and reference volumes are separated and the pressure decay due to gas transport from the working volume into the membrane is very accurately monitored by the DPT.

Since the gas permeation experiment should be initiated by a step increase in feed pressure from the initial high vacuum to a finite value, and at the same time the working and reference volumes should also be at the same pressure, the working volume is further split into two sub-sections by another valve. When the latter valve is closed and the valve between the working and reference volumes is opened, the desired feed pressure can be set, while the upstream part of the membrane remains under high vacuum. Ideally, once the desired feed pressure is set, the valve between the working and reference volumes should be closed, and the experiment should be initiated by opening the valve inside the working volume. However, in this scenario there would be a sudden expansion in the working volume orders of magnitude greater than the range of the DPT, which would preclude recording any pressure decay data. To solve this problem, the actual gas permeation experiment is started by first opening the valve in the working volume, while the valve between the working and reference volumes is opened, followed by immediate closing of the latter valve. Although this approach precludes recording the pressure decay in the first couple of seconds of the experiment, it allows to accurately monitoring the pressure decay afterwards (Al-Ismaily et al., 2012). Also, during the entire gas permeation experiment, the downstream section is continuously evacuated to ensure that the boundary condition, $C(L,t) = 0$, is satisfied.

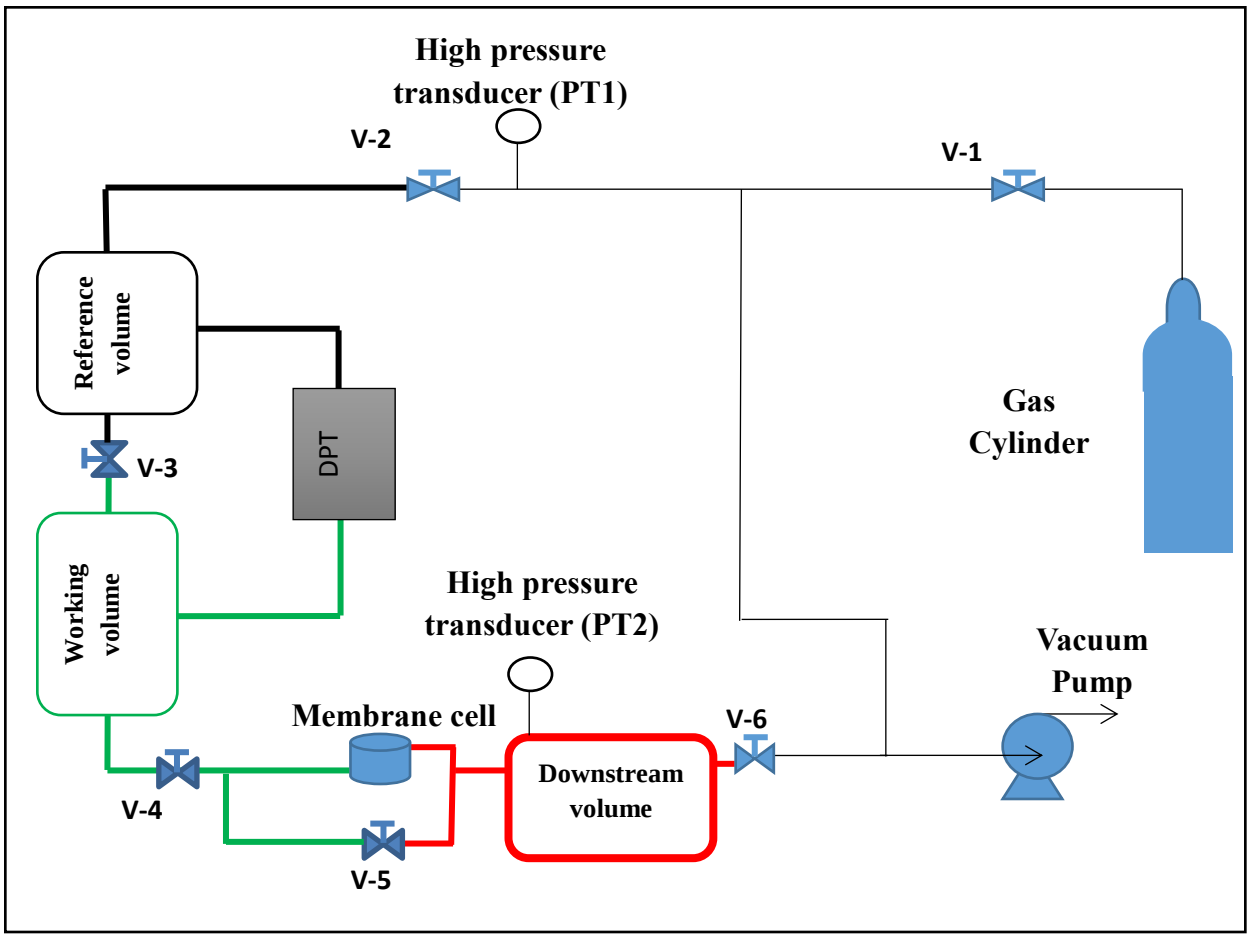

Figure 3.2: Schematic diagram of the experimental set up, showing the working volume, reference volume and downstream volume

The actual gas permeation experiments were carried out using pure nitrogen from a gas cylinder and a polyphenylene oxide (PPO) membrane of thickness L = 23.5 µm. PPO is a well-known membrane material, which has been thoroughly studied in our laboratory.

Figure 3.3 presents the experimentally recorded pressure decay as a function of the square root of time from the experiment in which p_o = 17 kPa. To increase the range of ΔP measurement, the zero point of the DPT was moved to -20 Pa. A constant pressure in the first second of experiment represents the time elapsed between pressurizing the membrane and closing the valve between the working and the reference volumes. It can be noticed that right after closing the valve between the two volumes, the pressure decay rapidly increases for another couple of seconds. This rapid pressure increase is referred to as a compression effect due to

closing the valve between the two volumes (Al-Ismaily et al., 2012). However, eventually the expected linear behavior due to gas transport into a semi-infinite membrane is observed. The red section of the curve was used to determine the slope, which is directly proportional to $S\sqrt{D}$. It can also be noticed that as time increases, the pressure decay curve shows an upward deviation from the semi-infinite behaviour as expected.

Figure 3.4 provides a closer look at the experimental data presented in Figure 3.3, by forcing the intercept to be equal to zero. In principle, the membrane should behave as a semi-infinite medium right after initiation of the gas permeation experiment. Consequently, by forcing ΔP versus $\sqrt{t}$ through the origin should allow correcting the pressure decay data for the compression effect and a delay in recording ΔP. However, as seen in Figure 3.4, when extending the red linear section from Figure 3.3 for the entire time frame of the experiment, it is evident the actual linear behaviour is observed only after $\sqrt{t} > 3$. This initial deviation cannot be explained by the compression effect discussed by Al-Ismaily et al. (2012). Instead, the following explanation is proposed. When the valve separating the working and reference volume is being closed, the gas from the entire upstream section flows toward the membrane and, right after closing the valve, there is a pressure imbalance in the reference volume. More specifically, the pressure far away from the valve separating the two volumes is slightly greater than the pressure close to the valve, where the DTP is connected. Since the pressure in the reference volume must equilibrate, during the time in which this equilibration occurs the pressure at the point where the DPT is connected slightly increases, which causes artificially higher pressure decay that is evident in Figure 3.3. The fact that the pressure in the reference volume is not instantaneously constant following the closure of the valve between the working and the reference volumes precludes correcting the upstream pressure decay data with absolute certainty. Consequently, the currently used system is not suitable for the determination of the upstream time lag, which would provide yet another alternative for the complete membrane characterization.

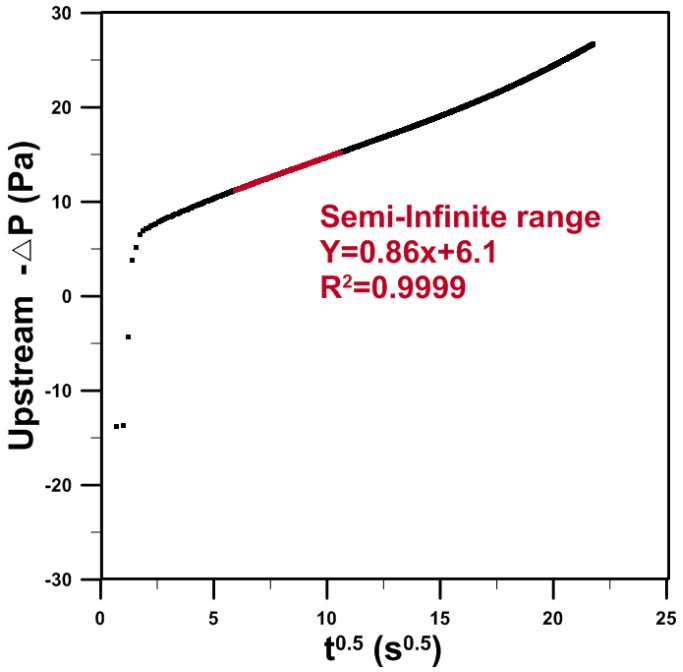

Figure 3.3: Experimental upstream pressure decay as a function of square root of time. Experiment was carried out T=298 K, Feed pressure p_0=17 kPa, membrane thickness L=23.5 µm, using nitrogen gas.

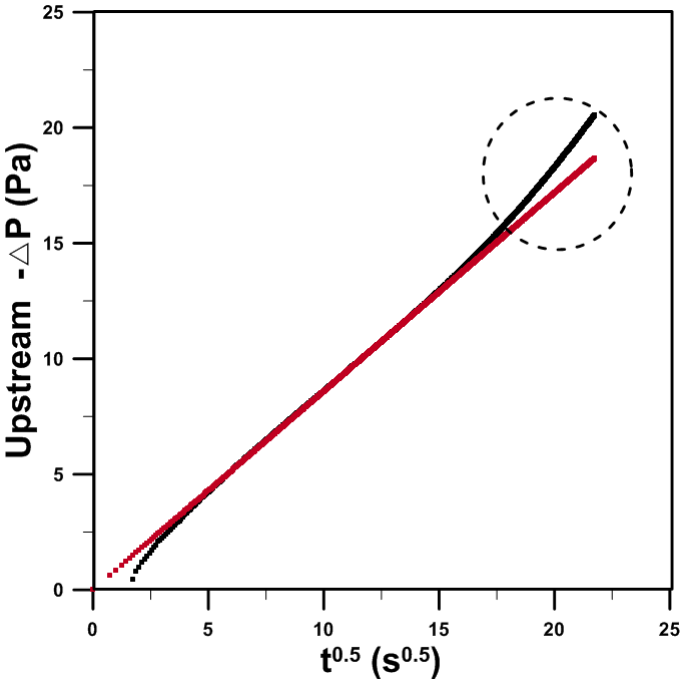

Figure 3.4: Correcting the experimental pressure decay data presented in Figure 3.2 by forcing the intercept of the linear region through the origin.

It is important to emphasize that the method proposed in this paper does not require correcting the upstream pressure decay data, as long as there is a sufficient time frame during which a linear behavior, as well as a deviation from the linear behavior, can be observed. In other words, the difference between the two curves, as a function of $\sqrt{t}$ is the same in both Figure 3.3 and Figure 3.4.

Using five randomly chosen points from the circled region in Figure 3.4, the diffusivity coefficient was determined from the experimental difference between the two curves and the slope of the red line by solving Eq. (3.8). Then, knowing *D* and the slope of the red line, solubility *S* was determined. Such determined values of *D* and *S* are plotted in Figs. 3.5a and 3.5b, respectively. It is important to emphasize that differences when using Eq. (3.8) and Eq. (3.9) were negligible, which suggest the disappearance of the exponential term and thus reaching the steady state permeation.

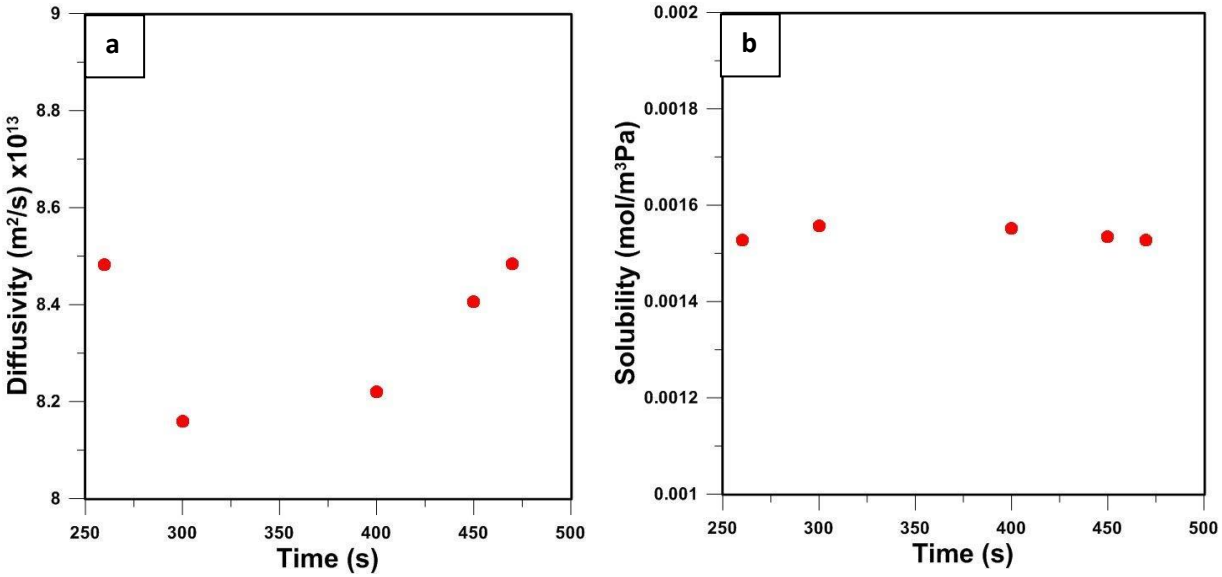

Figure 3.5: Diffusivity (a) and solubility (b) coefficients of N_2 in PPO determined from the experimental pressure decay and Eq. (3.9) at different times.

The average diffusivity and solubility coefficients based on the five data points shown in Figure 4 are 8.34×10^{-13} m^2/s and 1.540×10^{-3} mol / m^3 Pa. These values are considerably different from the diffusivity and solubility coefficients of 4.52×10^{-12} m^2/s, and 2.74×10^{-4} mol/m^3 that were reported by Al-Ismaily et al. (2012). Interestingly, the permeability coefficient of 1.28 x 10^{-15} mol/s m Pa, which is the product of *DS*, in the current investigation, is remarkably similar to

the permeability coefficient reported by Al-Ismail et al. of 1.24 x 10^{-15} mol/s m Pa (2012). The major source of error in the new method reported in this paper is the uncertainty in the actual feed pressure. Considering Eq. (3.9), if for a given difference between the curves p_o was smaller than the used value, the calculated D would increase while S would decrease. The problem with an uncertainty in the actual feed pressure can be rectified by modifying the current configuration of the upstream section of the system. The details of this modification and the corresponding results of membrane characterization will be reported in a future publication.

3.4 Conclusions

A mathematical basis for a new method for the characterization of gas transport in membrane has been presented. The method requires accurate monitoring of the upstream pressure decay due to gas transport into the membrane, which allows continuous evacuation of the downstream side of the membrane. The latter, allows obeying the boundary condition at the downstream face of the membrane, which is unique compared to a conventional time-lag method. In turn, the method relies on (1) monitoring the initial pressure decay that is characteristic to the transport into a semi-infinite membrane, (2) observing a clear deviation from the semi-infinite model at longer times, and (3) the analysis of the experimental pressure decay in the square root of time domain rather than linear time domain. At this point, the major challenge in the implementation of this method is an uncertainty in the actual feed pressure during a gas permeation test, which can be rectified by modification of the current experimental set up. Nevertheless, the experimentally determined permeability coefficient on N_2 in a PPO membrane using the new method was remarkably similar to the value obtained previously in our lab using different characterization methods.

3.5 Nomenclature

A	Cross sectional membrane area, m^2	p_o	Initial pressure, Pa
C	Gas concentration, mol/m^3.	P	Permeability, mol/m s Pa
D	Gas diffusivity in membrane, m^2/s	R	Universal gas constant, Pa m^3/ mol K
F_O	Fourier number, dimensionless	S	Solubility of membrane, mol/Pa m^3
L	Thickness of membrane, m	T	Temperature, K
p	Pressure, Pa	V_u	Upstream volume, m^3

3.6 References

- Al-Ismaily, M, Wijmans, J.G., Kruczek, B. “A shortcut method for faster determination of permeability coefficient from time lag experiments” Journal of Membrane Science, 234-424 (2012), 165-174.
- Barrer, R.M., “ Permeation, Diffusion and Solution of gases in organic polymers”, Transactions of Faraday Society, 35, (1939), 629-643
- Daynes, H.A., “The process of diffusion through a rubber membrane”, Proc. R. London, 97A (1920), 286.
- Jenkins, R.C.L., Nelson, P.M., and Spirer, L, “Calculations of the transient diffusion of gas through a solid membrane in to a finite outflow volume”, Transactions of the Faraday Society, 66 (1970), 1391-1401.
- Kruczek, B., Frisch, H.L., Chapanian, R., “Analytical solution for the effective time lag of a membrane in a permeate tube collector is which Knudsen flow regime exists”, Journal of membrane Science, 256, (2005) 57-63.
- Nguyen, X.Q., Broz, Z., Uchytil, P., “Methods for the determination of transport parameters of asses in membranes”, Journal of Chemical Society Faraday Trans., 88 (24), (1992), 3553-3560.
- Nguyen, X.Q., Broz, Z., Vasak, F., and Nguyen, Q.T, “Manometric techniques for determination of gas transport parameters. Application to the study of dense and asymmetric poly (Vinyltrimethylsilane) membranes”, Journal of Membrane Science, 91 (1994), 65-76.
- Rutherford, S.W, and Do, D.D., “Review of time lag permeation technique as a method for characterisation of porous media and membranes”, Adsorption, 283-312, 1997.
- Villaluenga, J.P.G, and Seoane, B., “Experimental estimation of Gas-Transport properties of linear low – density polyethylene membranes by an integral permeation method.” Journal of applied polymer Science, 82, (2001), 3013-3021.

Chapter 4

Simulation of Time-lag Permeation Experiments Using Finite Differences

Haoyu Wu, Neveen Al-Qasas, Boguslaw Kruczek, Jules Thibault

Department of Chemical and Biological Engineering, University of Ottawa
161 Louis Pasteur, Ottawa, Ontario, Canada K1N 6N5

Abstract

Membrane-based pressure driven processes are used in an increasing number of applications. To properly design membrane applications, it is necessary to have a good estimate of membrane properties. To characterize membrane permeation properties, the time-lag method is commonly used. A study has been undertaken to gain a deeper understanding on the accuracy of the time-lag method under realistic boundary conditions using numerical methods. Numerical simulations offer the opportunity to obtain a solution to the Fick's diffusion equation under various boundary conditions and for nonlinear sorption behaviour for which analytical solutions are difficult or impossible to obtain. This paper is mainly concerned with the selection of the optimal finite difference scheme for solving the Fick's diffusion equation that leads to the accurate determination of the membrane time lag. Pressure responses in the upstream and downstream reservoirs at both membrane interfaces are determined from the concentration gradients. The concentration gradient at the upstream side of the membrane is initially very steep and to accurately extract membrane properties, it is important to predict it very accurately. Simulation results for the prediction of concentration profiles and gradients at both interfaces are compared with known benchmark analytical equations to assess the precision of numerous numerical schemes where the effect of mesh size and time step is quantified. Results show that a variable mesh size is required to predict accurately the concentration gradient at the upstream interface. The choice of a variable mesh size scheme is important as a compromise must be struck between the smallest mesh size and the time step as it greatly impacts on the computation

time. Results also showed that both the implicit and explicit finite difference schemes gave very similar results.

Keywords: Membrane characterization, finite differences, time lag, upstream pressure decay, variable mesh scheme
Publication status: Journal of Fluid flow, Heat and Mass Transfer, 2 (2015), 14-25.

4.1 Introduction

Membrane-based pressure driven processes are used in an increasing number of applications, and are the subject of intensive research and development [1]. To characterize simple permeation processes as well as more complex processes involving diffusion with simultaneous adsorption, the time-lag method initially proposed by Daynes [2] and then modified by Barrer [3] is the method that is currently being used by most researchers. The determination of the time lag allows finding the membrane diffusion coefficient for a target solute. The downstream time lag is based on the downstream pressure increase, while the upstream time lag is based on the detection of the pressure decay in the upstream chamber. Our research group has undertaken an experimental research program to devise new and improved methods to rapidly and accurately determine membrane properties. To complement the experimental program, numerical simulations are also performed to gain a deeper understanding on the flow of molecules across the membrane. Numerical simulations offer the opportunity to obtain solutions for the Fick's diffusion equation under various boundary conditions at which analytical solutions are difficult or impossible to obtain, in addition to consider diffusion within membranes that is characterized with nonlinear sorption behaviours.

This paper is mainly concerned with the selection of the optimal finite difference scheme for solving the Fick's diffusion equation that leads to the accurate determination of the upstream and downstream membrane time lags. For the experimental determination of the time lag, the system usually consists of a thin membrane separated by two fixed-volume chambers, which are initially maintained under high vacuum (see Figures 4.1 and 4.2). The experiment starts when the upstream chamber is rapidly filled with a high pressure gas. The gas then progressively permeates through the membrane leading to a decrease in the pressure in the upstream chamber

and an increase in the pressure of the downstream chamber. Based on the plots of the upstream and downstream pressure differences as a function of time, it is possible to determine the upstream and downstream time lags, respectively. The time lags are obtained by evaluating the intercept of the linear portion of the pressure difference curves with the time axis as schematically shown in Figure 4.3. The time lag θ is directly proportional to the reciprocal of the membrane diffusion coefficient *D* [2] Eqs. (4.1) and (4.2) give, respectively, the relationships that exist between the upstream and downstream time lags with the membrane diffusion coefficient and thickness.

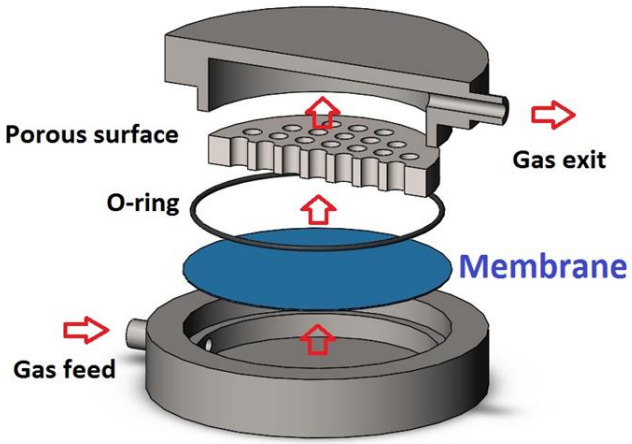

Figure 4.1: Schematic diagram of a typical membrane testing module.

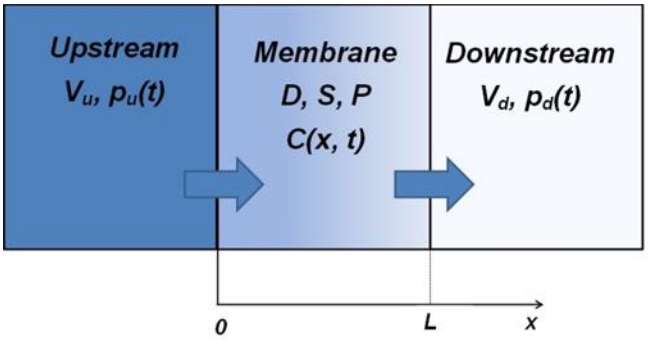

Figure 4.2: Schematic model of the membrane-based pressure driven processes in a constant volume (CV) system.

At time $t = 0^-$, the system is maintained under high vacuum and at $t = 0^+$ the system is suddenly exposed to high pressure gas that rapidly fills the upstream chamber. V_u and V_d are the

upstream and downstream volumes, $p_u(t)$ and $p_d(t)$ are the upstream and downstream pressure changes as a function of time, $C(x,t)$ is the concentration profile within the membrane as a function of permeation distance x and time t and D, S and P are the membrane properties: diffusion coefficient, solubility and permeability, respectively.

$$\theta_{up} = -\frac{L^2}{3D} \tag{4.1}$$

$$\theta_d = \frac{L^2}{6D} \tag{4.2}$$

where L is the membrane thickness, D is the diffusion coefficient, and θ_u and θ_d are the upstream and downstream time lags, respectively.

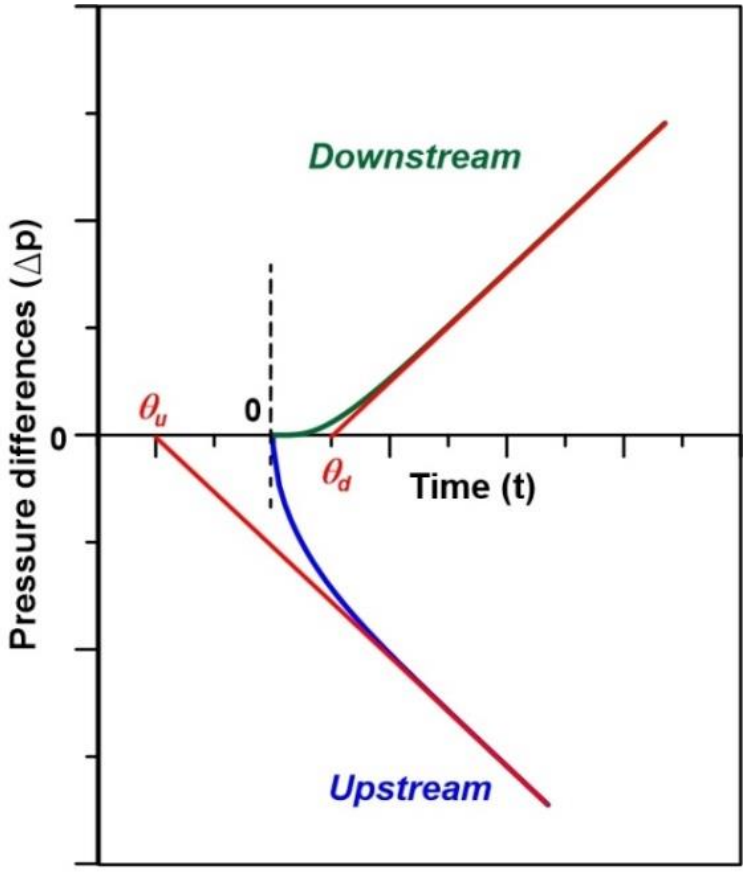

Figure 4.3: Schematic representation of the time lag determination from the upstream and downstream pressure difference curves.

The change in gas pressure in both chambers as a function of time is determined from the concentration gradients at their respective gas-membrane interfaces. Because the upstream interface of the membrane is subjected to a step change in the gas pressure, the concentration gradient at the upstream side of the membrane is initially very steep compared to the concentration gradient observed at the downstream side of the membrane. To accurately extract membrane properties from the upstream pressure difference curve, it is important to predict as accurately as possible the concentration gradient at that interface. A numerical model was developed to simulate the gas permeation process and predict the concentration profile as a function of time. The derivative of the concentration profile at the interfaces leads to the calculation of the interface gradients, which in turn allows calculating the pressure change in the upstream and downstream chambers of known volumes as a function of time. The time lag can then be obtained. In this investigation, the finite difference method (FDM) is used to discretize the one-dimensional Fick's second law of diffusion over the membrane into a number of finite thin slices and to solve numerically the partial differential equation to obtain the concentration profile of the gas permeating within the membrane.

In this paper, to support the experimental and numerical research program undertaken to determine the conditions under which the evaluation of the upstream and downstream time lags leads to better accuracy, numerical permeation experiments are performed to assess this precision. For quantifying this precision, simulation results for the prediction of concentration profiles, the concentration gradients at the two gas-membrane interfaces, the upstream and downstream pressure profiles and the time lag as a function of time were compared with benchmark analytical solutions. The paper is divided as follows. The benchmark analytical solutions for conventional boundary conditions are first presented, followed by a description of the various numerical schemes that have been investigated. Results of the various numerical studies are presented and discussed before concluding.

4.2 Analytical Solutions

A series of benchmark analytical solutions for the concentration profiles, the gradients at both interfaces, and the changes in pressures in the upstream and downstream volumes have been

used to compare the different numerical schemes. These analytical solutions are presented in this section.

For the simplest case, the gas permeation via diffusion through the membrane follows Fick's second law of diffusion which allows representing the concentration *C(x, t)* of the permeating species as a function of time (*t*) and position (*x*) via Eq. (4.3) where the diffusion coefficient (*D*) of the permeating gas within the membrane is assumed to be constant.

$$\frac{\partial C}{\partial t} = D\frac{\partial^2 C}{\partial x^2} \tag{4.3}$$

For deriving one of the benchmark solutions, the two chambers separating the membranes are initially under high vacuum such that the initial concentration throughout the membrane is equal to zero. The experiment starts when the upstream chamber is rapidly filled with the permeating species to reach a relatively high pressure, which is maintained constant during the experiment. The permeating gas molecules start diffusing through the membrane and eventually emerge into the downstream chamber. The amount of the gas that accumulates in the downstream chamber is considered to be negligible so that the concentration of the gas at the permeate interface of the membrane is assumed to be zero during the experiment. Based on these assumptions, the initial condition (IC) and the two boundary conditions (BC1 and BC2) used to derive the analytical solution are given in Eq. (4.4).

$$\text{IC: } C\left(x,0\right) = 0 \tag{4.4a}$$

$$\text{BC1: } C\left(0,t\right) = p_0 \cdot S \tag{4.4b}$$

$$\text{BC2: } C\left(L,t\right) = 0 \tag{4.4c}$$

where *C* is the concentration of the permeating gas, p_0 is the constant pressure in the upstream chamber, S is the solubility of the membrane and *L* is the thickness of the membrane. The two boundary conditions are ideal boundary conditions for which it is possible to derive an analytical solution. The solution of Eq. (4.3) subjected to the initial and ideal boundary conditions of Eq. (4.4) can be obtained using the method of separation of variables and is given in Eq. (4.5) [4]. This equation gives the concentration profile as a function of time t and permeation distance x.

$$C(x,t) = p_0 S\left(1-\frac{x}{L}\right) - \frac{2p_0 S}{\pi} \times \sum_{n=1}^{\infty} \frac{1}{n} \sin\left(\frac{n\pi x}{L}\right) \exp\left(-\frac{Dn^2\pi^2 t}{L^2}\right) \tag{4.5}$$

The concentration profiles inside the membrane at five different times following a step change in the upstream pressure are presented in Figure 4.4.

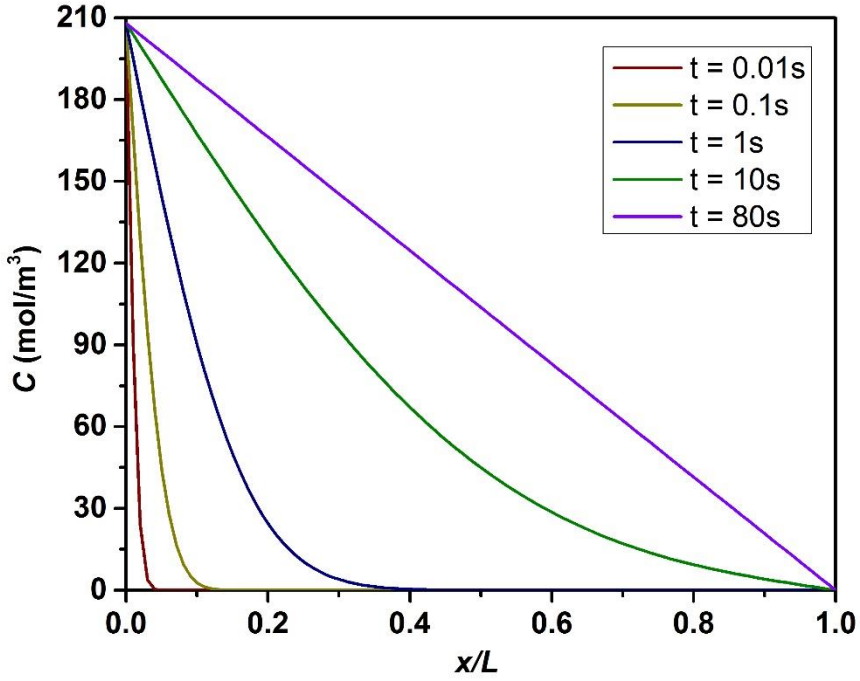

Figure 4.4: Concentration profiles inside the membrane for five different times following a step change in the upstream pressure. These concentration profiles were obtained using Eq. (4.5).

Figure 4.4 shows a very steep variation in the concentration profile at the upstream boundary condition at very small times. On the other hand, a smooth variation in concentration at the downstream boundary condition is observed. As the steady state is progressively established, the concentration profile will assume a straight-line relationship as observed for the concentration profile at 80 s.

To determine the concentration gradients at both interfaces, the Fick's first law can be used where, as expressed by Eq. (4.6), the flux J is the negative of the product of the diffusivity and the gradient.

$$J = -D\frac{\partial C}{\partial x} \tag{4.6}$$

The benchmark analytical solutions for the gas fluxes at the upstream side (x = 0) and downstream side ($x = L$) of the membrane are evaluated using Eqs. (4.7) and (4.8), respectively:

$$J_u = J(0,t) = \frac{Dp_0S}{L} + \frac{2Dp_0S}{L} \times \sum_{n=1}^{\infty} \exp\left(\frac{-n^2\pi^2Dt}{L^2}\right) \tag{4.7}$$

$$J_d = J(L,t) = \frac{Dp_0S}{L} + \frac{2Dp_0S}{L} \times \sum_{n=1}^{\infty} \cos(n\pi) \exp\left(\frac{-n^2\pi^2Dt}{L^2}\right) \tag{4.8}$$

To develop the analytical solutions for the concentration profile (Eq. (4.5)) and the mass fluxes at the interfaces (Eqs. (4.7) and (4.8)), it was necessary to use the boundary conditions given in Eq. (4.4). To determine the time lag, a pressure difference needs to be recorded in the upstream and/or downstream chambers such that the two boundary conditions of Eq. (4.4) are not perfectly satisfied. However, the pressure changes in both chambers are relative small such that the deviations from the theoretical boundary conditions are relatively small and do not have a major impact on the determination of the time lag. As a result, the mass flux at the two interfaces are calculated with the prevalence of the two boundary conditions of Eq. (4.4) even if the two gradients at the interfaces would be in reality slightly different than the ones calculated with the assumptions of Eq. (4.4).

The pressures in the upstream and downstream chambers can be calculated by performing a simple mass balance in each chamber while integrating Eqs. (4.7) and (4.8) with time. The following expressions were derived for the upstream and downstream pressures as a function of time:

$$p(0,t) - p_0 = \frac{ART}{V_u} \int_0^t J(0,t)\,dt \tag{4.9}$$

$$\begin{aligned} \Delta p_u &= p(0,t) - p_0 \\ &= -\frac{p_0 ARTDS}{V_u L}\left[t + \frac{L^2}{3D} - \frac{2L^2}{\pi^2 D} \times \sum_{n=1}^{\infty} \frac{-1}{n^2} \exp\left(-\frac{Dn^2\pi^2 t}{L^2}\right)\right] \end{aligned} \tag{4.10}$$

$$p(L,t) - 0 = -\frac{ART}{V_d} \int_0^t J(L,t)\,dt \tag{4.11}$$

$$\begin{aligned}\Delta p_d &= p(L,t) - 0 \\ &= \frac{p_0 ARTDS}{V_d L}\left[t - \frac{L^2}{6D} + \frac{2L^2}{\pi^2 D} \times \sum_{n=1}^{\infty} \frac{(-1)^{n+1}}{n^2} \exp\left(-\frac{Dn^2\pi^2 t}{L^2} \right) \right]\end{aligned} \tag{4.12}$$

where $p(0, t)$ and $p(L, t)$ are the respective pressure at the upstream and downstream interfaces, p_u and p_d are the pressure decrease at the upstream interface and pressure increase at the downstream interface, A is the cross sectional area of the membrane and R is the gas constant.

At long permeation time ($t \cdot D/L^2 > 1$), the transient terms in Eqs. (4.10) and (4.12) become negligible and these equations reduce to the following two linear equations:

$$\lim_{t\to\infty} \Delta p_u = -\frac{p_0 ARTDS}{V_u L}\left(t + \frac{L^2}{3D} \right) \tag{4.13}$$

$$\lim_{t\to\infty} \Delta p_d = \frac{p_0 ARTDS}{V_d L}\left(t - \frac{L^2}{6D} \right) \tag{4.14}$$

The intercept of the linear portion of the pressure difference curves with the time axis (see Figure 4.3), obtained after a long permeation time, gives the upstream and downstream time lags. The time lags, evaluated from the pressure changes on both sides of the membrane, are directly proportional to the reciprocal of the membrane diffusion coefficient, as shown in Eqs. (4.1) and (2).

4.3 Numerical Solutions

4.3.1 Finite difference numerical model.

The benchmark analytical solutions derived in the previous section under ideal boundary conditions can be used to evaluate the accuracy of the numerical solutions. The evaluation was performed for the following variables: concentration profiles, gradients at the interfaces, changes in the upstream and downstream pressures, and time lag. Eq. (4.3), subject to the initial and boundary conditions of Eq. (4.4), was solved numerically using finite differences [5]. The continuous domain of the membrane was discretized into a number of grid points and the Fick's second law of diffusion was approximated by finite differences for each of these grid points. For each point of the grid, it is therefore possible to write an algebraic equation to approximate the differential equation using Taylor's series expansion with respect to a change in time, Δt. For all grid points in the solution domain, Eq. (4.3) can be approximated as follows.

$$\frac{\partial C}{\partial t} = D\frac{\partial^2 C}{\partial x^2} \rightarrow \frac{C_x^{t+\Delta t} - C_x^t}{\Delta t} = D\frac{\partial}{\partial x}\left(\frac{\partial C}{\partial x}\right) = D\frac{\left(\frac{\partial C}{\partial x}\right)_{x+\frac{\Delta x_2}{2}} - \left(\frac{\partial C}{\partial x}\right)_{x-\frac{\Delta x_1}{2}}}{\frac{\Delta x_1}{2} + \frac{\Delta x_2}{2}} \tag{4.15}$$

where Δx_1 and Δx_2 are the grid sizes upstream and downstream of the grid point located at x, respectively. For a uniform grid size, Δx_1 would be equal to Δx_2. The concentration profile can be obtained numerically via Eqs. (4.16) and (4.17) respectively, using an explicit or implicit numerical scheme. For the explicit scheme, the concentration can be calculated directly at time $t+\Delta t$ at every grid point whereas for the implicit scheme the concentration profile at time $t+\Delta t$ is obtained by solving a tridiagonal matrix [5]. For the explicit scheme, the Courant number [6] or dimensionless time increment $(D\Delta t / \Delta x_s^2)$ must be smaller than or equal to 0.5 to ensure numerical stability. Δx_s is smallest mesh size (in this investigation it corresponds to the first mesh size) for both the variable and uniform mesh schemes. The implicit scheme is unconditionally stable but in this investigation we have used the same criterion to select the integration time step. In addition, the Crank-Nicolson algorithm [5], which is a combination of explicit and implicit algorithms, was also implemented.

$$C_x^{t+\Delta t} = C_x^t + 2D\Delta t\left(\frac{C_{x+\Delta x_2}^t - C_x^t}{\Delta x_2\left(\Delta x_1 + \Delta x_2\right)} - \frac{C_x^t - C_{x-\Delta x_1}^t}{\Delta x_1\left(\Delta x_1 + \Delta x_2\right)}\right) \tag{4.16}$$

$$\left(-\frac{2D\Delta t}{\Delta x_1\left(\Delta x_1 + \Delta x_2\right)}\right)C_{x-\Delta x_1}^{t+\Delta t} + \left[1 + \frac{2D\Delta t}{\Delta x_1 \Delta x_2}\right]C_x^{t+\Delta t} + \left(-\frac{2D\Delta t}{\Delta x_2\left(\Delta x_1 + \Delta x_2\right)}\right)C_{x+\Delta x_2}^{t+\Delta t} = C_x^t \tag{4.17}$$

Eqs. (4.16) and (4.17) are valid for all interior grid points. To satisfy the two boundary conditions, Eqs. (4.18) (a) and (b) are used for the first and last grid points, respectively.

$$(x = 0) \qquad C_0^t = p_0 S \tag{4.18a}$$

$$(x = L) \qquad C_L^t = 0 \tag{4.18b}$$

The concentration gradients at both surfaces of the membranes are calculated from the concentration profile using Eqs. (4.19) and (4.20).

$$G_u = \frac{C(\Delta x_1, t) - C(0,t)}{\Delta x_1} \tag{4.19}$$

$$G_d = \frac{C(L,t) - C(L - \Delta x_{N-1}, t)}{\Delta x_{N-1}} \tag{4.20}$$

where N is the number of grid points in the solution domain. The pressure differences are calculated from the gradient on both sides of the membrane via Eqs. (4.21) and (4.22) where T is the absolute temperature, G_u and G_d are the upstream and downstream concentration gradients, V_u and V_d are the upstream and downstream volumes of the chambers and n is the number of time increments Δt for which the simulation was run.

$$\Delta p_u = \sum_{i=1}^{n} \frac{DART\Delta t}{V_u} G_{ui} \tag{4.21}$$

$$\Delta p_d = \sum_{i=1}^{n} \frac{DART\Delta t}{V_d} G_{di} \tag{4.22}$$

4.3.2 Numerical schemes for variable mesh sizes

Since the gradient at upstream interface of the membrane is very steep, especially at a short permeation time, it is desired to resort to a relatively small mesh size at this interface to predict very accurately the concentration gradient. In this investigation, both uniform and variable mesh sizes were used. For the scheme with variable mesh size, a number of uniform grid sizes at the two membrane boundaries were transformed into a number of progressively increasing mesh sizes starting with a very small mesh size at the surface. Figure 4.5 shows one of the variable mesh schemes that were used in this study where 3 uniform mesh sizes were converted into 10 variable mesh sizes.

To obtain an exponentially increasing mesh size, a multiplication factor was defined for each variable mesh scheme such that the smallest mesh point at the boundary is progressively increased until the uniform central mesh size is obtained. The uniform mesh size is then used for all the other interior points. For the variable mesh scheme illustrated in Figure 4.5, the factor to convert the 3 uniform mesh sizes into 10 variables mesh is 1.311129915. The size of the first

mesh is calculated using Eq. (4.23) where the uniform mesh size (=$L/(N_0$ - 1)) is divided by the factor to the 10th power. N_0 is the number of grid points used with a uniform mesh size.

$$\Delta x_1 = \frac{L}{(N_0 - 1) \times Factor^{10}} \tag{4.23}$$

The sizes of the subsequent variable meshes are calculated using Eqs. (4.24) and (4.25) for the upstream and downstream boundaries, respectively.

$$\Delta x_i = \Delta x_{i-1} \times Factor \qquad (2 \le i \le 10) \tag{4.24}$$

$$\Delta x_i = \frac{\Delta x_{i-1}}{Factor} \quad (i \ge (N_0 - 1) + 2(N_2 - N_1) - 10) \tag{4.25}$$

Three different factors were tested in this investigation and their values are given in Table 1. In Eqs. (4.23) and (4.25), N_0 represents the original number of mesh points in a uniform grid. N_1 represents the number of uniform mesh sizes that were converted into N_2 variable mesh sizes. The number of grid points will therefore increase from N_0 to N_0+2(N_2 - N_1) when a variable grid scheme is used. For both mesh schemes, the total number of mesh points will be denoted N.

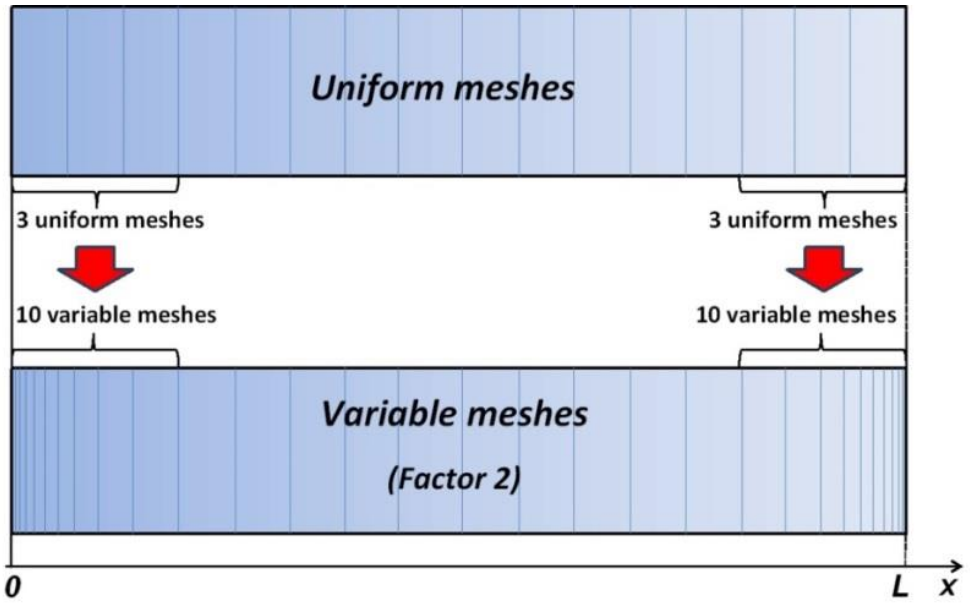

Figure 4.5: Schematic illustration of the transformation of a uniform mesh into a variable mesh with Factor 2.

It is important to reiterate that in practice, the upstream and downstream pressure changes cannot be observed under ideal boundary conditions (Eq. (4.4)) and analytical solutions are only available under these ideal conditions. However, in this investigation, these ideal boundary conditions were used to estimate the pressure changes that would occur in the upstream and downstream chambers. Since the changes in pressures for real boundary conditions are usually very small, errors associated with these ideal boundary conditions are also very small. The concentration profiles, concentration gradients, pressure differences and time lags calculated numerically were compared with the analytical benchmark solutions and average percentage errors were calculated to determine the accuracy of various numerical schemes. The numerical scheme was then used to gain a deeper understanding of the time lag method.

Table 4.1: Factors used in variable mesh schemes. N_1 is the number of uniform mesh sizes converted into N_2 variable mesh sizes.

Factor	**Factor 1**	**Factor 2**	**Factor 3**
Factor	1.490777275	1.311129915	1.150984101
$\mathbf{N_1}$	2	3	5
$\mathbf{N_2}$	10	10	10

4.4 Results and Discussion

In this investigation, analytical calculations and numerical simulations were performed under typical laboratory operating conditions that were used in actual experimental membrane tests. The typical experimental parameters are listed in Table 4.2.

Table 4.2: Simulation conditions and membrane system parameters.

Parameter		Value	Units
Operating conditions	Temperature T	273.15	K
	Operating pressure p_0	689 (100)	kPa (psi)
Membrane properties	Membrane solubility S	2.74×10^{-4}	mol/(m^3 Pa)
	Membrane diffusivity D	4.52×10^{-12}	m^2/s
	Membrane thickness L	$23.5x10^{-6}$	m
	Membrane area A	0.00125	m^2
Membrane system parameters	Upstream volume V_u	9.68×10^{-5}	m^3
	Downstream Volume V_d	9.68×10^{-5}	m^3

4.4.1 Concentration profiles

Figure 4.6 presents the dimensionless average percentage error for the prediction of the concentration profiles as a function of the number of mesh points. In Figure 4.6 results are presented for both uniform and variable (Factor 2) schemes using both explicit and implicit finite difference methods. The dimensionless concentration percentage average error ε(C), calculated using Eq. (4.26), corresponds to the average error for the prediction of the concentration profiles for all mesh points (N) and m different times. In the present investigation, m was equal to 8 which corresponds to the times the numerical and analytical solutions were compared which, in this investigation, the comparison was performed each 10 s up to 80 s. Superscript A in Eq. (4.26) designates the evaluation with the analytical solution (Eq. (4.5)).

$$\varepsilon(C)=\frac{\sum_{i=1}^{N}\sum_{j=1}^{m}\left|C_{ij}-C_{ij}^{A}\right|^2}{N\times m}\times\frac{100\%}{S\cdot p_0} \tag{4.26}$$

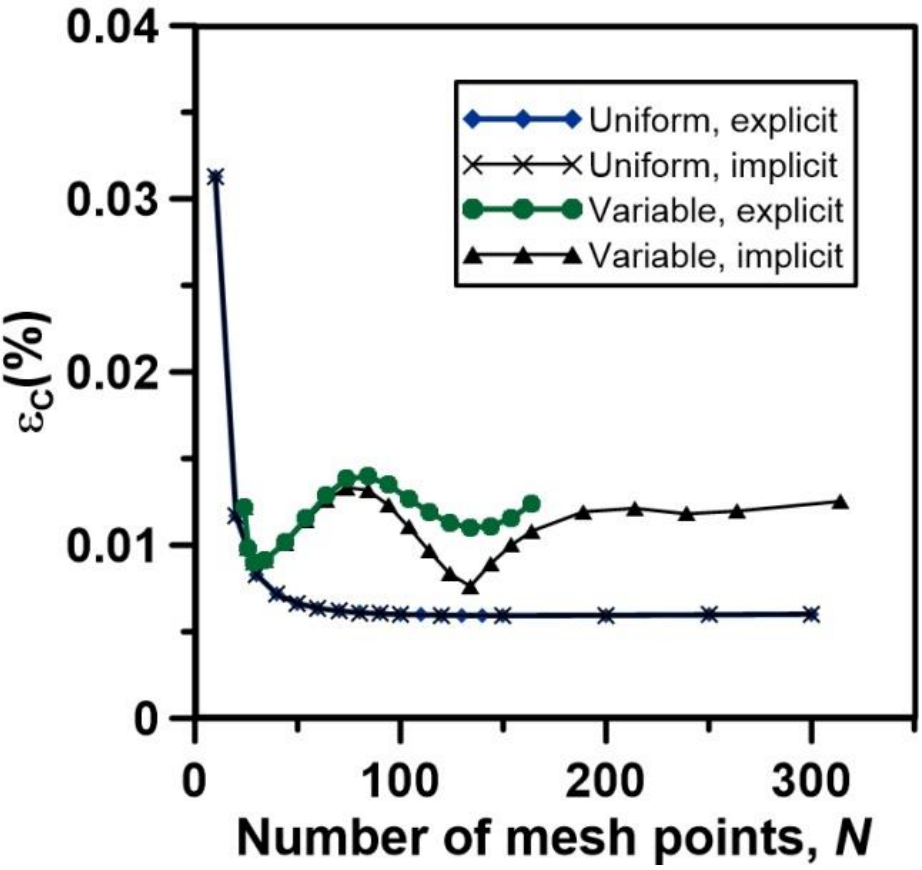

Figure 4.6: Dimensionless percentage average error ε(*C*) of the concentration profiles versus the number of mesh points (*N*). An integration time step of 0.00001 s was used for both explicit and implicit methods and for uniform and variable mesh (Factor 2) schemes.

Results of Figure 4.6 clearly show that the concentration profiles are obtained very accurately with an average percentage error of less than 0.015% when the number of mesh points is larger than about 25. For the prediction of the concentration profiles, both the explicit and implicit finite difference schemes lead to very small errors with slightly better predictions obtained with the implicit scheme. Similar results were obtained with the Crank-Nicolson algorithm where the error was always between the explicit and implicit methods. Since no benefits using the Crank-Nicolson algorithm were observed, only the explicit and implicit methods were considered in this investigation. In addition, results were identical for the uniform and variable mesh size. It can be safely stated that the numerical scheme used in this

investigation led to very accurate concentration profile predictions and that it can be used with confidence for other problems for which analytical solutions do not exist or were not yet derived.

4.4.2 Concentration gradients

Figures 4.7 and 4.8 present the plots of the upstream and downstream gradient percentage errors evaluated at three different times: 2, 4 and 10 s. The gradients were computed numerically (Eqs. (4.19) and (4.20)) and compared with the analytical gradients in order to determine the error in its prediction as defined by Eqs. (4.27) and (4.28)

$$\varepsilon\left(G_u\right)=\frac{G_u^A-G_u}{G_u^A}\times 100\% \tag{4.27}$$

$$\varepsilon\left(G_d\right)=\frac{G_d^A-G_d}{G_\infty^A}\times 100\% \tag{4.28}$$

where G_u and G_d are the upstream and downstream gradients, respectively. Superscript A designates the analytical solution. Since the downstream gradient is initially zero, the steady-state analytical gradient G_∞^A was used in Eq. (4.28) to avoid dividing by zero or by an extremely small number.

Results for the upstream gradient (Figure 4.7) obtained with a uniform mesh size show a progressively decreasing percentage error starting with 10 grid points with relatively high percentage error values of 4.915%, 2.395% and 0.953% at 2, 4 and 10 s, respectively. As the number of grid points increases, the percentage error becomes very small and reaches a value below 0.013% when the number of mesh points is 300. The percentage error in the case of the variable mesh size starts with relatively small negative values of -0.437%, -0.402% and -0.067% evaluated at 2, 4 and 10 s, respectively. The percentage errors then decrease to cross the zero-error line and to assume small positive percentage errors before progressively decreasing to very small percentage errors as the number of mesh points is increased. For a number of mesh points greater than 100, both uniform and variable mesh schemes lead to very small percentage errors. The insert in Figure 4.7 shows that the percentage errors are slightly smaller for a uniform mesh size when a higher number of mesh points is used and times larger than 2 s.

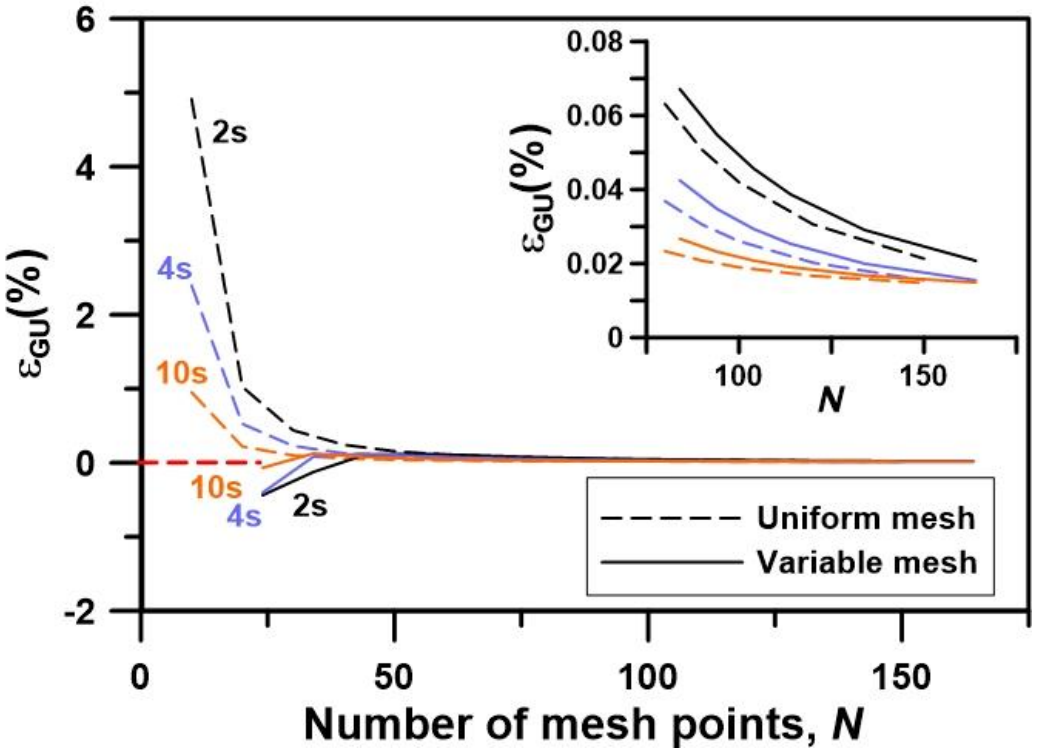

Figure 4.7: Upstream gradient percentage error $\varepsilon(G_u)$ versus the number of mesh points (N) with an integration time step of 0.00001s and at 2, 4 and 10 s for uniform and variable mesh schemes.

Results for the downstream gradient (Figure 4.8) obtained with a uniform and a variable mesh size show a progressively decreasing percentage error as the number of mesh points is increased. For the downstream gradient, the percentage error for the variable mesh size is slightly higher than for the uniform mesh size. The use of a variable mesh size for the downstream side of the membrane is therefore not required. The percentage prediction error for the downstream gradient is extremely low for small simulation times because the permeating gas has not yet emerged from the membrane. At higher times, the downstream gradient becomes more pronounced and approaches the steady-state analytical gradient (G_{∞}^{A}). For all simulation times, the percentage errors were always below 0.02% for a number of mesh points of 150 or more.

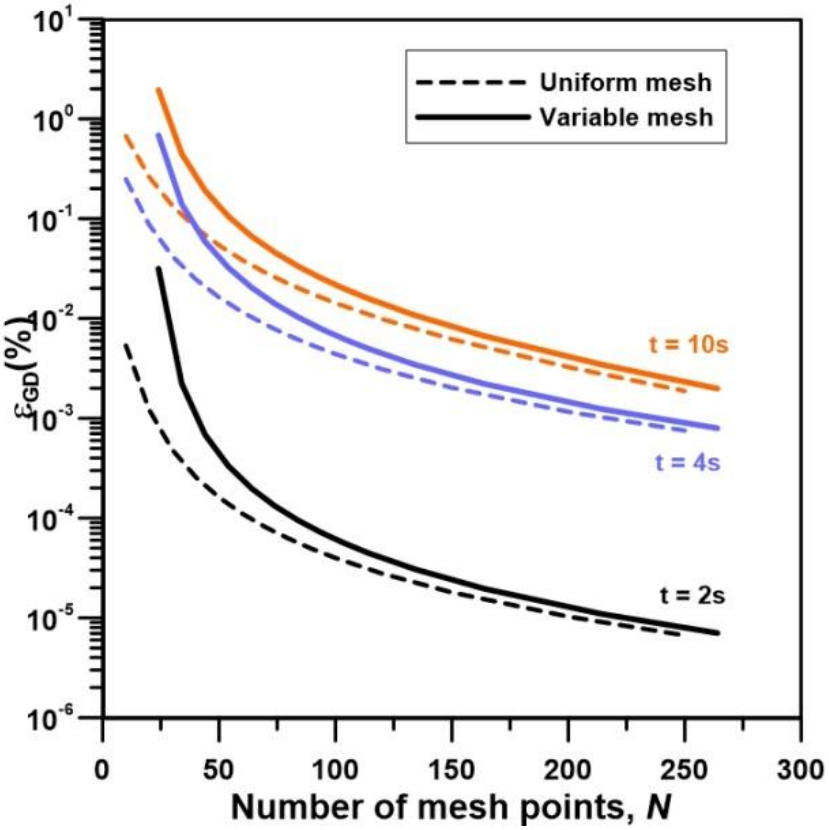

Figure 4.8: Downstream gradient percentage error ($\varepsilon(G_d)$) versus the number of mesh points (N) with an integration time step of 0.00001 s and at 2, 4 and 10 s for uniform and variable mesh schemes.

4.4.3 Pressure changes

With the instantaneous values of the gradients being calculated at the membrane boundaries, it is possible to determine the pressure changes in the upstream and downstream chambers using Eqs. (4.21) and (4.22). Figure 4.9 presents the plots of the upstream pressure decay percentage error at 10 and 80 s. The pressure decay is computed with the results of the implicit finite difference method and the pressure decay relative percentage error equation is calculated by comparing the analytical and numerical values using Eq. (4.29).

$$\varepsilon\left(\Delta p\right) = \frac{\Delta p^{A} - \Delta p}{\Delta p^{A}} \times 100\% \tag{4.29}$$

Results show that the upstream pressure decay percentage error for both uniform and variable meshes decreases steadily with an increase in the number of mesh points. For a given number of mesh points, the percentage error is smaller by an order of magnitude when a variable mesh size

is used. Since the change in pressure is the integration of the permeating gas flux at the interface, any error in the determination of the gradient will progressively accumulate as a function of time. The insert of Figure 4.7 shows that for a sufficiently large number of mesh points, smaller positive percentage prediction errors were observed for a uniform mesh point for simulation time greater than 2 s. To better explain the significant difference observed between the uniform and variable mesh sizes of Figure 4.9, it is important to examine the percentage errors of the upstream gradient at very short permeation time where the upstream gradient is the steepest (Figure 4.4) Figure 4.10 presents the variation of the percentage error of the upstream gradient for short permeation times. It is clear from this graph that the gradient percentage error for the variable mesh size is much smaller at short permeation time and decreases by two orders of magnitude in the first 0.5 s. The difference observed in Figure 4.9 between the uniform and variable mesh sizes is mainly due to the integration performed at early time and this difference persists for larger time. This is certainly for the upstream pressure change that the use of variable mesh points takes all its importance.

The percentage error for the downstream pressure change as a function of the number of mesh points is presented in Figure 4.11. In general, regardless of the number of mesh points and the permeation time, the percentage error for the downstream pressure change is similar for the uniform and variable mesh schemes. For a number of mesh points greater than 120 and a shorter permeation time (10 s), the pressure change is over-predicted by approximately 0.09% and the error decreases with an increase in the number of mesh points. On the other hand, at a longer permeation time (80 s) and N = 120, the pressure change is under-predicted by roughly 0.01%. For both upstream and downstream pressure differences, the errors are relative percentage errors.

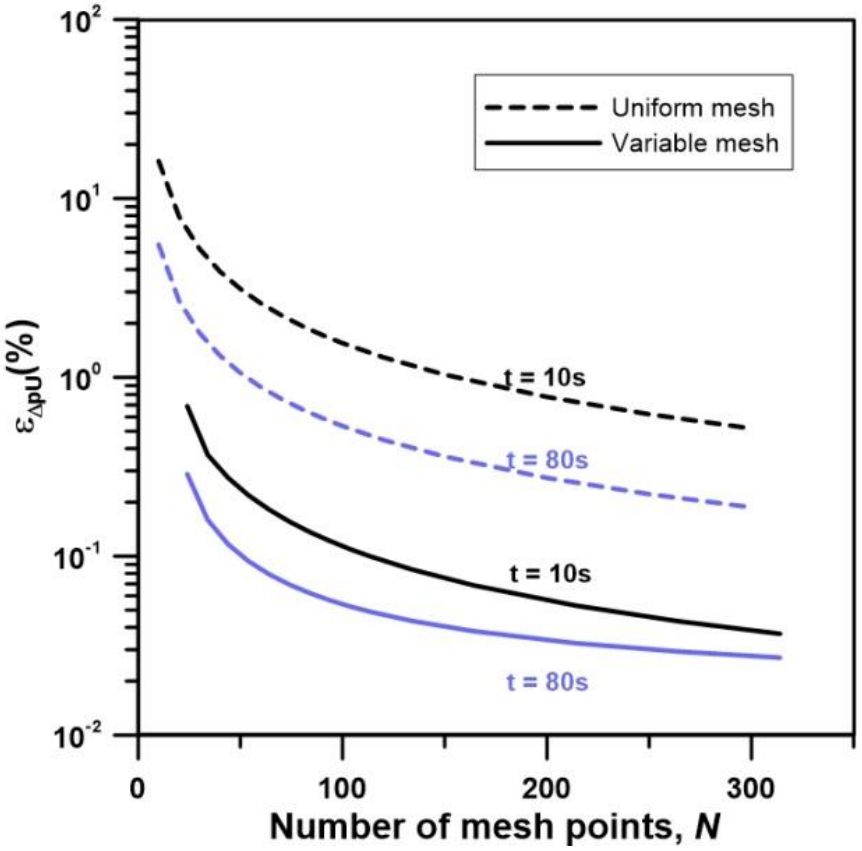

Figure 4.9: Upstream pressure decay percentage error ($\varepsilon(\Delta P_u)$)versus the number of mesh points (N) with an integration time step of 0.00001 s and at 10 s and 80 s for uniform and variable mesh schemes.

However, if the absolute errors were considered instead of the relative errors, results would show that the error accumulates with time. For instance, for a variable scheme with 150 mesh points, the absolute error at 10 s is 0.525 Pa while the error at 80 s is 0.548 Pa whereas for a uniform scheme with 164 mesh points, the absolute error at 10 s is 0.035Pa while the error at 80 s is 0.058 Pa. These results clearly show the importance of using a variable mesh scheme to capture adequately the concentration gradient at the upstream interface and that the absolute error strongly depends on the prediction error occurring at very short time where the concentration gradient is very steep.

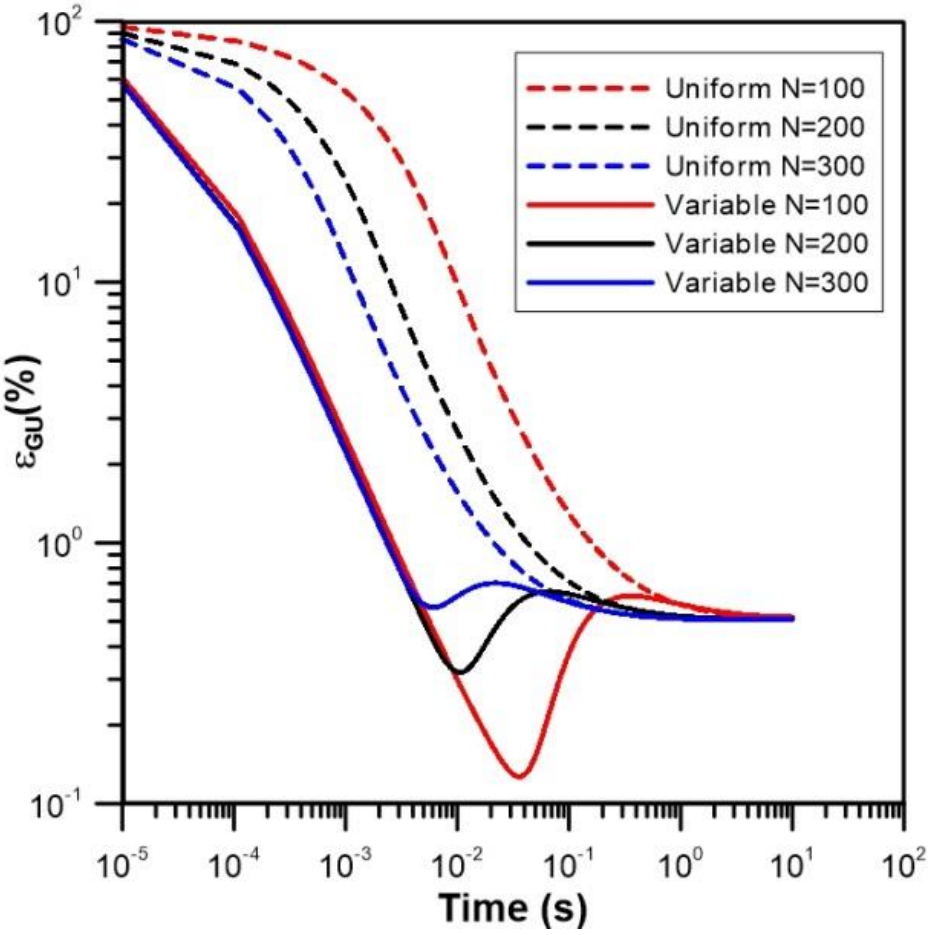

Figure 4.10: Upstream gradient percentage error $\varepsilon(\Delta G_u)$ versus time (s) at the first 10 seconds with an integration time step of 0.000001 s and the number of mesh points (N) of 100, 200 and 300 for uniform and variable mesh schemes.

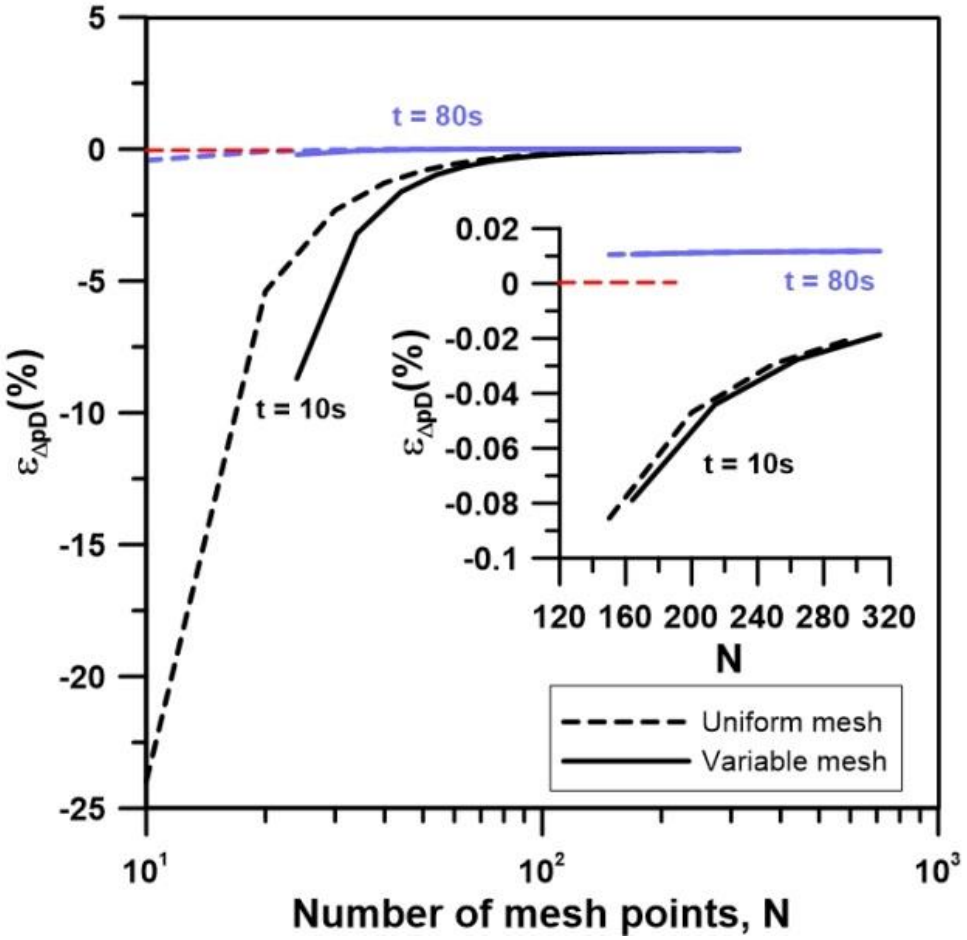

Figure 4.11: Modified downstream pressure increase percentage error $\varepsilon(\Delta P_d)$ versus the number of mesh points (N) with an integration time step of 0.00001 s and at 10 and 80 s for uniform and variable mesh schemes.

4.4.4 Time lags

Figures 4.12 and 4.13 show the plots of the upstream and downstream time lag percentage errors as a function of the number of mesh points, respectively. The evaluation of the time lag, that is the extrapolation of the linear portion of the pressure curve as a function of time, was performed at a permeation time of 190 s. The time lag is computed with the implicit finite difference method and the percentage time lag prediction error is calculated via Eq. (4.30).

$$\varepsilon(\theta) = \frac{\theta^A - \theta}{\theta^A} \times 100\% \tag{4.30}$$

Figure 4.12 shows that the percentage error of the upstream time lag is strongly influenced by the mesh scheme used to solve the problem. For a greater accuracy in the determination of the time lag, it is important to use a variable mesh scheme to capture the steep gradient at early permeation times (refer to Figure 4.4) because the determination of the time lag relies strongly on total upstream pressure change which results from the integration of the permeation flux at the upstream interface. Variable mesh schemes V1, V2 and V3 correspond to variable mesh scheme using Factors 1, 2 and 3, respectively. It appears that the variable mesh size with Factors 1 or 2 lead to very good results. Simulations presented in Figure 4.10 with Factor 2 for very short permeation times were also performed for Factors 1 and 3. Results (not shown) were nearly identical for Factors 1 and 2 but significantly better that those for Factor 3 and uniform mesh. Since the smallest mesh size for Factor 1 is significantly smaller than for Factor 2, the time step needs also to be smaller which leads to higher computation time. Factor 2 was therefore used for most results presented in this investigation.

For the downstream time lag, results of Figure 4.13 show that the percentage time lag prediction error is a function of the number of mesh points, but unlike the upstream time lag, the uniform mesh size is slightly better than the variable mesh size, but the difference is rather insignificant. The reason for the insignificant difference is the smooth concentration profile for the downstream interface (Figure 4.4). The accuracy of the time lag stabilizes to a percentage error of less than 0.015% for a number of mesh points greater than 150.

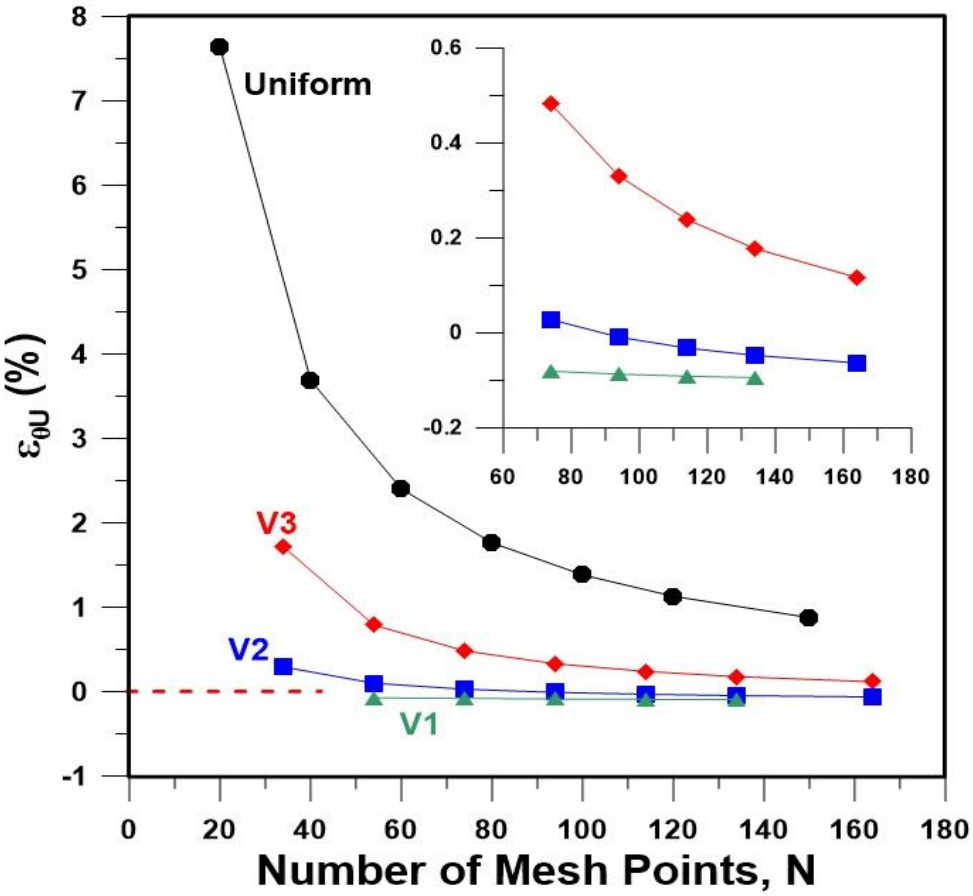

Figure 4.12: Upstream time lag prediction error ($\varepsilon(\theta_u)$) versus the number of mesh points (N) with an integration time step of 0.00001 s for uniform and variable mesh (with different factors) schemes. Time lag was evaluated at 190 s.

4.4.5 Computation time

Figure 4.14 presents the magnitude of dimensionless percentage average error $\varepsilon(C)$ for the concentration profile within the membrane as a function of the integration time step to study the accuracy of the numerical method with respect to the time step. Results clearly show that for the range of time steps that was investigated, the percentage error is very small in all cases. However, for a greater accuracy, a time step of 0.00005 s could be chosen as an optimal value and a compromise between accuracy and computation. Indeed, using a smaller time step would only lead to greater computation time and not to a greater accuracy.

Figure 4.15 presents an analysis to determine the computation time as a function of the number of mesh points. The computation time increases linearly with the number of mesh points.

Comparing the two numerical methods, the implicit method with the same time step required a larger computation time than the explicit method because it is required to solve at each time step the resulting tridiagonal matrix. Since the explicit finite difference led most of the time to a similar accuracy and it requires much less computation time, it is recommended to use explicit finite differences to solve the type of problems encountered in this investigation.

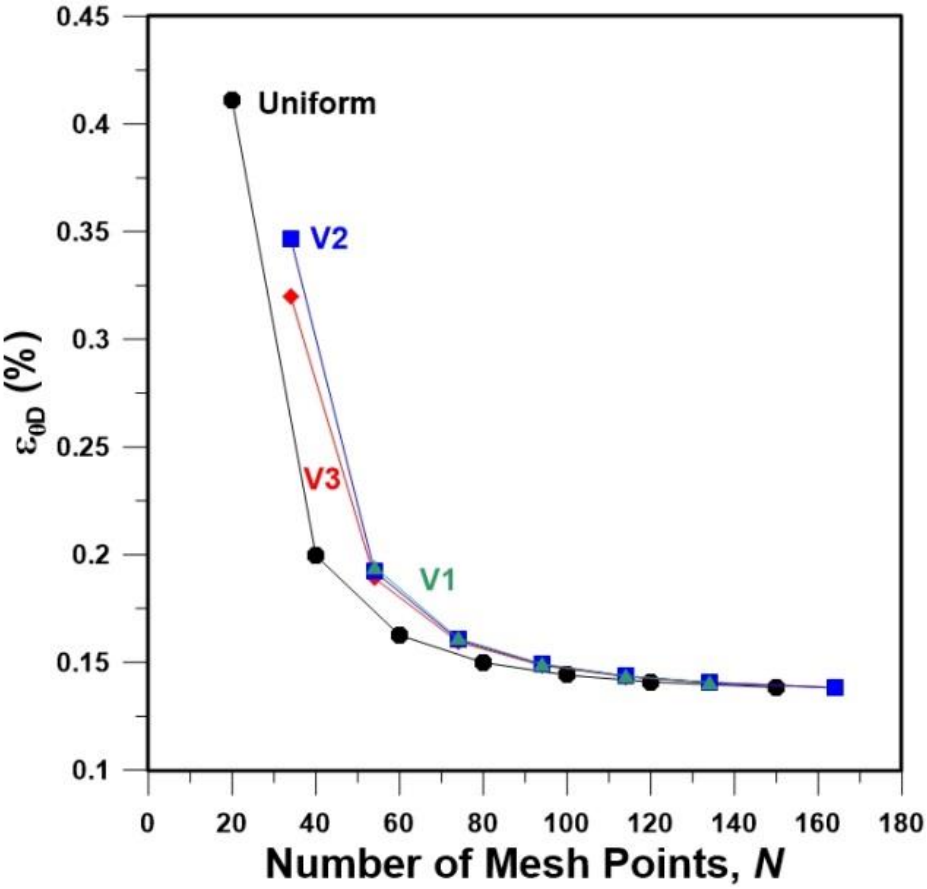

Figure 4.13: Downstream time lag error $\varepsilon(\theta_d)$ versus the number of mesh points (N) with an integration time step of 0.00001 s for uniform and variable mesh (with different factors) schemes. Time lag was evaluated at 190 s.

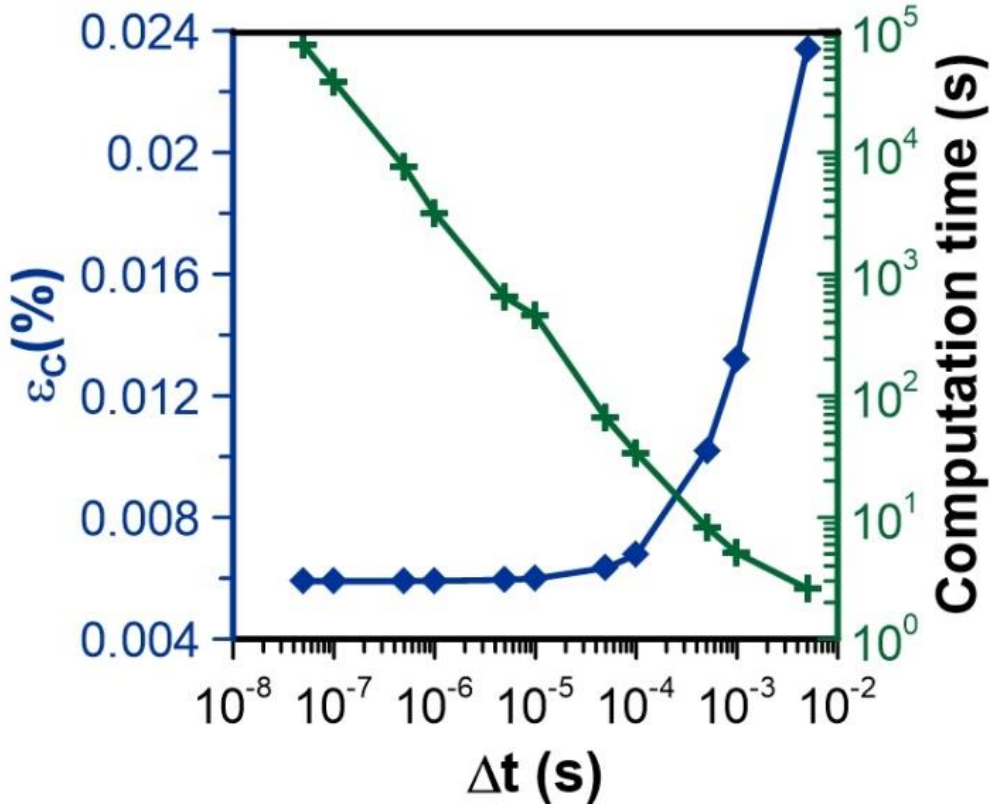

Figure 4.14: The average percentage error ε(C) of the concentration profiles versus the size of the integration time step with a uniform mesh scheme and a number of mesh points N = 100 and the corresponding computation time for each experiment.

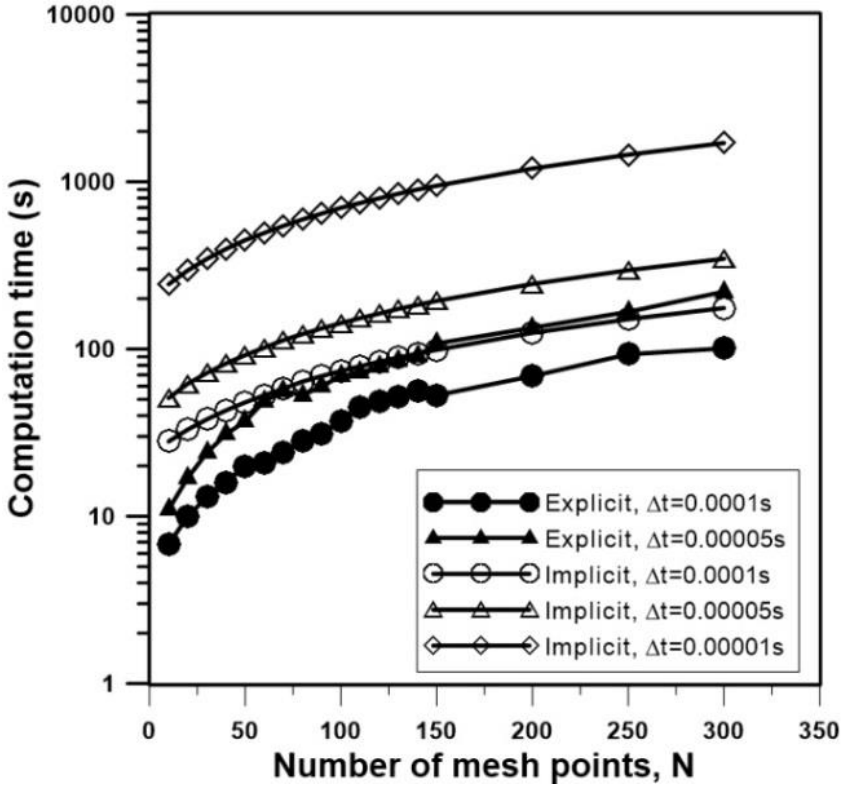

Figure 4.15: Computation times for different mesh points and for explicit and explicit schemes with uniform mesh size and simulation time of 80 s. Computer and processor used are Dell OptiPlex 780 and Intel Core 2 Duo E8400 (3.00 GHz), respectively.

4.5 Conclusion

Results have shown that the concentration profiles can be solved very accurately regardless of the finite difference scheme used to solve the Fick's second law of diffusion. The concentration gradients obtained with a uniform mesh scheme can predict the downstream time lag with a very good accuracy. However, to predict the upstream time lag, using a variable mesh size to have a small mesh size at the interface is required. Results have shown that the gradient percentage errors obtained with a variable mesh size are significantly smaller that the gradients percentage errors obtained with a uniform mesh size, especially at earlier permeation time when the gradient is very steep. Since the pressure change is the time-integration of the flux at the interface, the prediction errors on the gradients have a major impact on the upstream pressure difference curve from which the time lag is evaluated. Results have shown that a variable mesh

scheme where the first three uniform mesh sizes are transformed into 10 variable meshes (Factor 2) is a good compromise between accuracy and computation time.

This investigation has also allowed showing that both explicit and implicit finite difference schemes led to similar results. It is recommended to use an explicit scheme because of lower computation time for the same accuracy. However, the implicit scheme would be advantageous over the explicit method when 1) the time interval is too large for the explicit method to remain stable; 2) solving "stiff" initial value/boundary value problems and 3) solving nonlinear problems where stability criteria are very sensitive to nonlinearity. Crank-Nicolson algorithm [5] was also tested and the accuracy was found to be between the explicit and implicit schemes.

It is concluded that the numerical scheme used in this investigation can be used with confidence to solve problems with various boundary conditions and for systems where nonlinear diffusive behaviour is observed.

4.6 Nomenclature

A Cross sectional membrane area, m^2

C Permeating gas concentration, mol/m^3

D Diffusion coefficient, m^2/s

G^A Analytical concentration gradient, $mol/(m \cdot m^3)$

G_{∞}^{A} Steady-state analytical concentration gradient, $mol/(m \cdot m^3)$

G_u Upstream concentration gradient, $mol/(m \cdot m^3)$

G_d Downstream concentration gradient, $mol/(m \cdot m^3)$

J Flux, $mol/(m^2 \cdot s)$

L Membrane thickness, m

n Number of time increments

N Total number of mesh points for both uniform and variable mesh schemes

N_0 Number of original uniform mesh sizes before conversion to variable mesh

N_1 Number of uniform mesh sizes converted to variable mesh sizes

N_2 Number of converted variable mesh sizes from uniform mesh sizes

p^A Analytical pressure change, kPa

p^0 Constant pressure in the upstream chamber, kPa

p_u Upstream pressure, kPa

p_d Downstream pressure, kPa

P Permeability, mol·m/(m^2·Pa·s)

R Universal gas constant, J/(K·mol)

S Solubility, mol/(m^3 Pa)

t Simulation time, s

T Absolute temperature, K

V_u Upstream volume, m^3

V_d Downstream volume, m^3

x Permeation distance, m

ε Error between analytical results and numerical results

Δt Simulation time step, s

Δx_1 Grid size upstream of the grid point located at x, m

Δx_2 Grid size downstream of the grid point located at x, m

Δx_s First and smallest mesh size for both the variable and uniform mesh schemes.

Δp_u Upstream pressure decrease, kPa

Δp_d Downstream pressure increase, kPa

θ^A Analytical time lag, s

θ_u Upstream time lag, s

θ_d Downstream time lag, s

4.7 References

[1] P. Bernardo, and G. Clarizia, "30 Years of Membrane Technology for Gas Separation," Chemical Engineering Transactions, vol. 32, pp. 1999-2004, 2013.

[2] H.A. Daynes, "The process of diffusion through a rubber membrane", Proceedings of the Royal Society of London., vol. 97A, pp. 286-307, 1920.

[3] R. Barrer, and E. Rideal, "Permeation, diffusion and solution of gases in organic polymers," Transactions of the Faraday Society, vol. 35, pp. 628-643, 1939.

[4] S.W. Rutherford, and D.D. Do, "Review of time lag permeation technique as a method for characterisation of porous media and membranes", Adsorption, vol. 3, pp. 283-312, 1997

[5] B. Carnahan, H.A. Luther, and J. O. Wilkes, Applied numerical methods, New York, USA: Wiley, 1969.

[6] A. Iserles, A first course in the numerical analysis of differential equations. No. 44. Cambridge University Press, 2009.

Chapter 5

The Effect of the Downstream Pressure Accumulation on the Time-Lag Accuracy for Membranes with Non-Linear Isotherms.

Neveen Al-Qasas, Jules Thibault and Boguslaw Kruczek*

Department of Chemical and Biological Engineering, University of Ottawa
161 Louis Pasteur, Ottawa, Ontario, Canada K1N 6N5

Abstract

The time-lag method based on downstream measurements is one of the most popular methods for gas membrane characterization. This method is commonly used to characterize all types of membranes, either glassy or rubbery, and regardless of the type of isotherm for a gas molecule/membrane system. The time-lag method has originally been derived for a linear isotherm system (Henry's relation) under the assumption of vacuum at the downstream side of the membrane. This zero-pressure assumption is obviously violated as a finite downstream volume is required to record a pressure change necessary to estimate the time lag. The objective of this investigation is therefore to critically assess the degree of validity of the downstream time-lag method under more realistic boundary conditions and for systems characterized with nonlinear isotherms such as dual-mode sorption. To achieve this objective, the mass diffusion equation was solved numerically by finite differences and numerical results were compared with known analytical solutions. This study provides a deeper understanding on the behaviour of adsorption and the transport of molecules inside a membrane for the cases of linear isotherm and dual-mode sorption with complete immobilization and instantaneous equilibrium. Results clearly show that the sorption parameters have a major impact on the time required to achieve steady state as well as on the transient behaviour before reaching steady state under ideal boundary conditions. Under the realistic boundary conditions, steady state can never be achieved and can

only be approached due to gas accumulation in the downstream compartment. Conditions under which higher accuracy is obtained in the determination of the diffusion coefficient are discussed.

Keywords: Downstream time-lag method; Finite difference numerical modeling; Membrane characterization;
Publication status: Partially accepted at the Journal of Membrane science with minor revision.

5.1 Introduction

In the 1980s, polymeric gas separation membranes became an industrial reality and since then the range of their applications continuously increases **[**1**].** Gas transport in polymeric membranes is governed by the solution-diffusion mechanism, in which the gas is first dissolved at the high pressure side of the membrane and then, driven by the concentration gradient, diffuses towards the low pressure side. Consequently, gas permeability in the membrane (P) is conveniently represented as a product of the solubility (S) and the diffusivity (D) of the gas in the membrane. Accurate determination of these transport coefficients is the key to the development of improved polymeric materials for gas separation membranes **[**2- 4**].**

Typically, the three transport coefficients are determined in a single dynamic gas permeation experiment, often referred to as a time-lag experiment. A membrane, which is initially degassed, is exposed to a step increase in feed pressure while time-dependent gas permeation across the membrane is determined from the rate of pressure increase in a fixed downstream volume on the other side of the membrane. The permeability is determined from the linear portion of the pressure versus time graph; extrapolation of that linear portion to the time axis gives a time lag (θ_d), which is related to the diffusivity by:

$$\theta_d = \frac{L^2}{6D} \tag{5.1}$$

where L is the membrane thickness. The solubility is simply the ratio of the permeability and diffusivity. The mathematical basis for the time-lag measurements was originally provided by Daynes in 1920 [5]. Eq. (5.1) is based on the assumption that the concentration of the gas in the membrane at the permeate side is zero at all time during the gas permeation experiment, which is obviously not the case, because for the downstream time-lag method to be used the permeating

gas must be allowed to accumulate downstream from the membrane. Nevertheless, due to its simplicity, the time-lag analysis described above is widely used for the characterization of gas transport coefficients in membranes.

The problem of the oversimplified boundary conditions used by the time-lag method has been addressed in the literature. Barrer [6] derived a more general form of the time-lag equation by allowing a nonzero concentration at the permeate side, and a nonzero initial concentration profile in the membrane. Paul and DiBenedetto [7] modified the time-lag method by using the actual boundary conditions that existed in their experimental setup. They derived a correction factor to accommodate for gas accumulation at the permeate side of the membrane in order to correct the experimentally-determined transport coefficients. Spacek and Kubin [8] further modified the time-lag analysis taking into consideration the pressure changes at both sides of the membrane. Barrie et al. [9] considered four different sets of initial and boundary conditions resembling practical experimental conditions. For each set of conditions, they obtained a general equation describing the rate of pressure increase and calculated the respective diffusivity via an iterative procedure by solving a set of nonlinear equations.

To minimize the error due to gas accumulation downstream from the membrane, the receiving volume should be as large as possible. Moreover, the sooner the linear extrapolation is taken, the smaller the effect of gas accumulation on the experimental time lag. On the other hand, a sufficient time must elapse from the beginning of the experiment to allow gas permeation to reach steady state. As a rule of thumb, it is recommended that the pressure data used for the linear extrapolation should be taken in the time frame between $3\theta_d$ and $4\theta_d$ [2, 10, 11]. Jenkins et al. [12] conducted a numerical investigation on the effect of the size of the receiving volume and the time frame used for extrapolation. They concluded that even when the downstream volume is very large and the boundary conditions are equivalent to those imposed by the simplified time-lag analysis, the linear extrapolation of the pressure response between $3\theta_{\mathrm{d}}$ and $4\theta_d$ leads to an overestimation of the diffusivity by approximately 4%. An extended version of the numerical analysis of Jenkins et al. [12] was more recently presented by Taveira et al. [13]. In that study, the effect of performing a linear regression over a time frame in which the membrane concentration profile is not yet fully developed was discussed.

Equation (5.1) also assumes that gas sorption in the membrane follows Henry's law, which is the case for rubbery polymers and non-interactive gases. In the case of glassy polymers, a dual-mode sorption model, in which both Henry's dissolution and Langmuir's hole filling are present, is applicable. Dual-mode sorption leads to a non-linear sorption isotherm and the diffusivity from the time-lag experiment represents an apparent rather than the real diffusivity of the gas in the membrane [14-17]. Different models for glassy polymers have been proposed depending on the mobility of molecules associated with Henry's and Langmuir molecules and the driving force [18-21]. The case, in which gas molecules in Henry's sites are the only ones contributing to diffusion, is referred to as a complete immobilization model [14, 17]. Other workers [18, 19, 21-24] proposed that the molecules adsorbed in Langmuir's sites are not completely immobilized, and thus contributing to diffusion; this case is referred to as a partial immobilization model. The original complete immobilization model assumes instantaneous equilibrium between gas molecules adsorbed in Henry`s and Langmuir's sites. However, some workers suggested relaxing this assumption and instead to consider a reversible reaction between the two populations of gas molecules [25-28]. Other models attempting to explain nonlinear sorption in glassy polymers were also proposed [29, 30].

Dual-mode sorption in glassy polymers makes the derivation of the expression relating the diffusivity with the time lag more complex. For the simplest case of dual-mode sorption with complete immobilization of gas molecules in Langmuir sites, Paul [21] derived an expression for the time lag using the concept asymptotic solution proposed by Frisch [31]. The asymptotic solution provides only the steady state pressure response, which is sufficient to obtain the expression for the time lag. On the other hand, the asymptotic solution does not allow estimating the time required to reach the steady state permeation. Moreover, to our best knowledge, the effect of gas accumulation on the error in time lag of membranes with non-linear sorption isotherms has not been addressed in the literature.

In this paper, numerical simulations of time-lag experiments for membranes in which dual-mode sorption with complete immobilization of gas molecules in Langmuir sites exists are presented. Assuming a zero gas concentration at the permeate-side of the membrane, the effect of sorption parameters and the feed pressure on the time required to reach steady state is investigated. The analysis is then extended by allowing the gas to accumulate at the permeate

side of the membrane. For this more realistic case, the combined effect of sorption parameters, feed pressure and the volume downstream from the membrane on the magnitude of the minimum error and the time at which this minimum error occurs is analyzed and discussed.

5.2 Theoretical background.

A membrane of thickness L, initially degassed, is subjected to a step change in pressure (from 0 to a constant value p_0). Due to instantaneous equilibrium, the concentration of the gas at the feed surface of the membrane (x = 0) remains constant (C_0) during the entire experiment, while the gas diffuses towards the permeate surface of the membrane ($x = L$). If the gas concentration at the permeate surface of the membrane remains zero, and gas diffusivity in the membrane is constant, the time-lag experiment is described by Fick's 2nd law of diffusion given in Eq. (5.2), subject to the initial and boundary conditions (IBC) given by equations (5.3-5.5):

$$\frac{\partial C}{\partial t} = D\frac{\partial^2 C}{\partial x^2} \tag{5.2}$$

$$C\left(t<0,x\right)=0 \tag{5.3}$$

$$C\left(t,0\right)=C_0=p_0S \tag{5.4}$$

$$C\left(t,L\right)=0 \tag{5.5}$$

Eq. (5.4) implies linear sorption of gas in the membrane (e.g. Henry's law). Eq. (5.2) can be solved analytically by the method of separation of variables using the IBC specified by equations (5.3-5.5). Expression for the time lag given by Eq. (5.1) is then derived from the pressure response at the permeate side of the membrane, which is obtained from the concentration gradient at the permeate interface of the membrane.

Unless the permeate side of the membrane is continuously evacuated, Eq. (5.5) is not valid. Consequently, in a more rigorous analysis Eq. (5.5) should be replaced by:

$$\frac{V_L}{RT}\frac{dp_L}{dt} = -DA\left.\frac{\partial C}{\partial x}\right|_{x=L} \tag{5.6}$$

where V_L is the volume downstream from the membrane, A is the membrane area; R is the universal gas constant and T the absolute temperature. The 2nd BC specified by Eq. (5.6) prevents

obtaining analytical solution for Eq. (5.2). However, a semi-analytical solution based on the use of an iterative process requiring the computation of infinite summations and root determination can be obtained [2, 7, 12]. Alternatively, Eq. (5.2) with the 2nd BC specified by Eq. (5.6) can be also solved using Laplace transforms, but returning to the time domain involves numerical evaluation of the inverse Laplace transform using a fast Fourier transform [13]. In principle, to avoid complexity of the time-lag analysis resulting from using Eq. (5.6), the volume downstream from the membrane could be increased to make Eq. (5.5) approximately applicable. However, this approach is limited by the sensitivity of absolute pressure transducers, which are used to monitor gas accumulation downstream from the membrane [32]. Moreover, increasing the downstream volume may require adding extra accumulation tank(s) to the downstream configuration. In turn, this may greatly magnify the error due to resistance of gas transport at high vacuum in tubing connecting membrane cell with the accumulation tank(s) [33-34].

The problem of finding the expression for the time lag is further complicated in the case of membranes made from glassy polymers, in which gas sorption does not follow Henry's law. It is generally agreed that gas sorption in glassy polymers follows a dual-mode sorption model, in which the total gas concentration in the membrane is a sum of linear sorption in Henry's sites (C_D) resulting from normal dissolution in the continuous polymer phase, and nonlinear Langmuir sorption (C_H) in holes originating from unrelaxed free volume that exists in glassy state [14-17]:

$$C = C_D + C_H = Sp + \frac{C'_H bp}{1+bp} \tag{5.7}$$

where C'_H is the hole saturation constant and b is the hole affinity constant. Assuming that gas molecules in Langmuir sites are completely immobilized, and are in instantaneous equilibrium with gas molecules dissolved in Henry's sites [16], Eq. (5.2) is rewritten as:

$$\frac{\partial}{\partial t}\left(C_D + C_H\right) = D\frac{\partial^2 C_D}{\partial x^2} \Leftrightarrow \frac{\partial}{\partial t}\left(C_D + \frac{C'_H bp}{1+bp}\right) = D\frac{\partial^2 C_D}{\partial x^2} \tag{5.8}$$

Recognizing that $p = C_D/S$ and differentiating the term in the brackets lead to:

$$\frac{\partial C_D}{\partial t}\left(1 + \frac{C'_H b/S}{\left(1+C_D b/S\right)^2}\right) = D\frac{\partial^2 C_D}{\partial x^2} \tag{5.9}$$

Eq. (5.9) is the governing partial differential equation (PDE) describing dynamic gas permeation in glassy polymer membranes.

Using the concept of asymptotic solution [31], Paul [21] solved Eq. (5.9) for the following set of the IBC:

$$C_D\left(t<0,x\right)=C_{Di} \tag{5.10}$$

$$C_D\left(t,0\right)=C_{D0} \tag{5.11}$$

$$C_D\left(t,L\right)=C_{DL} \tag{5.12}$$

The corresponding expression for the time lag is given by:

$$\theta_d=\frac{L^2}{6D}\left\{1-3\delta+6K\left[\frac{\left(\delta+0.5\right)\alpha^2+\alpha-\left[1+\left(1+\delta\right)\alpha+\delta\alpha^2\right]\ln\left(1+\alpha\right)}{\left(1+\delta y\right)\left(1+\varepsilon y\right)\alpha^3}\right]\right\} \tag{5.13}$$

where:

$$\delta=\frac{\left(C_{Di}-C_{DL}\right)}{\left(C_{D0}-C_{DL}\right)} \tag{5.14a}$$

$$\varepsilon=\frac{C_{DL}}{C_{D0}} \tag{5.14b}$$

$$K=\frac{C_H' b}{S} \tag{5.14c}$$

$$y=C_{D0}\frac{b}{S} \tag{5.14d}$$

$$\alpha=\frac{y\left(1-\varepsilon\right)}{\left(1+\varepsilon y\right)} \tag{5.14e}$$

In the special case, for which $C_{Di} = C_{DL} = 0$, Eq. (5.13) simplifies to:

$$\theta_d=\frac{L^2}{6D}\left[1+Kf\left(y\right)\right]=\frac{L^2}{6D'} \tag{5.15}$$

where:

$$D' = \frac{D}{1 + Kf(y)} \text{ and } f(y) = 6y^{-3}\left[0.5y^2 + y - (1+y)\ln(1+y)\right] \tag{5.16}$$

Furthermore, if gas sorption follows Henry's law, the coefficient *K* defined by Eq. (5.14c) becomes zero and Eq. (5.15) simplifies to Eq. (5.1).

It is important to emphasize that the asymptotic solution of Eq. (5.9) does not provide information about the transient part of the experiment, and therefore does not allow estimating the time required to reach the steady state permeation. The latter would require a complete analytical solution. Moreover, allowing the gas to accumulate at the permeate side of the membrane; Eq. (5.12) should be replaced by:

$$\frac{V_L}{RT}\frac{dp_L}{dt} = -DA\left.\frac{\partial C_D}{\partial x}\right|_{x=L} \tag{5.17}$$

Eq. (5.17) is similar to Eq. (5.6). In both equations the concentrations refer to the mobile phase, which is equivalent to the total concentration for the linear sorption, but not in the case of nonlinear sorption. Similarly to linear sorption, there is no analytical solution of the governing PDE when gas accumulation at the permeate side of the membrane occurs. A numerical solution for this case is discussed next.

5.3 Numerical simulations

The governing PDE, Eq. (5.9), is nonlinear and it was not possible to determine analytically its solution. Eq. (5.9) was therefore solved numerically using a finite difference method. This method requires the discretization of Eq. (5.9) by applying Taylor's series expansion for the second derivative in space using a central difference in an explicit finite difference scheme to create a network of grid points throughout the membrane thickness. In addition, the time derivative is also discretized using a forward difference using a small integration time step Δt. This procedure gives a set of algebraic equations which allows determining the concentration at all grid points for each integration time step. The concentration at the subsequent time step for each interior mesh point was calculated from [35, 36]:

$$C_{D\,x}^{t+\Delta t} = C_{D\,x}^{t} + \frac{2D\Delta t}{\beta}\left(\frac{C_{D\,x+\Delta x_2}^{t} - C_{D\,x}^{t}}{\Delta x_2\left(\Delta x_1 + \Delta x_2\right)} - \frac{C_{D\,x}^{t} - C_{D\,x-\Delta x_1}^{t}}{\Delta x_1\left(\Delta x_1 + \Delta x_2\right)} \right) \tag{5.18}$$

where β is defined as follows:

$$\beta = 1 + \frac{K}{\left(1 + \frac{b}{S} C_{Dx}^{t}\right)^2} \tag{5.19}$$

Considering the other terms in Eq. (5.18), t is the current time, Δt the time step, Δx_1 is the backward mesh size, Δx_2 is the forward mesh size.

The governing PDE was solved for two sets of boundary conditions, which are referred to as ideal and real boundary conditions, respectively. As shown in Fig. 5.1, the ideal boundary conditions imply that, at the downstream interface, the concentration of the mobile phase in the membrane is not only constant, but also equal to zero:

$$C_{DL} = 0 \tag{5.20}$$

Eq. (5.20) requires Eq. (5.11) to be modified to:

$$C_D\left(t < 0, x\right) = 0 \tag{5.21}$$

For the real boundary conditions, Eq. (21) is also applicable, but at the downstream interface Eq. (5.17) is used, which in a discretized form is written as:

$$\frac{V_L}{RT}\frac{\Delta p_L}{\Delta t} = DA\left[\frac{C_{D,L\text{-}\Delta x} - C_{D,L}}{\Delta x}\right]_{x=L} \tag{5.22}$$

The upstream interface of the membrane for both the ideal and real boundary conditions is represented by Eq. (5.11). It is important to note that Eq. (5.11) also represents an ideal boundary condition, which however can be easily attained in practice by having a large volume upstream from the membrane.

Numerical solutions utilize a variable mesh size, with tighter mesh points at the two membrane boundaries. A separate comprehensive study was undertaken to determine the precision of various numerical schemes, using known analytical benchmark solutions, in view of

finding the optimal integration step and number of mesh points required to discretize the membrane [36]. Based on that study and to adequately represent the interface concentration gradients, a total of 120 mesh points were used in the current investigation and, to ensure numerical stability ($D\Delta t/\Delta x^2 < 0.5$), an integration time step of 0.00002 s was used. Indeed, the tighter mesh points allow for a more accurate evaluation of the concentration gradient at the permeate-side, which is then numerically integrated to obtain the downstream pressure versus time data.

The numerically generated pressure data is used to determine the apparent diffusivity (D_{app}) and then the diffusivity error (ε) as a function of time in the following way. For a given time t, the pressure data in a 10 s window (t – 5s, t + 5s) is used to obtain a linear trend line, which is extrapolated to the time axis. The resulting time-axis intercept, the simulated time lag, is converted into D_{app} using Eq. (5.1) and then compared with D', the expected apparent diffusivity, to obtain the relative percentage error ε:

$$\varepsilon = \frac{D_{app} - D'}{D'} \times 100\% \tag{5.23}$$

The relationship between the expected apparent diffusivity and the actual diffusivity is given by Eq. (5.16). The diffusivity error is a convenient measure of closeness to steady state permeation at a given time. A zero error indicates that steady state permeation has been attained. It is important to note that zero error is possible only with the ideal boundary conditions. In the case of real boundary conditions, the diffusivity error is expected to reach a minimum value, which may or may not be equal to zero. To generalize the analysis of the time required to reach the zero or minimum error, the dimensionless time (τ) is introduced:

$$\tau = \frac{t}{\theta_d} \tag{5.24}$$

where θ_d is defined by Eq. (5.1) using the actual diffusivity and the membrane thickness.

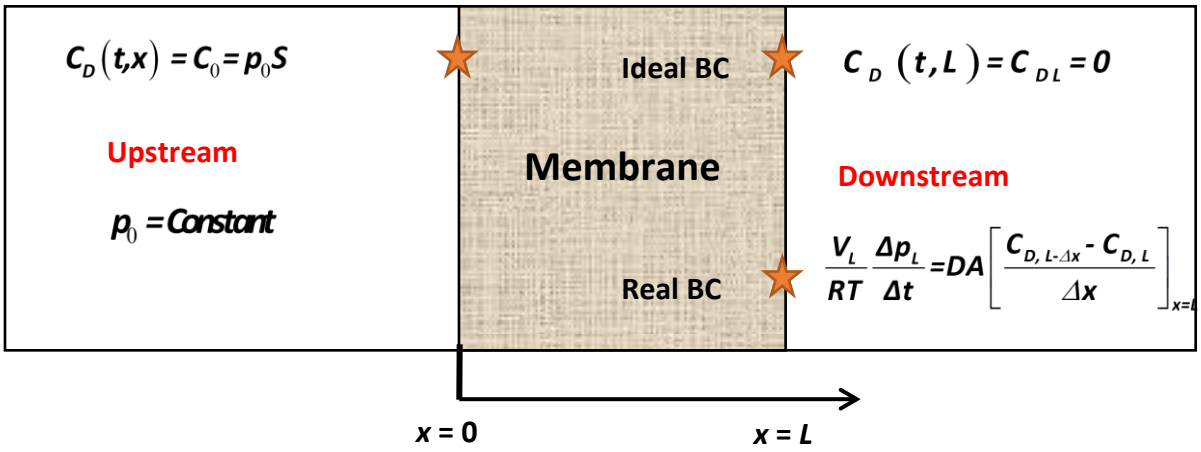

Figure 5.1: Representation of boundary conditions in a time-lag experiment.

5.4 Results and discussion

The results of the numerical simulations are presented in two subsections that are categorized according to type of boundary conditions.

5.4.1 Ideal boundary conditions

It is well known that the existence of Langmuir sites in glassy polymers, as shown by Eq. (5.15), increases the time lag of the membrane compared to what would be expected based on gas diffusivity in Henry's sites [21, 37-40]. This implies that there is also a delay in reaching steady, or rather pseudo-steady state permeation. However, based on the asymptotic solution, one does not know exactly how long it takes for gas permeation to reach steady state permeation, or to reach it within a certain percentage. This problem is illustrated in Fig. 5.2, which presents the simulated progress of the time-lag experiments for a hypothetical membrane with three different values of C'_H : 0, 3 and 20 cm^3(STP)/cm^3. All other sorption parameters and the feed pressure remain the same. The dotted lines in Fig. 5.2 represent the linear asymptotes for the prediction of the time lag given by Eq. (5.13). It is important to note that C'_H = 0 corresponds to linear sorption, which is indicated by the dimensionless time lag equal to unity.

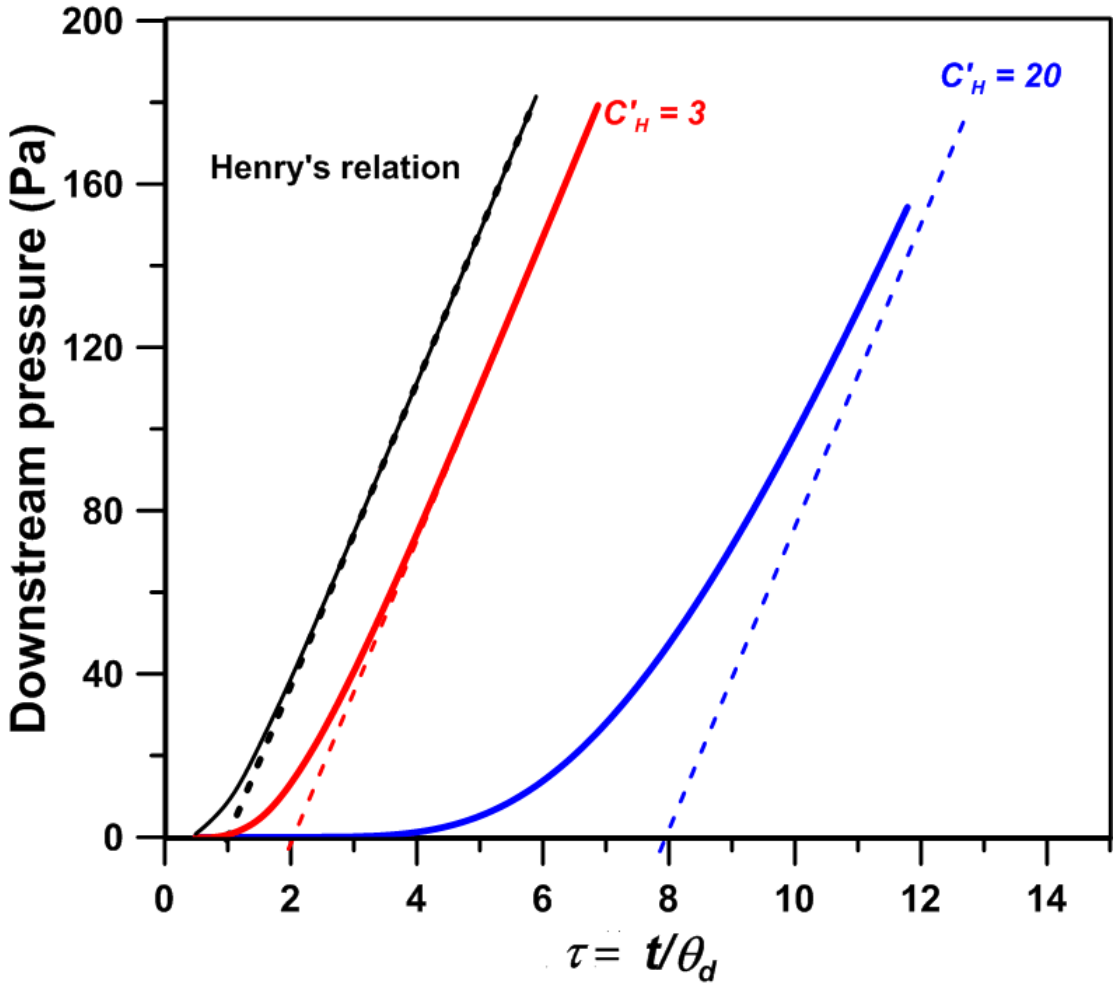

Figure 5.2: Effect of the hole saturation constant C'_H ($cm^3(STP)\cdot cm^{-3}$) on the downstream pressure profile and time lag; simulation parameters: p = 5 atm, b = 0.5 atm^{-1}, $L = 2.35\times10^{-5}$ m, $D = 4.52\times10^{-12}$ $m^2\cdot s^{-1}$, S = 0.685 $cm^3(STP)\cdot cm^{-3}\cdot atm^{-1}$.

It is evident that as C'_H increases, the steady state permeation is reached not only later, but also at much larger downstream pressures. In other words, the shape of the transient pressure curve is strongly affected by C'_H. More generally, an increase in C'_H, while other sorption parameters are unchanged, results in more sorption in Langmuir sites relative to Henry's sites. This is evident by considering Eq. (5.7) in a slightly different form:

$$C = C_D + C_H = p\left(S + \frac{C'_H b}{1+bp}\right) = p\left(\text{Term 1} + \text{Term 2}\right) \tag{5.25}$$

Term 2 in Eq. (5.25), which describes Langmuir portion of the dual-mode isotherm, is directly proportional to C'_H. A question arises: is the magnitude of Term 2 relative to Term 1 the only factor affecting the shape of the pressure curves shown in Fig. 5.2? Before addressing this question, it is important to realize that Fig. 5.2 allows only for a qualitative assessment of closeness to the steady state; as the closeness to the steady state is a convenient measure of the pressure curve shape. On the other hand, closeness to the steady state can be assessed quantitatively in terms of the error in diffusivity defined by Eq. (5.23) at a given value τ. Alternatively, the delay in reaching steady state permeation can be assessed in terms of the τ value required for the error in diffusivity to be within 1% of the actual value.

It is also important to note that a given value of Term 2 can be obtained with an infinite number of combinations of C'_H, *b* and *p*, but the relationship relating Term 2 to either *b* or *p* is more complex than that between Term 2 and C'_H. Table 1 presents the literature values of sorption parameters for several gases in both glassy polymers and rubbery polymers with inorganic fillers. It is evident that there is a significant variation in individual sorption parameters depending on the polymer, gas and temperature. For example, C'_H varies from 0.31 to 147 $cm^3(STP)\cdot cm^{-3}$ whereas *b* from 0.012 to19.84 atm^{-1}. In the simulations performed in this investigation, the nominal values of C'_H and *b* were 30 $cm^3(STP)\cdot cm^{-3}$ and 0.5 atm^{-1}, respectively, which are within the respective ranges in Table 1. The nominal pressure used in simulations was p = 5 atm. In addition, numerical simulations of time-lag experiments require the membrane thickness, the diffusivity and solubility. For the latter parameters, the following values were used: $L = 2.35\times10^{-5}$ m, $D = 4.52\times10^{-12}$ $m^2\cdot s^{-1}$, S = 0.685 $cm^3(STP)\cdot cm^{-3}\cdot atm^{-1}$. The chosen diffusivity and solubility coefficients correspond to those of N_2 in poly(p-phenylene oxide) (PPO) [32, 41]. For *D* and *L* specified above, the corresponding θ_d = 20.4 s. It should be emphasized that one could choose any values for *L* and *D*. This is because similarly to Fig. 5.2 the analysis are carried out in terms of dimensionless time defined by Eq. (5.24). The selected *S* determines the magnitude of Term 1; the effect of *S* will also be considered in the following analysis.

Table 5.1: Sorption data for various gases in different membrane materials.

Type of polymer	**Gas**	***T*** °C	C'_H $cm^3(STP)\cdot cm^{-3}$	***b*** atm^{-1}	***S*** $cm^3(STP)\cdot cm^{-3}\cdot atm^{-1}$
PIM-1 [42]	He	25	6.60	0.037	0.065
	H_2	25	49.1	0.013	0.040
	N_2	25	31.0	0.076	0.493
	O_2	25	18.6	0.132	1.327
	CH_4	25	65.0	0.150	0.592
	CO_2	25	107	0.421	2.351
	C_2H_4	25	93.5	0.556	1.806
	C_2H_6	25	81.1	1.085	2.762
	C_3H_6	25	88.7	2.604	10.14
	C_3H_8	25	78.1	3.428	10.52
Silicon rubber filled with 5A [40]	CO_2	30	147	19.84	1109
	CH_4	30	39.4	0.958	430.9
PPOBr (36%)[43]	CO_2	35	35.4	0.244	0.941
	CH_4	35	24.9	0.113	0.344
	N_2	35	11.8	0.053	0.162
PPOBr (91%)[43]	CO_2	35	37.5	0.292	0.969
	CH_4	35	26.9	0.120	0.379
	N_2	35	15.1	0.057	0.169
PPO[43]	CO_2	35	32.7	0.195	0.921
	CH_4	35	22.2	0.107	0.321
	N_2	35	9.95	0.048	0.153
Maylar polyester film [16]	CO_2	40	5.30	0.440	0.380
Glassy oriented Polystyrene [17]	CH_4	-	3.25	0.164	0.193
Glassy polyimide [44]	CH_4	35	29.6	0.126	0.173
	CO_2	35	33.4	1.076	1.973
Polycarbonate [23]	He	35	0.31	0.012	0.015

	N_2	35	2.11	0.056	0.091
	CH_4	35	8.38	0.084	0.147
	CO_2	35	18.8	0.262	0.685
PTCDC [45]	CO_2	15	24.0	0.430	1.510
Polyethylene terephthalate PET [24]	CO_2	25	7.91	0.351	0.362
Silicon rubber-filled with 5A [39]	CO_2	30	102.6	7.053	1.100
	CH_4	30	43.4	0.480	0.430
	N_2	30	14.6	1.201	0.130

Figures 5.3-5.5 show the effect of Term 2 on the dimensionless time required for the apparent diffusivity to be within 1% of the real apparent diffusivity. Term 2 is varied from 0 to 6 by changing one of its three elements: C'_H, *b* and *p* while keeping the other two parameters fixed. Term 2 in Fig. 5.3 is varied by means of *b* while C'_H and *p* are kept constant to their nominal values; in Fig. 5.4 by means of C'_H while *b* and *p* are kept constant; in Fig. 5.5 by means of *p* while C'_H and *b* remain unchanged. In addition to S = 0.685 $cm^3(STP)\cdot cm^{-3}\cdot atm^{-1}$, the simulations are carried out for S = 0.40 $cm^3(STP)\cdot cm^{-3}\cdot atm^{-1}$ to also determine the impact of solubility. In general, the dimensionless time τ necessary to reach 1% error in D', i.e. to attain steady state permeation, increases with an increase of Term 2. This is consistent with simulations shown in Fig. 5.2. The only exception is Fig. 5.3, in which Term 2 is varied by means of *b*. For both solubilities, the time to reach steady state permeation reaches a maximum value at Term 2 ≈ 5.25. The magnitude of this maximum depends on *S*. For S = 0.685 $cm^3(STP)\cdot cm^{-3}\cdot atm^{-1}$, $\tau_{max} \approx$ 30, while for S = 0.400 $cm^3(STP)\cdot cm^{-3}\cdot atm^{-1}$, $\tau_{max} \approx$ 50. This illutrates a general trend seen in Figs. (5.3-5.5); for a given value of Term 2, the time to reach the steady state is always greater for the smaller *S*, i.e. for a smaller Term 1. It is important to note that up to Term 2 ≈ 4, Figs. (5.3-5.5) are quite similar, i.e. the magnitude of Term 2 regardless of individual values of C'_H, *b*, and *p* determines the time to reach the steady state. The manner in which each of these parameters affects the magnitude of Term 2 is obviously different.

As already mentioned, Term 2 is directly proportional to C'_H. On the other hand, Term 2 is inversely related with *p*. In principle, at $p \to 0$, Term 2 approaches infinity, but in practice gas permeation experiments are carried out at pressures greater than atmospheric pressure. Consequently, the effect of *p* on Term 2 is rather limited compared to that of C'_H, which as shown in Table 1 can vary by orders of magnitude depending on the membrane material and the type of gas. As for the hole affinity constant, when $b \to \infty$, Term 2 approaches C'_H/p which is the largest possible value. On the other hand, with few exceptions mostly for composite materials, *b* is generally less than unity (Table 1).

The physical interpretation of the observed maximum in Fig. 5.3 when varying Term 2 by means of *b* is not easy to comprehend. At this time, the following explanation is proposed. As *b* increases, the affinity of molecules towards Langmuir sites increases. At the same time, Langmuir sites have limited capacity to accommodate the molecules. A local distribution between Henry's and Langmuir's sites depends on *b*; the greater the value of *b*, the greater the number of molecules immobilized in Langmuir sites compared to mobile molecules in Henry's sites. Therefore, as *b* increases while all the other parameters remain unchanged, a larger number of gas molecules must enter the membrane to establish a steady state concentration profile, which implies an increase of the time required to reach steady state. This effect is clearly seen at low values of *b* (thus at low values of Term 2) in Fig 3. On the other hand, the Langmuir sites could be locally saturated at or near to the feed interface of the membrane. In this case, an increase of *b* would decrease the total number of gas molecules required to saturate the Langmuir sites implying a decrease of the time required to reach steady state. Since the permeate side of the membrane is under vacuum, Langmuir sites cannot be fully saturated near the permeate interface of the membrane. Consequently, while an increase of *b* would lead to a faster steady state concentration profile where Langmuir sites can be fully saturated, this effect is always associated with the opposite trend near the permeate interface of the membrane where Langmuir sites cannot be fully saturated. The net effect of *b* on the time required to reach steady state would therefore depend on the fraction of the membrane thickness in which Langmuir's sites could be fully saturated. Numerical verification of this hypothesis is beyond the scope of the current paper.

When Term 2 approaches zero (Henry's law is applicable), which occurs either when C'_H or b approach zero, τ required to reach 1% error in D' in Figs 5.3 & 5.4 is the same and equal approximately to 4. This is consistent with a general rule of thumb proposed by Jennings et al. [12] that the time lag of membranes, in which Henry's law is applicable, should be determined from the rate of pressure increase in the timeframe between 3 and 4 time lags of the membrane. It should be noted the minimum value of Term 2 in Fig. 5.5 is approximately 0.6 rather than 0; the former corresponds to the maximum pressure (p = 50 atm) at which simulation was carried out. In the timeframe (3 - 4θ_d), gas permeation is sufficiently close to steady state and at the same time, because of a relatively short time the amount of gas accumulated downstream from the membrane is small. As a result, Eq. (5.5) might be a good approximation of the downstream boundary condition. On the other hand, as shown in Figs. (5.3-5.5), the time for ε to be within 1% for a non-linear sorption could be very long. As a result, the pressure of the gas accumulated downstream might be too large to use Eq. (5.5) as the downstream boundary condition.

The issues related to time-lag measurements in glassy membranes using the real boundary condition at the permeate interface of the membrane are discussed next.

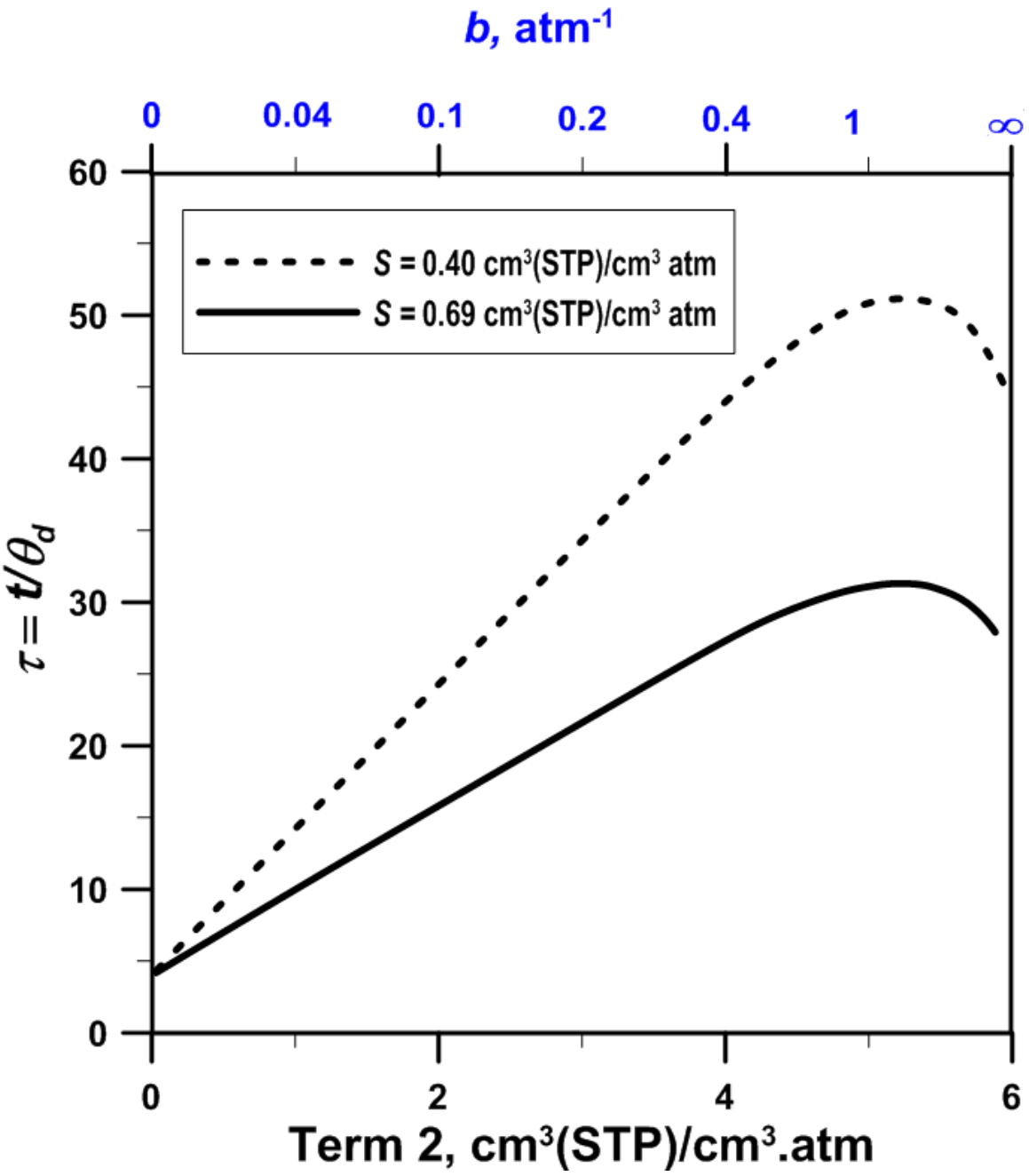

Figure 5.3: The effect of the affinity parameter b on the dimensionless time τ to reach steady state permeation (ε < 1%); simulation parameters: C'_H = 30 $cm^3(STP)\cdot cm^{-3}$, p = 5 atm, L = 2.35×10^{-5} m, D = 4.52×10^{-12} $m^2\cdot s^{-1}$.

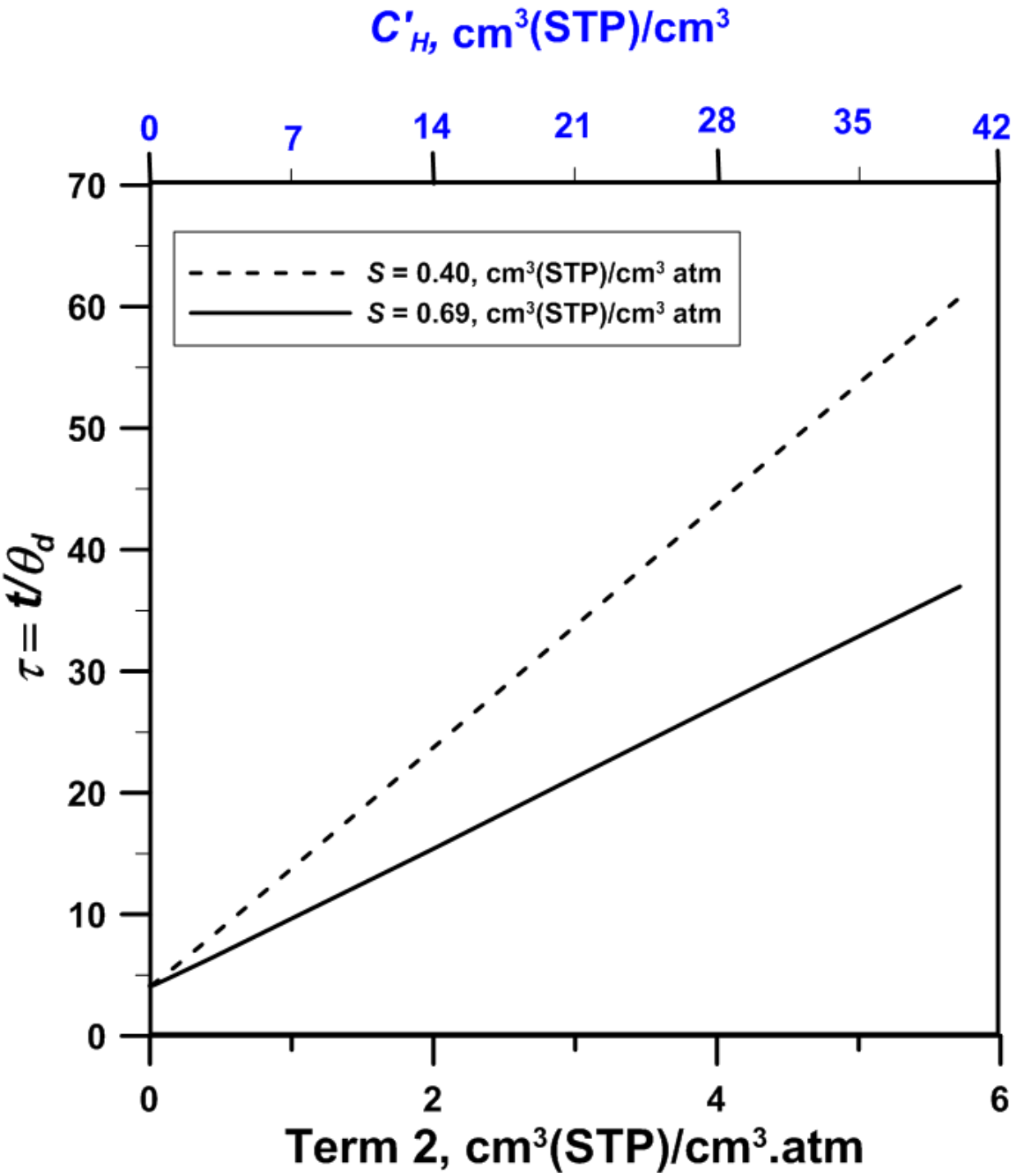

Figure 5.4: The effect of hole saturation constant C'_H the dimensionless time τ to reach steady state permeation ($\varepsilon < 1\%$); simulation parameters: b = 0.5 atm^{-1}, p = 5 atm, L = 2.35×10^{-5} m, D = 4.52×10^{-12} m^2·s^{-1}.

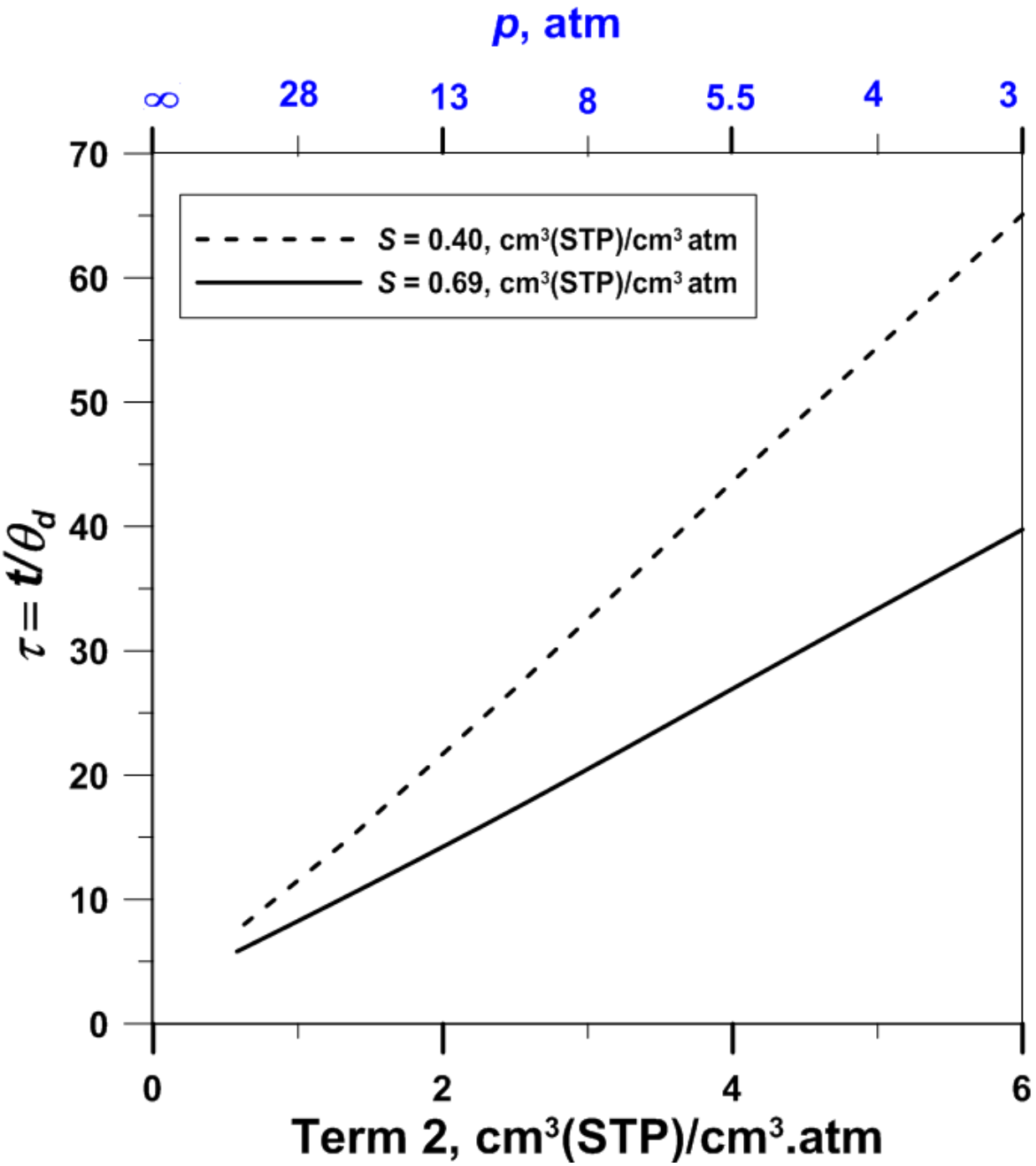

Figure 5.5: The effect of feed pressure p on the dimensionless time τ to reach steady state permeation, (ε < 1%); simulation parameters: C'_H = 30 $cm^3(STP)\cdot cm^{-3}$, b = 0.5 atm^{-1}, L = 2.35×10^{-5} m, D = 4.52×10^{-12} $m^2\cdot s^{-1}$.

5.4.2 Real boundary conditions

The ideal boundary condition at the permeate interface along with a constant feed pressure ensures reaching steady state permeation. Thus, as shown in Fig. 5.2, the simulated pressure responses approach the respective asymptotes regardless of the type of the isotherm. On the other hand, when gas accumulation at the permeate side is taken into consideration, i.e. using the real boundary condition, steady state permeation cannot be attained so that the simulated pressure response curve is expected to diverge from the respective asymptote.

Figure 5.6 presents the effect of dimensionless time (τ) on the relative percentage error in the apparent diffusivity (ε), defined by Eq. (5.23), for two downstream volumes, V_L = 25 and 100 cm^3, and two membranes having C'_H = 0 and 20 $cm^3(STP)\cdot cm^{-3}$. It is important to note that C'_H = 0 indicates the linear sorption isotherm regardless of the value of b. The other membrane properties (S = 0.685 $cm^3(STP)\cdot cm^{-3}\cdot atm^{-1}$, D = 4.52×10^{-12} $m^2\cdot s^{-1}$, L = 2.35×10^{-5} m) as well as the feed pressure (p = 5 atm) were kept the same for all simulations in Fig. 5.6. For the membrane having C'_H = 20 $cm^3(STP)\cdot cm^{-3}$, the corresponding hole afinity constant is b = 0.5 atm^{-1}. The parameter Ψ in Fig. 5.6 represents the dimensionless time, during which ε is less than 1%. In the case of the ideal boundary conditions, once ε drops below 1% it approaches zero so that the corresponding Ψ is infinity. The parameter Ψ' indicates the period of time, during which the error remains below the minimum error (ε_{min}) plus 1%. Since the magnitude of ε_{min} is not constant, the shape of the error curves in Fig. 5.6 is better reflected by the magnitude of Ψ' rather thanΨ.

The existence of ε_{min} in Fig. 5.6 indicates that the numerically simulated pressure response curve first approaches and then crosses the corresponding asymptote. Keeping in mind the definition of ε given by Eq. (5.23), after initiation of the experiment (transient conditions) the slope of the pressure curve and thus the apparent time lag increases with an increase of τ thereby leading to a decrease in ε. However, because of gas accumulation, the driving force for permeation gradually decreases and the slope of the pressure response curve never reaches the slope of the corresponding asymptote. As the driving force decreases, the pseudo-steady

permeation rate also decreases, leading to a decrease in the apparent time lag and thus an increase in ε with τ.

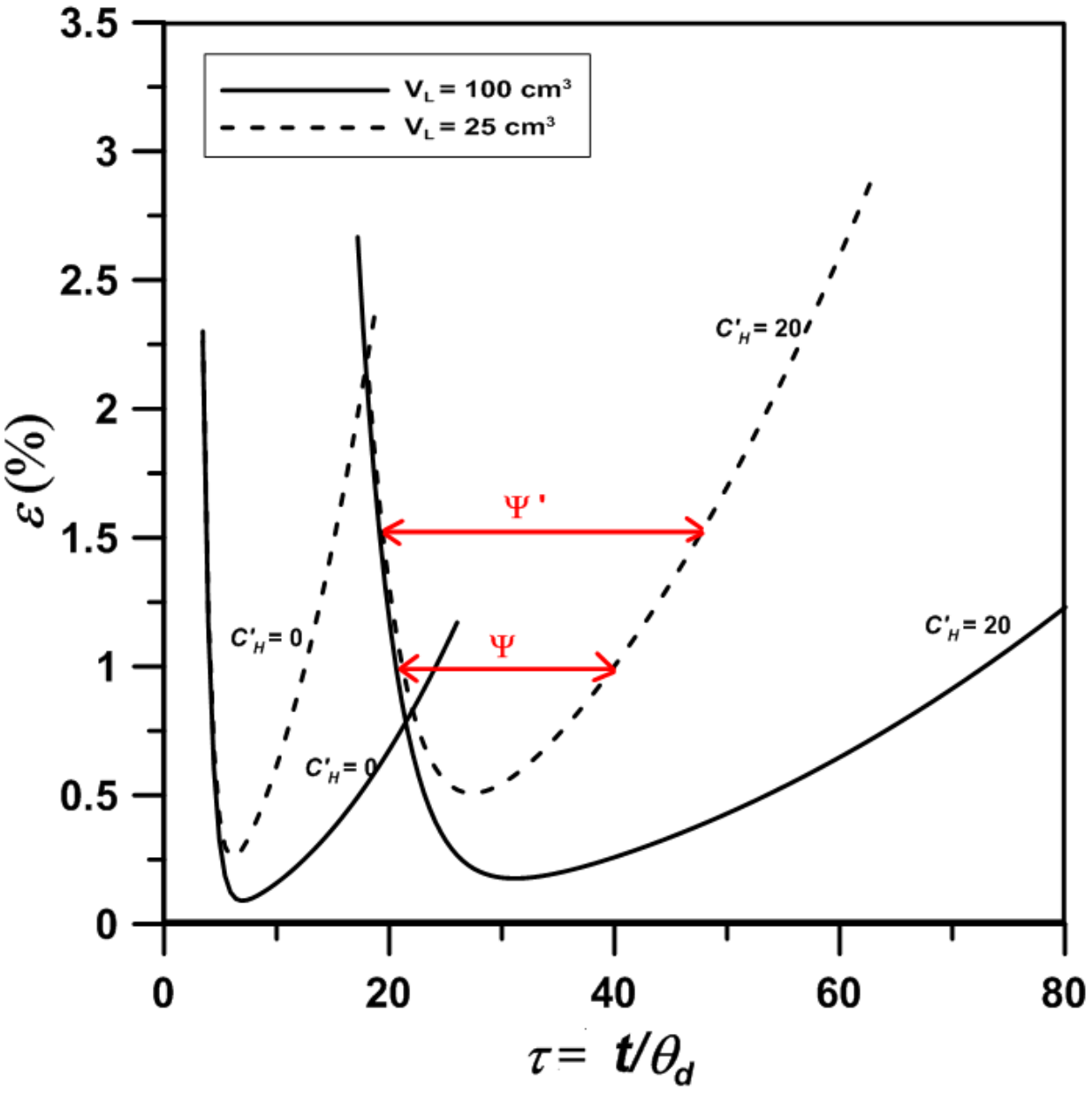

Figure 5.6: The effect of the hole saturation parameter C'_H and the downstream volume V_L on the error of the apparent diffusivity (ε) for two membranes having a linear isotherm C'_H =0 and nonlinear isotherm with C'_H = 20 $cm^3(STP)\cdot cm^{-3}$, b = 0.5 atm^{-1}. Simulation parameters are: p = 5 atm, L = 2.35×10^{-5} m, D = 4.52×10^{-12} $m^2\cdot s^{-1}$.

Consequently, the existence of ε_{min} in Fig. 5.6 is not surprising. Similarly, the effect of the downstream volume (V_L) on the shape of the error curve could be expected. This is because for a larger V_L, while all other parameters remain unchanged, the downstream pressure at a given τ must be smaller for a smaller V_L. Consequently, the rate of decrease of the driving force for gas permeation for V_L = 100 cm^3 must be smaller than that for V_L = 25 cm^3, leading to a more shallow error curve (increase in Ψ'). By the same argument, although the minimum error never reaches zero, ε_{min} for V_L = 100 cm^3 is smaller than that for V_L = 25 cm^3. It can also be observed that as the downstream volume increases the time required to reach ε_{min} slightly increases. On the other hand, the effect of C'_H on the time to reach ε_{min} is very clear; for a given V_L the time to reach ε_{min} is much shorter for C'_H = 0 than for C'_H = 20 cm^3(STP)·cm^{-3}. This is consistent with the results of Fig. 5.4 for the ideal boundary conditions, or more generally with the results of Figs. 3-5, where an increase in Term 2 delays reaching the steady state. In addition, the greater the C'_H, the greater the ε_{min} but the effect of C'_H on the magnitude of ε_{min} is not as strong as that of V_L.

On the other hand, the effect of C'_H on the shape of the error curves in Fig. 5.6 may appear to be rather surprizing. First of all, it should be kept in mind that for a given *S* and *D* regardless of C'_H, *b* and *p*, the membrane permeability (*P*) is constant and equal to the product *S* and *D*. This means that for the same V_L the slope of the simulated pressure response curves for different values of Term 2 at pseudo-steady state conditions should be comparable. At the same time, since an increase in C'_H leads to a delay in reaching pseudo-steady state, the corresponding downstream pressure also increases. Therefore, after reaching the pseudo-steady state, the rate of decrease of the pressure difference across the membrane should be slightly greater for a greater C'_H leading to a slightly steeper error curve. However, this is not the case in Fig. 5.6. In contrast, the error curve for C'_H = 0 is significantly steeper than that for C'_H = 20 cm^3(STP)·cm^{-3}. This indicates, that a change in pressure difference across the membrane is not directly related to the change in the actual driving force for gas permeation. From a practical point of view, this implies a more linear behaviour at pseudo-steady state for membranes with dual-mode sorption and

complete immobilization in Langmuir sites, and hence the possibility of their accurate characterization by the time-lag method despite gas accumulation at the permeate side.

For the membrane with C'_H = 0, once gas molecules reach the permeate interface of the membrane, they desorb and accumulate at the permeate side. Because of the linear isotherm, a decrease in the pressure difference across the membrane is directly related to the driving force for gas permeation. On the other hand, for the membrane with C'_H = 20 $cm^3(STP)\cdot cm^{-3}$, once gas molecules reach the permeate interface via Henry's sorption sites, they are not only desorbed but also transferred into Langmuir sites (it is assumed that the two populations are in instantaneous equilibrium). This is why as C'_H increases there is not only a delay in the molecules reaching the permeate interface of the membrane, but also the initial rate at which they desorb decreases (see Fig. 5.2). This phenomenon could be referred to as "sucking of molecules by Langmuir sites". In other words, the molecules reaching the permeate interface of the membrane are split into those that desorb and those that are transferred to Langmuir sites. The greater the downstream pressure, the smaller the fraction of gas molecules that are transferred to Langmuir sites, because the latter are already partly filled. Therefore, on the one hand, for membranes with $C'_H > 0$, as C'_H increases, the rate of decrease of the pressure difference across the membrane increases, which is supposed to result in faster deviation from asymptote pressure curve, but on the other hand, the fraction of molecules reaching the permeate interface of the membrane that can desorb increases therefore contributing in the slower deviation from the asymptote. The "sucking of gas molecules by Langmuir sites" could explain the more linear pressure response curve at pseudo-steady state for the membrane with C'_H = 20 $cm^3(STP)\cdot cm^{-3}$ compared to that with C'_H = 0. On the other hand, the "sucking effect" is not as strong as the effect of the decrease in the driving force, because for a given C'_H in Fig. 5.6 the error curves for V_L = 25 cm^3 (greater downstream pressure) are steeper than those for V_L = 100 cm^3.

To generalize the above discussion, the effect of Term 2 on τ required to reach ε_{min} and the magnitude of ε_{min} is now considered (Figs. 5.7a – 5.9a) along with the effect of Term 2 on Ψ and Ψ' (Figs 5.7b – 5.9b). Similarly to Figs. 5.3-5.5, Term 2 is varied from 0 to 6 by changing one of

its elements C'_H , b and p while keeping the other two parameters fixed. In Figs. 5.7a&b, Term 2 is varied by means of b while C'_H and p remain constant; in Figs. 8a&b by means of C'_H while b and p are kept constant; in Fig. 5.9 by means of p while C'_H and b remain unchanged. Two downstream volumes are considered, V_L = 25 cm^3 and V_L = 100 cm^3, while the other simulation parameters (S = 0.685 $cm^3(STP)\cdot cm^{-3}\cdot atm^{-1}$, D = 4.52×10^{-12} $m^2\cdot s^{-1}$, L = 2.35×10^{-5} m) are identical to the values used previously.

In general, regardless of which parameter of Term 2 is varied, Ψ' increases with an increase of Term 2. This indicates that a more nonlinear adsorption isotherm (due to dual-mode sorption), the wider the error curves become, thereby indicating a more linear behaviour at pseudo-steady state. However, the way Ψ' increases with respect to Term 2 depends on which one of the three parameters in Term 2 is varied. When Term 2 is increased by increasing b (Fig. 5.7b), the relation between Term 2 and Ψ' is approximately linear up to a value of Term 2 ≈ 4, and then the rate of increase in Ψ' greatly increases. On the other hand, when Term 2 is increased by changing C'_H (Fig. 5.8b) and p (Fig. 5.9b), the rate of increase in Ψ' decreases with an increase in Term 2, in particular when Term 2 is smaller than 2. A different dependence of Ψ' on Term 2 in Fig. 5.7b compared to that in Figs. 5.8b and 5.9b is a consequence of a unique dependence of the dimensionless time τ necessary to reach ε_{min} when Term 2 is varied by changing b (Fig. 5.7a). More specifically, the time required to attain ε_{min} reaches the maximum for a value of Term 2 ≈ 5.5. On the other hand, when Term 2 is varied by either C'_H or p, the time required to reach ε_{min} increases with an increase in Term 2. The relations between Term 2 and τ to reach ε_{min} are similar to those depicted in Figs. (5.3-5.5).

Another unique feature of Fig. 5.7a compared to Figs. 5.8a & 5.9a is the existence of the maximum value of ε_{min} at a specific value of Term 2 in Fig. 5.7a, while the magnitude ε_{min} in Figs. 5.8a & 5.9a generally increases with an increase of Term 2. As shown in Fig.5. 6, an increase in τ necessary to reach ε_{min} leads to an increase in the magnitude of ε_{min}. Consequently, the existence of the maximum value of ε_{min} in Fig. 5.7a likely results from previously discussed maximum τ required to reach ε_{min} when Term 2 is varied by means of b. At the same time, it should be emphasized that the maximum τ and the maximum ε_{min} occur at different values of

Term 2. More specifically, the maximum ε_{min} occurs at values of Term 2 ≈ 3.5 while the maximum τ necessary to reach ε_{min} occurs at Term 2 ≈ 5.5. This indicates that in addition to the unique effect of *b* on the time required to reach steady state discussed in the previous section, the presence of gas accumulation magnifies this effect.

The effect of downstream volume on both Ψ' and Ψ is similar to that already seen in Fig.5. 6. For a given Term 2, Ψ' and Ψ are greater for the larger volume. In comparison to Ψ', the corresponding Ψ at a given value of Term 2, regardless how Term 2 is varied is always smaller than Ψ'. This is because ε_{min} is always greater than zero. In general, the difference between Ψ' and Ψ increases as Term 2 increases. The exception is Fig. 5.7b, in which this difference first increases, and then decreases with an increase of Term 2. This is the consequence of the previously discussed unique relationship between ε_{min} and Term 2 when the latter is varied by means of *b*.

The most important outcome of the simulations of dual-mode sorption membranes with real downstream boundary condition, i.e. taking into consideration the gas accumulation occurring at the permeate side of the membrane, is that despite a delay in reaching pseudo-steady state resulting in a significantly greater downstream pressure (a greater change from the initial pressure difference across the membrane) compared to membranes following Henry's law, the pseudo-steady state permeation is more stable for the former than for the latter membranes. Moreover, the more nonlinear sorption isotherm, the more stable is the permeation at pseudo-steady state. Although the minimum error in the apparent diffusivity due to the real boundary condition generally increases with an increase of nonlinearity of the sorption isotherm, quantified by the magnitude of Term 2 (Eq. 5.25), ε_{min} was less than 1% in all performed simulations.

The above considerations can be qualitatively extended to a dual mode sorption with a partial immobilization in Langmuir sites model, in which the diffusivity in the Langmuir sites is a fraction of the diffusivity in Henry's sites [19]. In one limiting case, when the fraction is equal to zero, the partial immobilization model becomes the complete immobilization model. As the diffusivity of the molecules in Langmuir sites increases, the delay in reaching pseudo-steady state should decrease; in the other limiting case in which the diffusivity of molecules in Langmuir and Henry's were the same, there would be no delay in reaching the pseudo-steady

state, and the diffusivity could be directly determined from the apparent time lag [24]. Noting a similar effect of decreasing diffusivity in Langmuir sites and increasing nonlinearity of sorption isotherm on the delay in reaching pseudo-steady state, it is likely that decreasing diffusivity in Langmuir sites in the partial immobilization model should lead to more stable permeation at pseudo-steady state.

It is important to emphasize that the apparent time lag always underestimates the expected time lag. Therefore, to determine the conditions for $\varepsilon_{\min}$ it is recommended to use a relatively short time frame for the determination of the slope of the asymptote, and to monitor the variation in the slope with time. The maximum slope should correspond to the maximum apparent time lag and to $\varepsilon_{\min}$. At the same time, it should be kept in mind that the validity of this conclusion depends on the assumed instantaneous equilibria between the gas phase and the membrane phase, and between the molecules in Henry's and Langmuir's sites, as well as, on the complete immobilization of gas molecules in the Langmuir's sites.

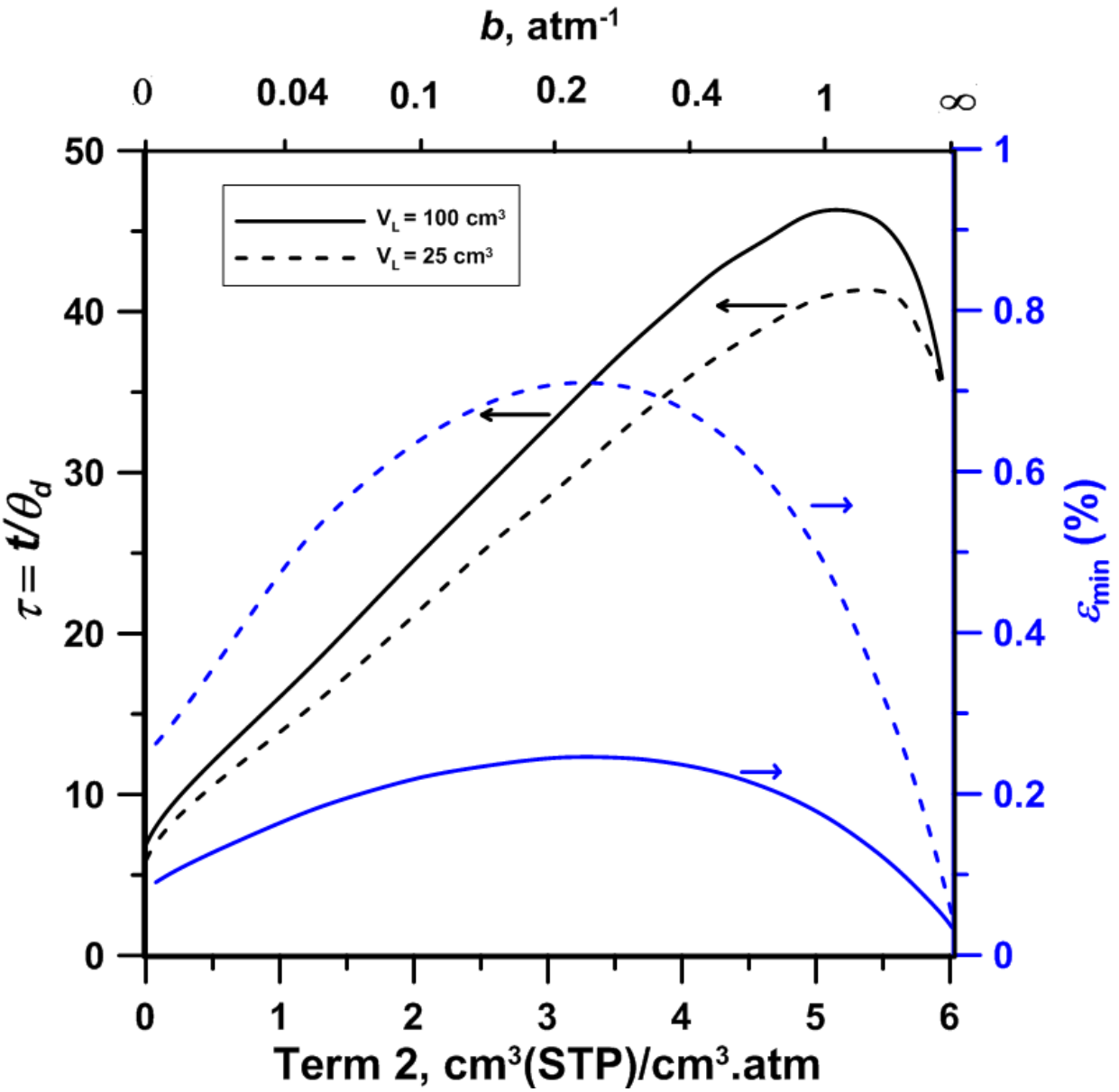

Figure 5.7a: The effect of changing the affinity parameter b, on the time of reaching minimum error (τ) and on the magnitude of this minimum (ε_{min}) for two different downstream volumes (25 & 100 cm^3), Simulation parameters: C'_H = 30 cm^3(STP)·cm^{-3}, p = 5 atm, L = 2.35×10^{-5} m, D = 4.52×10^{-12} m^2·s^{-1}.

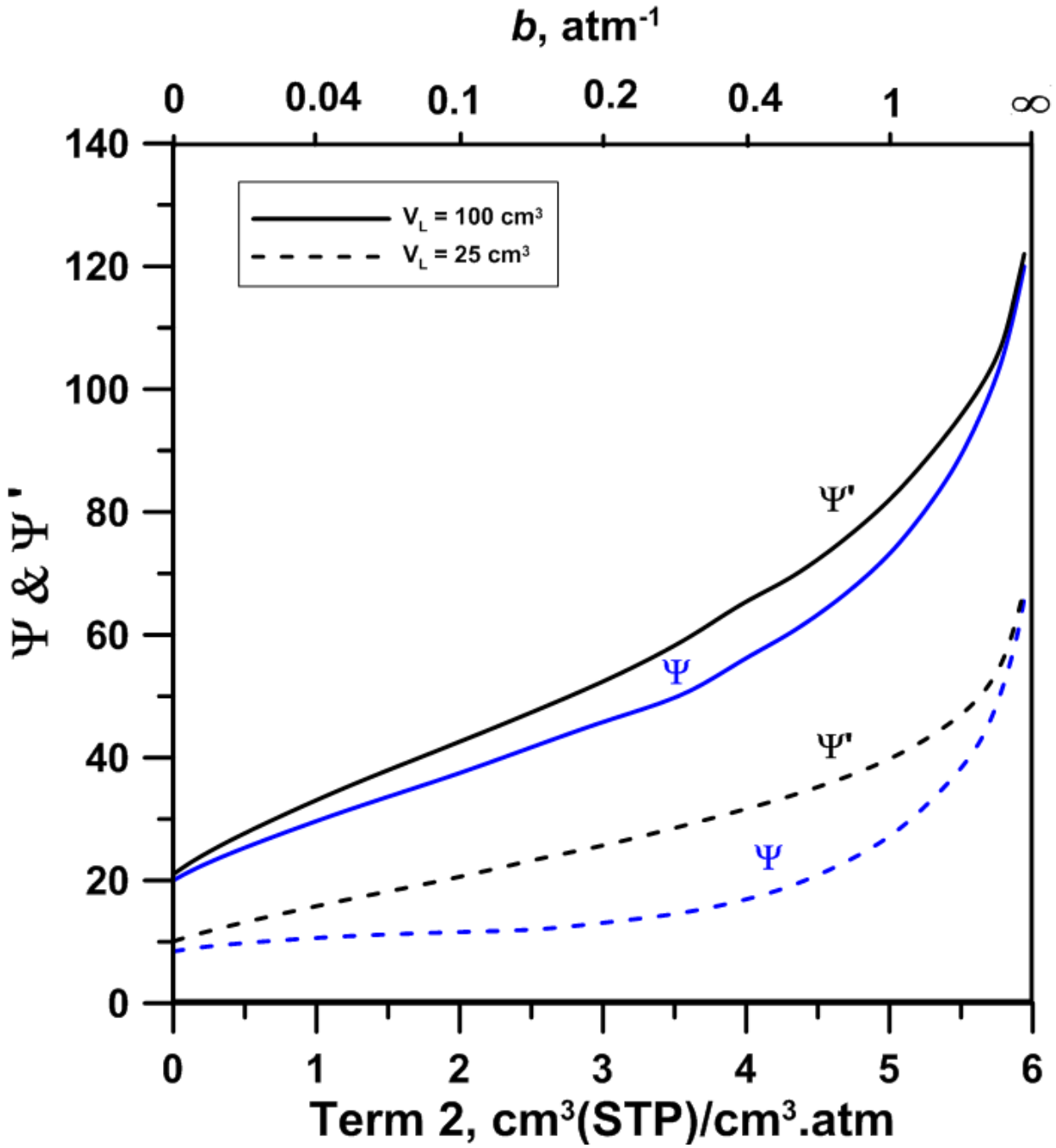

Figure 5.7b: The effect of changing the affinity parameter b on the period of time to stay within 1% and within ε_{min} + 1% (ψ and ψ' respectively) for two downstream volumes (25 & 100 cm^3). Simulation parameters are: C'_H = 30 cm^3(STP)·cm^{-3}, p = 5 atm, L = 2.35×10^{-5} m, D = 4.52×10^{-12} m^2·s^{-1}.

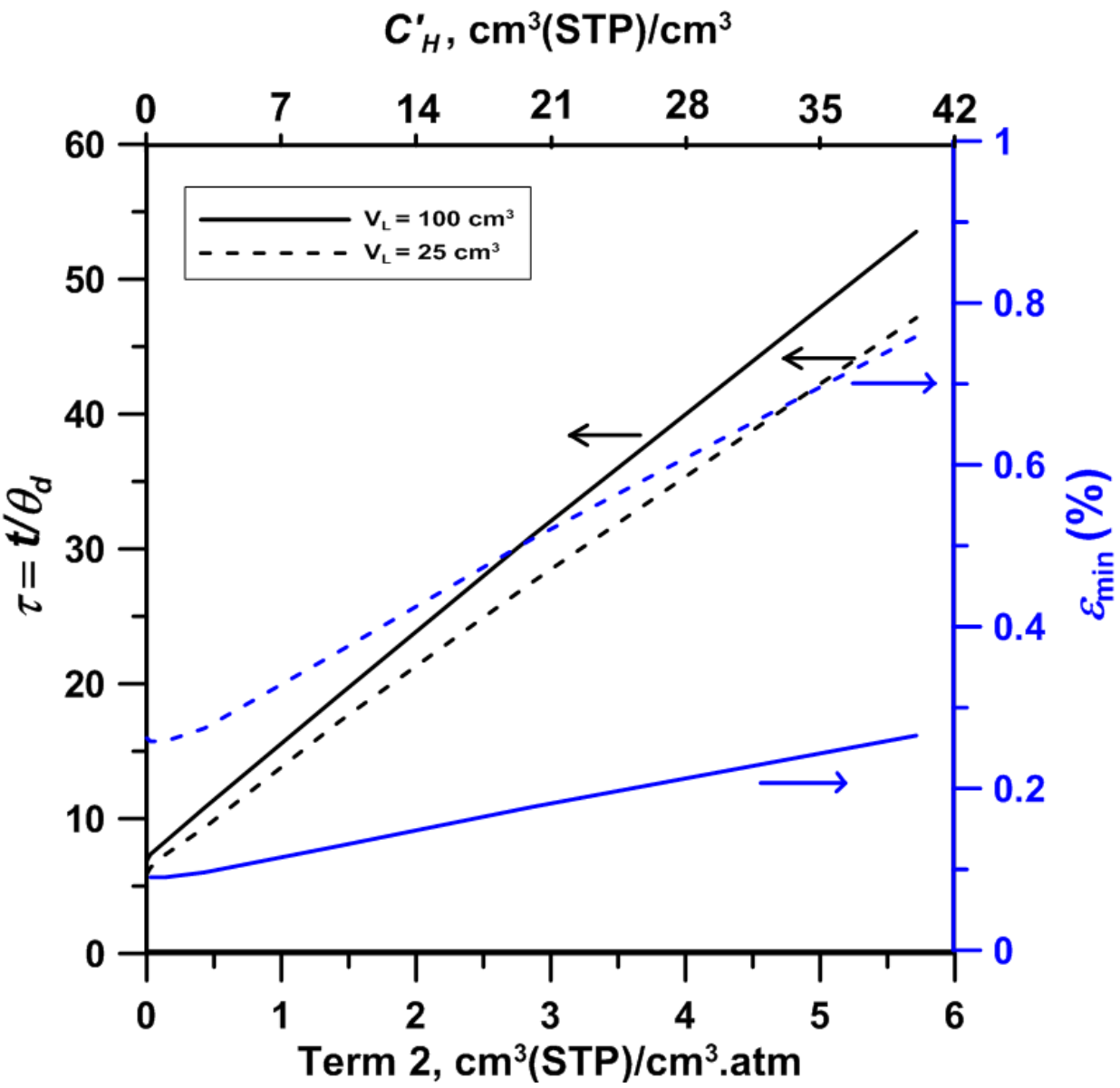

Figure 5.8a: The effect of the hole capacity parameter C'_H on the time necessary to reach the minimum error (τ) and on the magnitude of this minimum error (ε_{min}) for two different downstream volumes (25 & 100 cm^3). Simulation parameters: b = 0.5 atm^{-1}, p = 5 atm, L = 2.35×10^{-5} m, D = 4.52×10^{-12} $m^2\cdot s^{-1}$.

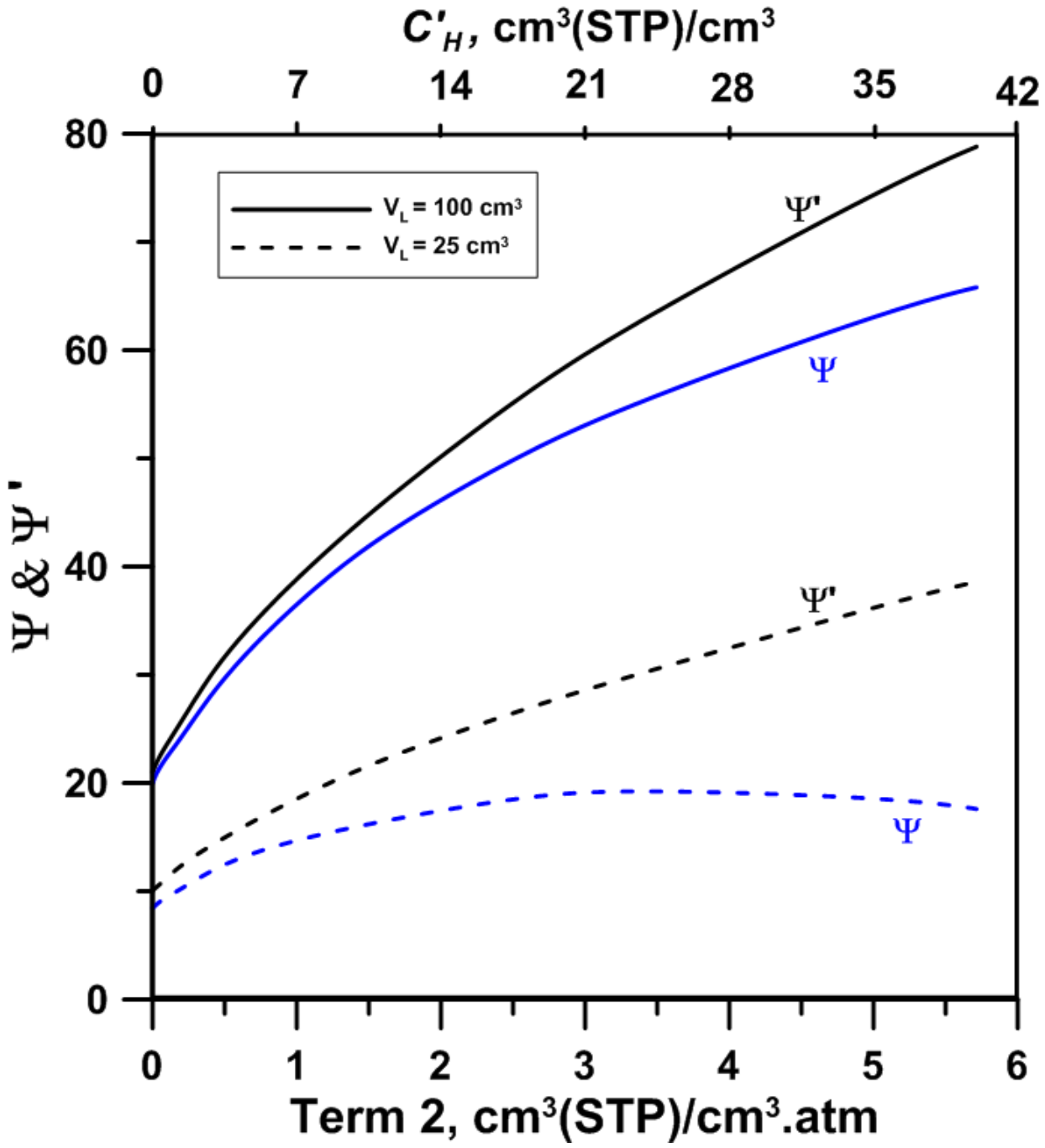

Figure 5.8b: The effect of the hole capacity parameter C'_H on the period of time to stay within 1% and within ε_{min} + 1% (ψ and ψ' respectively) for two downstream volumes (25 & 100 cm^3). Simulation parameters are: b = 0.5 atm^{-1}, p = 5 atm, L = 2.35×10^{-5} m, D = 4.52×10^{-12} $m^2 \cdot s^{-1}$.

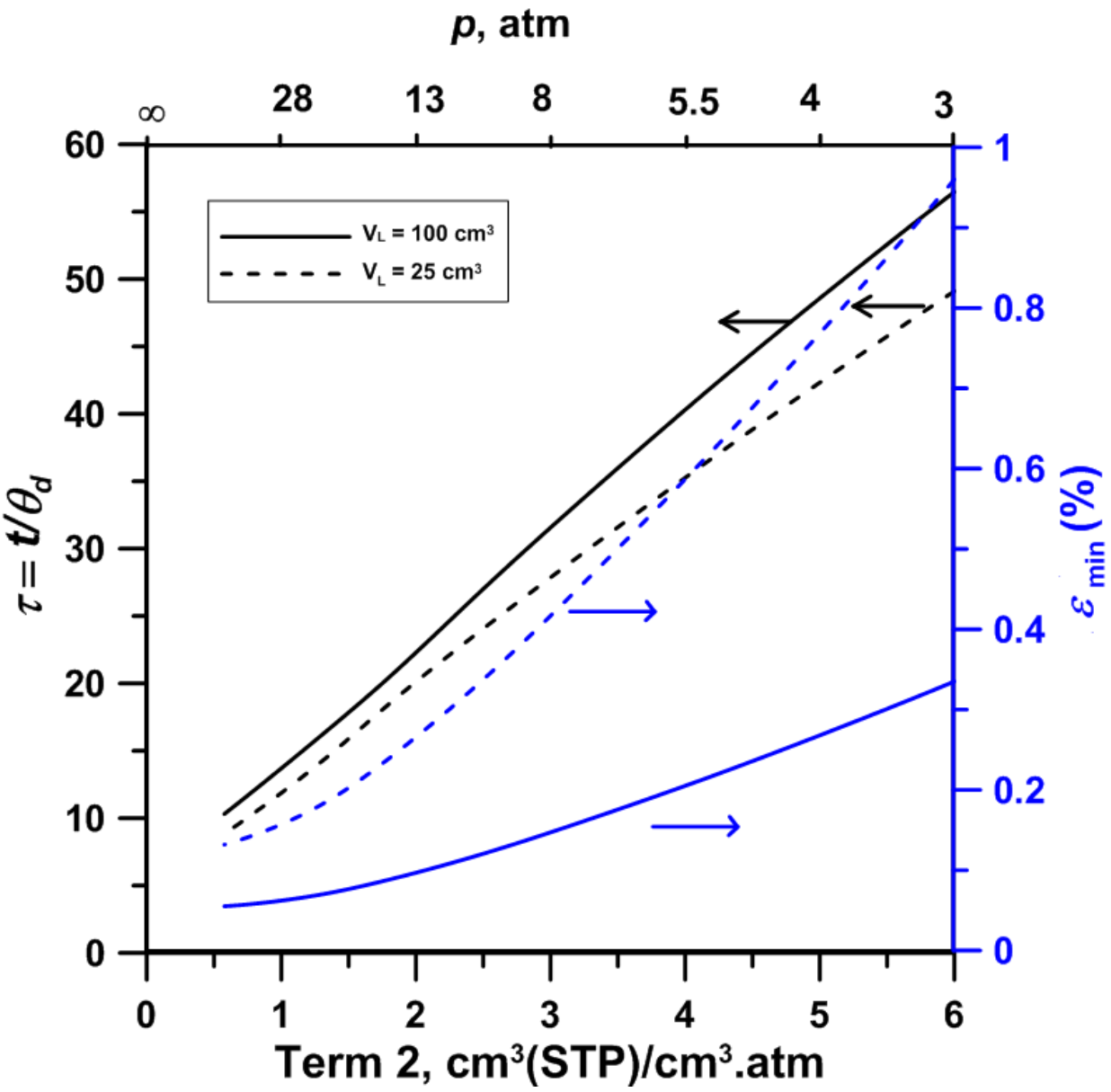

Figure 5.9a: The effect the operating pressure p on the time of reaching minimum error (τ) and on the magnitude of this minimum (ε_{min}) for two different downstream volumes (25 & 100 cm^3). Simulation parameters are: C'_H = 30 $cm^3(STP)\cdot cm^{-3}$, b = 0.5 atm^{-1}, L = 2.35×10^{-5} m, D = 4.52×10^{-12} $m^2\cdot s^{-1}$.

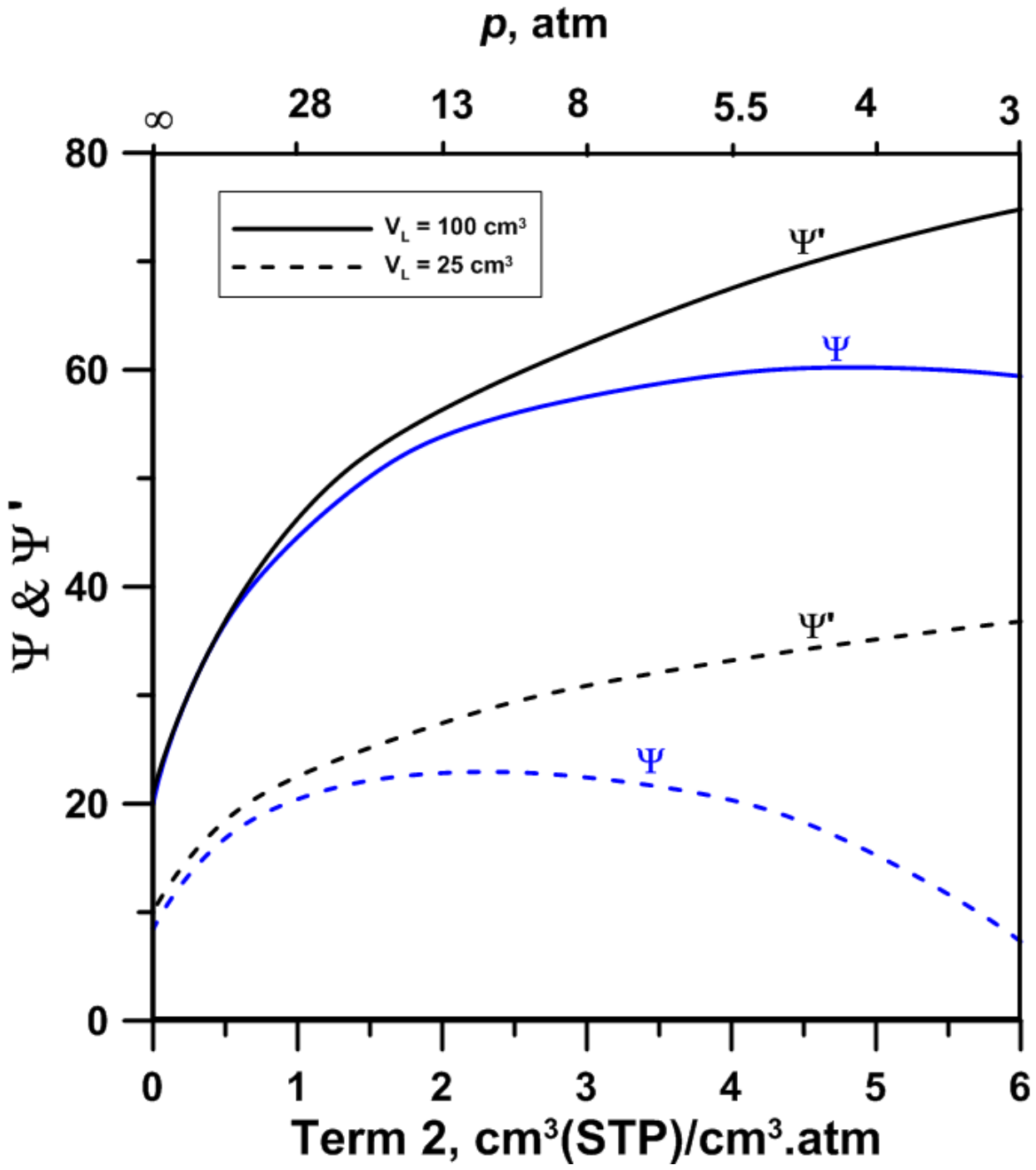

Figure 5.9b: The effect the operating pressure p on the period of time to stay within 1% and within ε_{min} + 1% (ψ and ψ' respectively) for two downstream volumes (25 & 100 cm^3). Simulation parameters are: C'_H = 30 $cm^3(STP)\cdot cm^{-3}$, b = 0.5 atm^{-1}, L = 2.35×10^{-5} m, D = 4.52×10^{-12} $m^2\cdot s^{-1}$.

5.5 Conclusions

Dynamic membrane gas permeation experiments have been simulated numerically in order to assess the effect of gas accumulation at the permeate side of the membrane on the accuracy the time-lag method. It was assumed that membranes followed a dual mode sorption with instantaneous equilibrium between gas molecules in the mobile Henry's sites and the immobile Langmuir sites. To establish a reference for comparison, simulations in which the permeate interface of the membrane was assumed to have a zero concentration during the entire experiment, were also carried out. The effect of non-linearity of the sorption isotherm, assessed by the magnitude of the Langmuir portion of the isotherm, on the dimensionless time to reach pseudo-steady state permeation, the minimum error due to gas accumulation, and the a rate of change in gas permeation at pseudo-steady state have been quantitatively evaluated and discussed. In general, as the sorption isotherm become more non-linear, the time to reach pseudo steady-state and the magnitude of the minimum error due to gas accumulation increase. However, the exact nature of these increases depends on the specific sorption parameter (capacity, affinity, pressure) by which non-linearity increases. Despite an increase in the time required to reach pseudo-steady state and thus a greater downstream pressure due to gas accumulation, an increase in non-linearity of sorption isotherm reduces the rate of decrease in permeation rate at pseudo steady-state. From the practical point of view, this indicates the possibility of accurate characterization of dual-mode sorption membranes by the classical time-lag method despite unavoidable error due to gas accumulation at the permeate side of membrane.

5.6 Nomenclature

Symbol	Description
b:	Affinity factor, atm^{-1}
C:	Concentration inside the membrane, mol/m^3
C_D:	Dissolved concentration by Henry's law, mol/m^3
C_H :	The immobilized species adsorbed on Langmuir sites, mol/m^3
C'_H:	Capacity parameter, cm^3STP/cm^3
D:	Diffusivity, m^2/s
D_{app}:	Apparent diffusivity, m^2/s

D': Asymptote diffusivity, m^2/s

L: Membrane thickness, m

P: Permeability, mol/m s Pa

p: Pressure, Pa

p_0 Upstream initial pressure, Pa

p_L Downstream pressure, Pa

S: Solubility, mol/Pa m^3

V_L: Downstream volume, m^3

x: Membrane coordinate, m

Greek symbols

Δx_1: Backward mesh size, m

Δx_2: Forward mesh size, m

ε: The relative error in the apparent diffusivity, %

ε_{min}: The minimum relative error on the apparent diffusivity, %

Ψ: The period of time at which ε is within 1%, [-]

Ψ': The period of time at which ε is within ε_{min} +1%, [-]

θ_d: Downstream time-lag, s

τ: Dimensionless time, [-]

5.7 Acknowledgement

The authors gratefully acknowledge the financial support for this project provided by the Natural Science and Engineering Research Council of Canada.

5.8 References

[1] R. W. Baker, Membrane Technology and Application, Third Edition, Membrane Technology and Research, Inc, John Wiley & Sons, Ltd, Newark, California, 2012.

[2] J. Crank, Mathematics of Diffusion, Second Edition, Clarendon Press, Oxford, Eng, 1975

[3] M. Mulder, Basic Principles of Membrane Technology, Kluwer Academic Publishers, Dordrecht, the Netherlands, 1992.

[4] R. E. Kesting, and A. K., Fritzsche, Polymeric Gas Separation Membranes, John Wiley and Sons, Inc, New York, NY, 1993.

[5] H. A. Daynes, The Process of Diffusion through a Rubber Membrane, R. Soc. Proc. A97 (1920), 286-307.

[6] R.M., Barrer, Permeation, Diffusion and Solution of Gases, Trans. Faraday Soc., 35 (1939), 628-64.

[7] D. R Paul, A., T. Dibenedetto, Diffusion in Amorphous Polymers, Journal of Polymer Science, Part C, No. 10 (1965), 17-44.

[8] P. Spacek, M. Kubin, Diffusion in Gels, Journal of Polymer Science, Part C, No. 16 (1967), 705-714.

[9] J. A. Barrie, H. G. Spencer, A. Quig, Transient Diffusion through a Membrane Separating Finite and Semi-infinite Volumes, Journal of Chemical Society: Faraday Transition 1, 71 (1975), 2459-2467.

[10] G.J Van-Amerongen, Influence of Structure of Elastomers on Their Permeability to Gases, 5 (1949), 307-332.

[11] J. C. Shah, Analysis of permeation data: evaluation of the lag time method, International Journal of pharmaceutics, 90 (1993) 161-169.

[12] R. C. L. Jenkins, P. M. Nelson, L Spirer, Calculations of the Transient Diffusion of Gas through a Solid Membrane in to A Finite Outflow Volume, Transactions of the Faraday Society, 66 (1970), 1391-1401.

[13] P. Taveira, A. Mendes, C. Costa, On the determination of diffusivity and sorption coefficients using different time-lag models, Journal of Membrane Science, 221 (2003), 123-133.

[14] P. Meares, The diffusion of Gases Through Polyvinyl Acetate, Journal of American Chemical Society, 76 (1954), 3415-3422.

[15] A. S. Michaels, W.R. Vieth, J. A. Barrie, Diffusion of Gases in Polyethylene Terephthalate, Journal of applied Physics, 34 (1963), 13-20.

[16] W. R. Vieth, K. J. Sladek, A model for diffusion in a glassy polymer, Journal of colloid Science, 20 (1965), 1014-1033.

[17] W. R. Vieth, C. S. Frangoulis, J. A. Rionda, Kinetics of sorption of Methane in Glassy polystyrene, Journal of Colloid and interface science, 22 (1966), 454-491.

[18] J. H. Petropoulos, Quantitative analysis of gaseous diffusion in glassy polymers, Part A-2, 8 (1970), 1797-1701.

[19] D.R. Paul, W. J. Koros, Effect of partially immobilizing sorption on permeability and the diffusion time-lag, Journal of Polymer science: Polymer physics edition, 14(1976), 675-685.

[20] M. A. Islam, H. Buschatz, Gas permeation through a glassy polymer membrane: chemical potential gradient or dual mobility mode?, Chemical Engineering Science, 57 (2002), 2089-2099.

[21] D. R. Paul, Effect of Immobilizing Adsorption on the diffusion time-lag, Journal of membrane science: Part A-2, 7(1969), 1811-1818.

[22] W. J. Koros, D. R. Paul, A. A. Rocha, Carbon Dioxide Sorption and Transport in Polycaronate, Journal of Polymer Science: Polymer Physics Edition, 14 (1976), 687-702.

[23] W. J. Koros, A. H. Chan, D. R. Paul, Sorption and transport of various gases in polycarbonate, Journal of Membrane Science, 2 (1977), 165-190.

[24] W. J. Koros, D. R. Paul, Transient and Steady-State Permeation in Poly(ethylene Terephthalate) above and below the glass transition, Journal of Polymer Science, Polymer Physics Edition, 16 (1978), 2171-2187.

[25] J. A. Tshudy, C. V. Frankenberg, A model Incorporating Reversible Immobilization for Sorption and Diffusion in Glassy Polymers, Journal of Polymer Science: Polymer Physics Edition, 11 (1973), 2027-2037.

[26] E. Favre, N. Morliere, D. Roizard, Experimental Evidence and Implications of an Imperfect Upstream Pressure Step for the Time-lag Technique, Journal of Membrane Science, 207 (2002), 59–72.

[27] Y.K. Zhang, N. M. Kocherginsky, Time lag for Transmembrane Transport without Interface Equilibrium, Journal of Membrane Science, 225 (2003), 105-114.

[28] J. Guo, T. A. Barbari, A Dual Mode, Local Equilibrium Relaxation Model for Small Molecule Diffusion in a Glassy Polymer, Macromolecules, 41 (2008), 238-245.

[29] D. Bhatia, W. R. Vieth, The penetrant time-lag for the Dual-sorption case with Langmuir Isotherms, Journal of Membrane Science, 6 (1980), 351-357.

[30] G. H. Fredrickson, E. Helfand, Dual-Mode Transport of Penetrant in Glassy Polymers, Macromolecules, 18 (1985), 2201-2207.

[31] H. L. Frisch, The time-lag in diffusion, The Journal of Physical Chemistry, 61. No. 1 (1957), 93-95.

[32] M. Al-Ismaily, J. G. Wijmans, B. Kruczek, A Shortcut Method for Faster Determination of Permeability Coefficient from Time Lag Experiments, Journal of Membrane Science, 423-424 (2012), 165-174.

[33] B. Kruczek, H. L. Frisch, R. Chapanian, Analytical solution for the effective time-lag of a membrane in a permeate tube collector is which Knudsen flow regime exists, Journal of membrane Science, 256 (2006), 57-63, 2006

[34] S. Lashkari, B. Kruczek, Effect of Resistance to Gas Accumulation in Multi-tank Receivers on Membrane Characterization by the Time lag Method: Analytical Approach for Optimization of the Receiver, Journal of Membrane Science, 360 Issues 1-2 (2010), 442-453,

[35] B. Carnahan, H. A. Luther, J. O. Wilkes, Applied Numerical Methods, John Wiley & Sons, New York, NY, 1969.

[36] H. Wu, N. Al-Qasas, B. Kruczek, J. Thibault, Simulation of Time-Lag Experiment Using Finite Differences, Fluid flow, Heat and Mass Transfer, 2 (2015), 14-25.

[37] K. F. Finger, A. P. Lemberger, L. W. Higuchi, L.W. Busse, D. E. Wurster, Investigation and Development of Protective Ointment IV: The influence of Active Fillers on the permeability of Semisolids, Journal of American pharmaceutical Association, 49 No.9 (1960), 569-573.

[38] C. F. Most, Some Filler Effects on Diffusion in Silicone Rubber, Journal of Applied Polymer Science, 14 (1970), 1019-1024.

[39] D. R. Paul, D. R. Kemp, The Diffusion Time lag in Polymer Membranes Containing Adsorptive Fillers, Journal of Polymer Science, 41(1973), 79-93.

[40] D. R. Kemp, D. R. Paul, Gas sorption in Polymer Membranes containing Adsorptive fillers, Journal of Polymer Science: Polymer Physics Edition, 12 (1974), 485-500.

[41] W. A. Rogers, R. S. Burtiz, D. Alpert, Diffusion Coefficient, Solubility and Permeability for Helium in Glass, Journal of Applied Physics, 25 (1954), 868-875.

[42] P. Li, T. S. Chung, D. R. Paul, Gas Sorption and Permeation in PIM-1, Journal of Membrane Science, 432 (2013), 50-57.

[43] J. Lianda, F. R. Sheu, R. R. Chern, H. B. Hopfenberg, Gas Sorption and Transport in Poly (phenylene oxide) (PPO) and Aryl-Brominated PPO Membranes, Chines Journal of Polymer Science, 7 No.4, (1989), 306-314.

[44] M. J. Thundyil, Y. H. Jois, W. J. Koros, Effect of Permeate Pressure on the Mixed Gas Permeation of Carbon Dioxide and Methane in Glassy Polyimide, Journal of Membrane Science, 152 (1999), 29-40.

[45] L. Garrido, M. Lopez-Gonzalez, E. Saiz, E. Riande, Molecular Basis of Carbon Dioxide Transport in Polycarbonate Membranes, Journal of Physical Chemistry, B, 112 (2008), 4253-4260.

Chapter 6

A New Characterization Method of Membranes with Nonlinear Sorption Isotherm Systems Based on Continuous Upstream and Downstream Time-Lag Measurements.

Neveen Al-Qasas, Jules Thibault and Boguslaw Kruczek*

University of Ottawa, Department of Chemical and Biological Engineering

161 Louis Pasteur, Ottawa, Ontario, Canada K1N 6N5

Abstract

The upstream time-lag method for complete immobilization and instantaneous equilibrium model has been derived using Frisch's asymptotic solution. The advantages of using simultaneously the upstream and downstream time-lag measurements have been discussed. This opens the possibility of fully characterizing a membrane with two dynamic gas permeation experiments at two different pressures. The analytically derived ratio between the upstream and downstream time lag for a nonlinear system is used as an extra equation that reduces the number of permeation experiments required to fully recover the kinetic and sorption parameters. Finite difference numerical modeling was utilized to examine the proposed method under realistic boundary conditions. The accuracy of the recovered kinetic and sorption parameters is promising and allows the elimination of challenging sorption measurement involving dense membranes.

Keywords: Membrane characterization; upstream and downstream time lags; nonlinear isotherm; Dual-mode sorption model.

Publication status: to be submitted to the Journal of Membrane science.

6.1. Introduction

Time-lag method, which originates from the analysis of Daynes [1], is the most common approach for complete characterization of polymeric gas separation membranes. In essence, one carefully executed gas permeation experiment allows evaluation of the gas diffusivity in membrane (D) from the observed time lag and the gas permeability in membrane (P) from steady-state rate of pressure rise. In turn, the gas solubility in membrane (S) is evaluated from the ratio of P and D. The conventional time-lag analysis is limited to membranes in which gas sorption follows Henry's law, i.e. to rubbery membranes and ideal gases. In practice most gas separation membranes are made from glassy polymers, in which gas sorption does not follow a linear isotherm, i.e. S is not constant, but depends on the gas concentration in the membrane (C).

It is generally accepted that gas sorption in glassy polymers follows a dual-mode sorption, first proposed by Meares [2]. More specifically, there are two different sorption mechanisms that occur simultaneously. One follows Henry's law in normally densified regions and the other one follows Langmuir's model in intersegmental defects that are unique to amorphous polymers below the glass transition temperature. Mathematically, the dual-mode sorption model is described by:

$$C = C_D + C_H = Sp + \frac{C'_H bp}{1 + bp} \tag{6.1}$$

where C_D and C_H refer to the gas concentrations in Henry's and Langmuir's sites, respectively, p is the gas pressure in contact with the membrane, and C'_H and b are the hole saturation and the hole affinity constants, respectively. Variations of dual-mode sorption to explain non-linear sorption in glassy polymers were also proposed. For example, Bhatia and Vieth [3] suggested the presence of two different types of Langmuir's sites with different affinities. Weiss et al. [4] went even further postulating a sorption model based on continuous distribution of Langmuir's sites.

In the simplest case of dual-mode sorption, it is assumed that gas molecules in Langmuir's sites are completely immobilized, but at the same time they are in instantaneous equilibrium with the mobile gas molecules, i.e. those dissolved in Henry's sites [5]. Some researchers postulate that gas molecules in Langmuir's sites are not completely immobilized and their diffusivity is a fraction of the diffusivity in mobile Henry's sites; this is referred to as a

partial immobilization model [6-12]. In addition, some researchers argue to relax the assumption of the instantaneous equilibrium between the two gas populations [13-16]. The complete characterization of membranes, which follow dual-mode sorption, using the time-lag method even in the simplest case of complete immobilization and instantaneous equilibrium between the Langmuir's and Henry's sites is challenging. It requires evaluation of five parameters, i.e., in addition to *S*, *D* and *P*, also C'_H and *b* must also be determined. Using the concept of asymptotic solution, originally proposed by Frisch [17], Paul derived an expression for the downstream time-lag, which is a function of *S*, *D*, C'_H and *b* [18]. Consequently, the evaluation of *D* from the downstream time lag requires *S*, C'_H and *b*, which are normally determined from a sorption isotherm. The time-lag expressions derived by Paul [18] assume that gas concertation at the feed and permeate interfaces of the membrane are constant at all time. In reality, this is not possible, because the rate of gas transport across the membrane in the time-lag experiments relies on gas accumulation at the permeate side of membrane.

To maintain constant gas concentration at the permeate interface of the membrane, Al-Qasas et al. proposed continuous evacuation of the permeate side of membrane and monitoring of the pressure decay at the feed side of the membrane [19,20], which is technically feasible [21]. In this approach, the concentration of the gas at the upstream interface of the membrane is not constant, but the concentration of the gas at the permeate interface is equal to zero at all time. In this case, one can measure the upstream time lag and carry out the analyses similar to those for the downstream time lag. The determination of the downstream and upstream time lags requires reaching steady state permeation, or more precisely pseudo steady-state permeation. On the other hand, by monitoring the upstream pressure decay one can characterize the membrane before the steady state conditions are attained [19,20]. Right after initiation of gas permeation, but before the gas molecules emerge at the permeate side of the membrane, the membrane behaves as a semi-infinite solid and the pressure decay at the feed side is a linear function of the square root of time [21]. A deviation from this linear behavior after the gas emerges at the permeate side, but before the steady-state permeation is reached provides the basis for membrane characterization [20]. The concept of deviation from semi-infinite behavior was extended to the case of two membranes in series, which is suitable for the characterization of composite membranes [19]. The analyses proposed by Al-Qasas et al. [19,20] are applicable only for membranes in which

sorption follows Henry's law. These methods have not yet been extended to membranes with dual-mode sorption.

Recently, we have numerically examined the downstream time-lag method for membranes which follow dual-mode sorption with complete immobilization and instantaneous equilibrium between the Langmuir's and Henry's sites, under realistic conditions when gas accumulation leads to time-dependent changes in gas concentration at the permeate interface of the membrane [22]. Due to gas accumulation, the time lag is not constant; it reaches a maximum value, which is always less than the ideal time lag, i.e. the time lag that would be measured if the concentration at the permeate interface of the membrane were constant. However, the difference between the ideal and the maximum time lag is generally within 1% [22]. This validates the application of the time-lag analysis developed by Paul [18] for the characterization of glassy polymer membranes under realistic boundary conditions. However, in absence of S, C'_H and b from independent sorption experiments, the complete characterization of this type of membranes would require the analysis of four time lag experiments carried out at four different feed pressures.

In this paper, we propose a new membrane characterization method that relies on simultaneous monitoring of pressure decay and pressure rise and continuous evaluation of the respective instantaneous upstream and downstream time lags as well as their ratio. For the membranes with a linear sorption isotherm under the ideal boundary conditions (constant upstream and downstream interfaces concentrations) the absolute value of this ratio is equal to 2, but for the membranes with nonlinear sorption isotherms this ratio is less than 2 and depends on the values of sorption parameters. The unique ratio of the upstream and downstream time lags, allows for the complete membrane characterization based two gas permeation experiments performed at two different feed pressures without relying on sorption isotherm. The theoretical basis of the proposed method is presented by assuming the ideal boundary conditions at both membrane interfaces. In the presence of the real boundary conditions the ratio of the time lags does not approach to a unique value corresponding to the ideal boundary conditions; however, the latter is recovered by using the maximum downstream time lag. The new method is tested numerically under real boundary conditions using S, D, C'_H and b of several literature-reported membranes.

6.2. Theoretical Background.

Applying Fick's second law of diffusion to a system that follows the dual-mode sorption with complete immobilization in Langmuir's sites and instantaneous equilibrium between Henry's and Langmuir's sites yields the following differential equation:

$$\frac{\partial C_D}{\partial t}\left(1+\frac{C'_H b/S}{\left(1+C_D b/S\right)^2}\right)=D\frac{\partial^2 C_D}{\partial x^2} \tag{6.2}$$

Using the concept of asymptotic solution of Frisch [17], Paul [18] solved Eq. (6.2) for the following set of the initial and boundary conditions (IBC):

$$C_D\left(t<0,x\right)=C_{Di} \tag{6.3a}$$

$$C_D\left(t,0\right)=C_{D0} \tag{6.3b}$$

$$C_D\left(t,L\right)=C_{DL} \tag{6.3c}$$

The corresponding expression for the downstream time lag is given by:

$$\theta_d=\frac{L^2}{6D}\left\{1-3\delta+6K\left[\frac{\left(\delta+0.5\right)\alpha^2+\alpha-\left[1+\left(1+\delta\right)\alpha+\delta\alpha^2\right]\ln\left(1+\alpha\right)}{\left(1+\delta y\right)\left(1+\varepsilon y\right)\alpha^3}\right]\right\} \tag{6.4}$$

where:

$$\delta=\frac{\left(C_{Di}-C_{DL}\right)}{\left(C_{D0}-C_{DL}\right)} \tag{6.5a}$$

$$\varepsilon=\frac{C_{DL}}{C_{D0}} \tag{6.5b}$$

$$K=\frac{C'_H b}{S} \tag{6.5c}$$

$$y=C_{D0}\frac{b}{S} \tag{6.5d}$$

$$\alpha = \frac{y(1-\varepsilon)}{(1+\varepsilon y)} \tag{6.5e}$$

In the special case, for which $C_{Di} = C_{DL} = 0$, Eq. (6.4) simplifies to:

$$\theta_d = \frac{L^2}{6D}\left[1 + Kf(y)\right] = \frac{L^2}{6D_L} \tag{6.6}$$

It follows from Eq. (6.6) that the apparent downstream diffusivity D_L is related to the actual diffusivity D as follows:

$$D_L = \frac{D}{1+Kf(y)} \text{ and } f(y) = 6y^{-3}\left[0.5y^2 + y - (1+y)\ln(1+y)\right] \tag{6.7}$$

If gas sorption follows Henry's law, the coefficient K defined by Eq. (6.5c) becomes zero and Eq. (6.6) simplifies to the conventional time-lag equation:

$$\theta_d = \frac{L^2}{6D} \tag{6.8}$$

The analysis of Paul [18] indicates that the apparent time lag of glassy polymer membranes is increased by a factor that depends on the sorption parameters of the tested membrane. This factor can be calculated using Eq. (6.7) provided that the sorption parameters of the membrane (S, C'_H and b) are known. The latter can be evaluated from a sorption isotherm of the membrane. However, generation of the sorption isotherm for a dense polymer membrane is challenging, and typically the required sorption experiments are carried out using a polymer powder rather than the actual membrane. Alternatively, one could also carry out a so-called desorption permeation experiment [18], with the corresponding time lag providing another piece of information for membrane characterization. However, desorption permeation experiments are not practical as they require a step decrease in pressure on one side of the membrane, and monitoring of the corresponding rate of pressure increase. In addition, the desorption permeation experiment would need to be carried out separately from the downstream (absorption) permeation experiment. On the other hand, the downstream permeation experiment could be carried out simultaneously with an upstream pressure decay experiment. More specifically, in addition to monitoring the rate of gas permeation from the membrane after a step change in feed pressure, the rate of gas

permeation into the membrane could also be monitored in a properly designed system [19-21]. However, to our best knowledge an expression equivalent to Eq. (6.4) for the upstream time lag is not available in the literature.

6.2.1 Expression for the upstream time lag of membrane

The following analysis presents a derivation of the upstream time lag using Frisch's method [17] for a membrane with dual-mode sorption, complete immobilization in Langmuir's sites and instantaneous equilibrium between Henry's and Langmuir's sites.

The governing PDE along with the IBC for the upstream time lag are identical to those for the downstream time lag, and are given by Eqs. (6.2-6.3). The total amount of gas that has entered the membrane from the start of the experiment, resulting in a decrease in gas molecules from the upstream reservoir, will be referred to gas accumulation (obviously negative) and it can be obtained by integrating Eq. (6.2) first with respect to position, from 0 to z and then with respect to time from 0 to t:

$$\int_0^t \int_0^z \left[1 + \frac{K}{\left(1 + \frac{b}{S} C_D\right)^2} \right] \frac{\partial C_D}{\partial t} dx dt = \int_0^t \int_0^z \frac{\partial}{\partial x}\left(D \frac{\partial C_D}{\partial x} \right) dx dt \tag{6.9}$$

Performing the internal integration on the right hand side of Eq. (6.9) and rearranging the left hand side give:

$$\int_0^t \int_0^z \frac{\partial C_D}{\partial t} dx dt + \int_0^t \int_0^z \frac{K}{\left(1 + \frac{b}{S} C_D\right)^2} \frac{\partial C_D}{\partial t} dx dt = \int_0^t \left(D \frac{\partial C_D}{\partial x} \right)_z - \left(D \frac{\partial C_D}{\partial x} \right)_0 dt \tag{6.10}$$

It can be recognized that the amount of negative gas accumulating upstream of the membrane is:

$$\frac{Q_{x=0}}{A} = \int_0^t \left(D \frac{\partial C_D}{\partial x} \right)_0 dt \tag{6.11}$$

Integrating the first term on the left hand side of Eq. (6.10) with respect to time, and substituting Eq. (6.11) leads, after rearrangement, to:

$$\frac{Q_{x=0}}{A}=\int_0^t\left(D\frac{\partial C_D}{\partial x}\right)_z-\int_0^z C_D dx+C_{Di}z-\int_0^t\int_0^z\frac{K}{\left(1+\frac{b}{S}C_D\right)^2}\frac{\partial C_D}{\partial t}dxdt \tag{6.12}$$

Integrating the last term on the right hand side of Eq. (6.12) with respect to time gives:

$$\frac{Q_{x=0}}{A}=\int_0^t\left(D\frac{\partial C_D}{\partial x}\right)_z-\int_0^z C_D dx+C_{Di}z-\int_0^z\frac{K\left(C_D-C_{Di}\right)dx}{\left(1+\frac{b}{S}C_D\right)\left(1+\frac{b}{S}C_{Di}\right)} \tag{6.13}$$

Integrating Eq. (6.13) with respect to z from 0 to L yields:

$$\int_0^L\frac{Q_{x=0}}{A}dz=\int_0^L\int_0^t\left(D\frac{\partial C_D}{\partial x}\right)_z dtdz-\int_0^L\int_0^z C_D dxdz+\int_0^L C_0 zdz-\int_0^L\int_0^z\frac{K\left(C_D-C_{Di}\right)}{\left(1+\frac{b}{S}C_D\right)\left(1+\frac{b}{S}C_{Di}\right)}dxdz \tag{6.14}$$

Thus:

$$\frac{Q_{x=0}}{A}=\frac{t\,D\left(C_{DL}-C_{D0}\right)}{L}-\frac{1}{L}\int_0^L\int_0^z C_D dxdz+\frac{LC_{Di}}{2}-\frac{1}{L}\int_0^L\int_0^z\frac{K\left(C_D-C_{Di}\right)}{\left(1+\frac{b}{S}C_D\right)\left(1+\frac{b}{S}C_{Di}\right)}dxdz \tag{6.15}$$

To obtain the asymptotic solution, the concentration C_D in Eq. (6.14) can be replaced by the steady state concentration which is given by following equation:

$$C_D=\left(C_{D0}-C_{DL}\right)\left(1-\frac{x}{L}\right)+C_{DL}=C_{D0}-\frac{x}{L}C_{D0}+\frac{x}{L}C_{DL} \tag{6.16}$$

Substituting Eq. (6.16) into Eq. (6.15) leads to:

$$\begin{aligned}\frac{Q_{x=0}}{A}&=\frac{tD\left(C_{DL}-C_{D0}\right)}{L}-\frac{1}{L}\int_0^L\int_0^z\left[C_{D0}-\frac{x}{L}C_{D0}+\frac{x}{L}C_{DL}\right]dxdz+\frac{LC_{Di}}{2}\\&-\frac{1}{L}\int_0^L\int_0^z\frac{K\left(C_{D0}-\frac{x}{L}C_{D0}+\frac{x}{L}C_{DL}-C_{Di}\right)}{\left(1+\frac{b}{S}C_{D0}-\frac{b}{S}\frac{x}{L}C_{D0}+\frac{b}{S}\frac{x}{L}C_{DL}\right)\left(1+\frac{b}{S}C_{Di}\right)}dxdz\end{aligned} \tag{6.17}$$

Performing the double integration of the remaining terms of Eq. (6.17) yields:

$$\frac{Q_{x=0}}{LA}=\frac{D\left(C_{DL}-C_{D0}\right)}{L^2}t-\frac{2C_{D0}}{6}-\frac{C_{DL}}{6}+\frac{C_{Di}}{2}-\frac{K}{2\frac{b}{S}\left(1+\frac{b}{S}C_{Di}\right)}$$
$$+K\frac{\left[\left(\frac{b}{S}C_{DL}+1\right)\log\left(\frac{b}{S}C_{DL}+1\right)-\frac{b}{S}C_{DL}+\frac{b}{S}C_{D0}-\left(\frac{b}{S}C_{D0}+1\right)\log\left(\frac{b}{S}C_{D0}+1\right)\right]}{\left(\frac{b}{S}\right)^3\left[C_{DL}-C_{D0}\right]^2} \quad (6.18)$$
$$-K\frac{\log\left(aC_{D0}+1\right)}{\left(\frac{b}{S}\right)^2\left[C_{DL}-C_{D0}\right]}$$

Eq. (6.18) represents the steady state rate of the negative gas accumulation upstream since pressure decreases at the upstream side) from the membrane, which is directly proportional to *t*. The intercept of Eq. (6.18) with time axis represents the upstream time lag. Thus, setting the left hand side of Eq. (6.18) to zero and solving for $t = \theta_u$ leads to:

$$\theta_u=-\frac{tD}{L^2}+\frac{2C_{D0}}{6\left(C_{DL}-C_{D0}\right)}+\frac{C_{DL}}{6\left(C_{DL}-C_{D0}\right)}-\frac{C_{Di}}{2\left(C_{DL}-C_{D0}\right)}+\frac{K}{2\frac{b}{S}\left(C_{DL}-C_{D0}\right)\left(1+\frac{b}{S}C_{Di}\right)}$$
$$-K\frac{\left[\left(\frac{b}{S}C_{DL}+1\right)\log\left(\frac{b}{S}C_{DL}+1\right)-\frac{b}{S}C_{DL}+\frac{b}{S}C_{D0}-\left(\frac{b}{S}C_{D0}+1\right)\log\left(\frac{b}{S}C_{D0}+1\right)\right]}{\left(\frac{b}{S}\right)^3\left[C_{DL}-C_{D0}\right]^3} \quad (6.19)$$
$$+K\frac{\log\left(\frac{b}{S}C_{D0}+1\right)}{\left(\frac{b}{S}\right)^2\left[C_{DL}-C_{D0}\right]^2}$$

Eq. (6.19) is the general form of the upstream time lag, which for $C_{Di}=C_{DL}=0$ simplifies to:

$$\theta_u=-\frac{L^2}{3D}\left[1+\frac{3K}{\left(\frac{b}{S}\right)^3{C_{D0}}^3}\left[\frac{\left(\frac{b}{S}\right)^2{C_{D0}}^2}{2}-\frac{b}{S}C_{D0}+\log\left(\frac{b}{S}C_{D0}+1\right)\right]\right] \quad (6.20)$$

Similarly to the downstream time lag, the expression for the upstream time lag can be written in a more compact form in terms of *y* defined by Eq. (6.5d):.

$$\theta_u = -\frac{L^2}{3D}\left[1 + KE(y)\right] \tag{6.21}$$

The apparent upstream diffusivity, D_0, is therefore related to the actual diffusivity in the mobile phase by the following equation:

$$D_0 = \frac{D}{1 + KE\ \ y} \text{ and } E\ \ y\ \ = 3y^{-3}\left[0.5y^2 - y + \ln\ \ 1 + y\ \ \right] \tag{6.22}$$

For the special case, when the sorption isotherm follows Henry's relation, term K will be zero and the expression of the upstream time lag reduces to the conventional upstream time lag:

$$\theta_u = -\frac{L^2}{3D} \tag{6.23}$$

6.2.2 Ratio of the upstream and downstream time lags

For a membrane under ideal boundary conditions, in which sorption follows Henry's law, the ratio of the of the upstream and downstream time lags (R_θ) is constant and equal to -2, regardless of the pressure at which gas permeation experiment is performed. On the other hand, in the case of membranes following dual-mode sorption with complete immobilization in Langmuir's sites and instantaneous equilibrium between Henry's and Langmuir's sites, this ratio is no longer constant:

$$R_\theta = \frac{\theta_u}{\theta_d} = -2R \tag{6.24}$$

where:

$$R = \frac{\left[y^3 + 1.5Ky^2 - 3Ky + 3K\ln(1+y)\right]}{\left[y^3 + 3Ky^2 + 6Ky - 6K(1+y)\ln(1+y)\right]} \tag{6.25}$$

R_θ is a function of y and K only and it varies from -1.1 to -2 (i.e., R varies from 0.55 to 1) depending on the degree of nonlinearity of the isotherm. The higher the degree of nonlinearity of the sorption isotherm, the smaller is the ratio. Using the definition of K given by Eq. (6.5c) and recognizing that $C_{D0} = pS$ and thus $y = pb$, Eq. (6.24) can be rewritten in terms of sorption parameters as follow:

$$R_\theta = -2\frac{\left[(bp)^3 + 1.5\frac{C'_H}{S}b^3p^2 - 3\frac{C'_H}{S}b^2p + 3\frac{C'_H}{S}b\ln(1+bp)\right]}{\left[(bp)^3 + 3\frac{C'_H}{S}b^3p^2 + 6\frac{C'_H}{S}b^2p - 6\frac{C'_H}{S}b(1+bp)\ln(1+bp)\right]} \tag{6.26}$$

It is important to note that the hole capacity constant and the solubility in the mobile phase in Eq. (6.26) are merged as a single parameter C'_H/S. Thus, R_θ depends only on C'_H/S, b and p, where p is the operating parameter that can be varied. In other words, assuming that the operating pressure is known, there are two unknowns in Eq. (6.26), C'_H/S and b. Thus, performing two gas permeation experiments at two different pressures, in which both the pressure rise at the permeate side and the pressure decay at the feed side are monitored simultaneously, should allow the determination of C'_H/S and b.

6.2.3 Numerical simulations

The ratio of the upstream and downstream upstream time lags given by Eq. (6.26) relies on the ideal initial and boundary conditions defined by Eqs. (6.3a-6.3c), in which $C_{Di} = C_{D0} = 0$. However, in reality because of the pressure decay at the feed side and pressure rise at the permeate side the concentrations at the respective interfaces will not be constant. Instead, the upstream and downstream boundary conditions are given by the following two equations:

$$\frac{V_u}{RT}\frac{dp_u}{dt} = -DA\left.\frac{\partial C_D}{\partial x}\right|_{x=0} \tag{6.27}$$

$$\frac{V_L}{RT}\frac{dp_d}{dt} = -DA\left.\frac{\partial C_D}{\partial x}\right|_{x=L} \tag{6.28}$$

where A, R, T, V_L, V_u, p_u and p_d are the membrane cross sectional area, the universal gas constant, the temperature, the downstream volume, the upstream volume, the upstream pressure, and the downstream pressure, respectively. The governing PDE, Eq. (6.2), cannot be solved using the asymptotic solution approach when the boundary conditions are specified by Eqs. (6.27-6.28).

To investigate the applicability of the concept of R_θ for more realistic boundary conditions, the governing PDE was solved numerically using a variable-mesh explicit finite difference method. Eq. (6.2) was discretized using Taylor's series expansion for the second derivative in space using a central difference in the explicit finite difference scheme. The concentration at the subsequent time step for each interior mesh point was calculated from [23,24]:

$$C_{D\,x}^{t+\Delta t} = C_{D\,x}^{t} + \frac{2D\Delta t}{\beta}\left(\frac{C_{D\,x+\Delta x_2}^{t} - C_{D\,x}^{t}}{\Delta x_2\left(\Delta x_1 + \Delta x_2\right)} - \frac{C_{D\,x}^{t} - C_{D\,x-\Delta x_1}^{t}}{\Delta x_1\left(\Delta x_1 + \Delta x_2\right)} \right) \tag{6.29}$$

where β is defined as follows:

$$\beta = 1 + \frac{K}{\left(1 + \frac{b}{S} C_{Dx}^{t}\right)^2} \tag{6.30}$$

Considering the other terms in Eq. (6.29), t is the current time, Δt the integration time step, Δx_1 is the backward mesh size, Δx_2 is the forward mesh size. The boundary conditions, Eq. (6.27) and Eq. (6.28), were also discretized and are given by:

$$\frac{V_0}{RT}\frac{\Delta p_u}{\Delta t} = DA\left[\frac{C_{D,\Delta x} - C_{D,0}}{\Delta x} \right]_{x=0} \tag{6.31}$$

$$\frac{V_L}{RT}\frac{\Delta p_L}{\Delta t} = DA\left[\frac{C_{D,L-\Delta x} - C_{D,L}}{\Delta x} \right]_{x=L} \tag{6.32}$$

The numerical simulations were carried out for the special case, in which initially the membrane is free from permeating species:

$$C_D\left(t < 0, x\right) = 0 \tag{6.33}$$

In addition, it was assumed that although the concentration of the mobile phase at the feed ($C_{D,0}$) and permeate ($C_{D,L}$) interfaces varied with time, they were linearly related with the respective feed and permeate pressures:

$$C_{D,0}\left(t\right) = Sp_u\left(t\right) \tag{6.34a}$$

$$C_{D,L}\left(t\right) = Sp_d\left(t\right) \tag{6.34b}$$

In all simulations, the feed and permeate volumes were the same, V_d = V_u = 100 cm^3; the temperature T = 298 K, the membrane area A = 0.00125 m^2, the membrane thickness L = 2.35×10^{-5} m, and the input diffusivity to the program D = 4.52×10^{-12} m/s^2.

Similarly to our previous work [22], numerical solutions utilized a variable-mesh size, with tighter mesh points at the two membrane boundaries. To adequately represent the interface concentration gradients, a total of 120 variable-size mesh points were used and to ensure

numerical stability ($D\Delta t/\Delta x^2 < 0.5$ based on the smallest step size), an integration time step of 0.00002 s was used [24]. The tighter mesh points at the interfaces allow for a more accurate evaluation of the concentration gradients, in particular at the feed side. The concentration gradients at both interfaces are then numerically integrated to generate the upstream and downstream pressure as a function of time.

The numerically-generated pressure data was used to determine the upstream and downstream time lags. For a given time t, the pressure data in a 10 s window (t – 5s, t + 5s) was used to obtain a linear trend line, which is extrapolated to the time axis. The resulting time-axis intercepts, the simulated time lags, were used to evaluate R_θ as a function of time. In addition, using the ideal initial and boundary conditions, the expression for the upstream time lag was verified numerically.

6.3. Results and Discussion

The purpose of the simultaneous determination of the upstream and downstream time lags is to facilitate a complete characterization of membranes following dual-mode sorption with complete immobilization in Langmuir's sites and instantaneous equilibrium between the permeant molecules in Henry's and Langmuir's sites. The following discussion explains the details of the proposed method, which is illustrated initially using the ideal boundary conditions. Considering unavoidable pressure decay at the feed side and pressure rise at the permeate side, the limitations of the proposed method in the case of real boundary conditions are then discussed.

6.3.1 The ratio of the upstream and downstream time-lags at ideal boundary conditions

Complete characterization of membranes that follow dual-mode sorption with complete immobilization in Langmuir's sites and instantaneous equilibrium between Henry's and Langmuir's sites requires evaluation of four parameters: S, C'_H, b and D. Then knowing S and D, the membrane permeability, P, is simply the product of S and D. In principle, four gas permeation experiments would be required to determine the four parameters, provided that the resulting apparent time lags were sufficiently different at different feed pressures. Assuming that it is possible to simultaneously monitor pressure decay and pressure rise in a single gas permeation experiment and that the ratio of the resulting upstream and downstream time lags depends on the feed pressure for membranes with nonlinear sorption, it is possible to reduce the

number of the required experiments. Moreover, recognizing that C'_H and S in Eq. (6.26), which correlates the ratio R_θ with sorption parameters are merged as C'_H/S, only two gas permeation experiments would be required.

Knowing the time-lag ratios $R_{\theta,1}$ and $R_{\theta,2}$ determined in experiments performed at pressures $p_{u,1}$ and $p_{u,2}$, respectively, Eq. (6.26) can be used to setup two equations with two unknowns, C'_H/S and b. Knowing C'_H/S and b, the constant K defined by Eq. (6.5c) can then be evaluated. In addition, recognizing that the surface concentration in the mobile phase is related to the upstream pressure through Eq. (6.34a), the parameter y defined by Eq. (6.5d) becomes simply $y = p_u b$. Consequently, using either the apparent upstream or downstream time lag, the diffusivity in the mobile phase (D) can be evaluated either from Eq. (6.22) or Eq. (6.7). The slope of the asymptote of the pressure versus time relation, $(dp/dt)_{t\to\infty}$, on either side of the membrane allows the determination of the membrane permeability:

$$P = \frac{VL}{p_u ART}\left(\frac{dp}{dt}\right)_{t\to\infty} \tag{6.35}$$

where V is either the upstream or the downstream volume for which the asymptote (upstream or downstream) is considered. Knowing P, the solubility in the mobile phase is simply, $S = P/D$ and then knowing S, C'_H can be evaluated from the previously determined C'_H/S.

The method outlined above will work provided that R_θ varies with feed pressure p_u, which is not immediately obvious from Eq. (6.26). Table 6.1 presents examples of sorption parameters for several membrane-gas combinations taken from the literature [7, 25-28] and the absolute R_θ values at different feed pressures. The dependence of the absolute value of R_θ on p_u for the case studies presented in Table 6.1 is fully explored in Figure 6.1.

Table 6.1: Recovery of C'_H/S and b for different combinations of gas/membrane systems (7 case studies) from the literature, using the ratio of the upstream and downstream time lags at two different feed pressures.

Case, Gas &Material		Sorption values		p_u [atm]	$\lvert R_\theta \rvert$ [-]	Used	Recovered values	
		b [atm^{-1}]	C'_H/S [atm]			p_u [atm]	C'_H/S [atm]	b [atm^{-1}]
1	CO_2 & PIM-1[25]	0.421	45.51	1	1.846	1 & 5	45.52	0.421
				2	1.748	2 & 5	45.53	0.421
				5	1.591	1 & 2	45.45	0.421
2	C_3H_6 & PIM-1[25]	2.604	8.748	0.5	1.671	1 & 2	8.739	2.605
				1	1.548	0.5 & 2	8.748	2.604
				2	1.446	2 & 5	8.748	2.604
				5	1.387	1 & 5	8.748	2.604
3	CO_2 & Silicon Rubber filled with 5A [7]	7.053	93.27	1	1.320	1 & 5	93.25	7.053
				2	1.221	3 & 5	93.25	7.053
				3	1.178	1 & 3	92.40	7.057
				5	1.138	2 & 5	93.25	7.053
4	CO_2 & Silicon Rubber filled with 5A [26]	19.84	132.5	0.15	1.479	0.15 &5	132.5	19.84
				1	1.176	1 & 5	132.5	19.84
				2	1.116	2 & 5	132.3	19.84
				5	1.071	0.15 &2	132.5	19.84
				10	1.060	2 & 10	132.5	19.84
5	CH_4 & PPoBr (36%) [27]	0.113	72.38	1	1.954	1 & 5	72.69	0.113
				5	1.823	1 & 15	72.46	0.113
				15	1.666	5 & 15	72.39	0.113
6	N_2 & PPO [27]	0.048	26.18	1	1.987	1 & 15	22.92	0.051
				15	1.882	1 & 30	26.11	0.048
				30	1.839	15 & 30	26.19	0.048
7	CH_4 & Glassy oriented polystyrene [28]	0.164	16.84	1	1.947	1 & 7	16.85	0.164
				7	1.789	7 & 30	16.84	0.164
				30	1.706	1 & 30	16.84	0.164

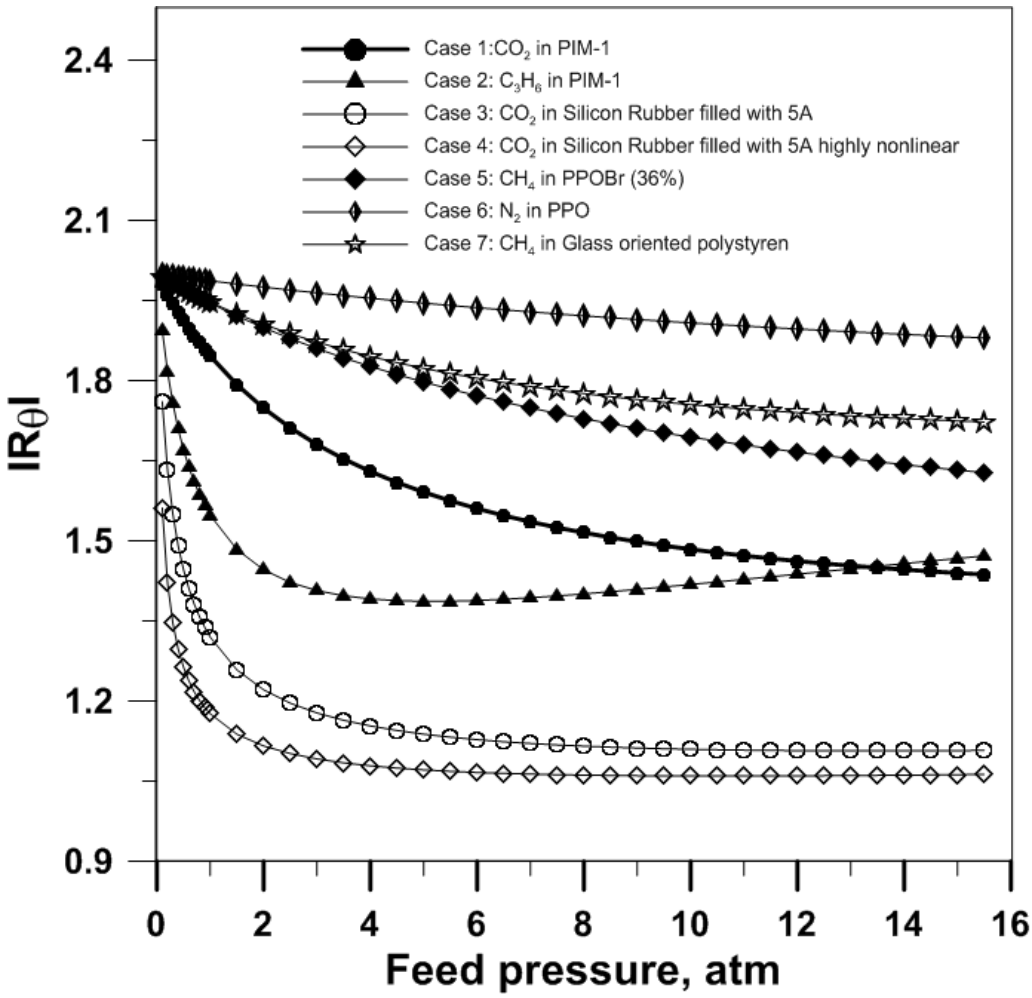

Figure 6.1: Effect of the feed pressure (p_u) on the absolute value of the ratio of the upstream and downstream time lags for different gas/membrane systems (7 case studies in Table 6.1) for which sorption parameters, C'_H/S and b, are available in the literature.

In general, with the exception of Case 2 in Figure 6.1, $|R_\theta|$ monotonically decreases with feed pressure. For Case 2, $|R_\theta|$ reaches the minimum at p_u c.a. 5 atm. In all cases, as $p_u \rightarrow 0$, $|R_\theta| \rightarrow 2$, which the value is characteristic for systems in which sorption isotherm follows Henry's law. The way $|R_\theta|$ decreases with p_u depends on the product of C'_H/S and b. The greater this product the more rapidly $|R_\theta|$ decreases with p_u at low feed pressures. On the other hand, $|R_\theta|$ for Cases 3 and 4, which have the largest product of C'_H/S and b among the cases studied in Table 6.1, is practically independent of p_u at high feed pressures. Case 2, for which $|R_\theta|$ reaches the minimum value, has the lowest C'_H/S yet because of a large b, it has the third highest product of

C'_H/S and b among the cases considered in Table 6.1. A large product of C'_H/S and b is indicative of highly nonlinear sorption isotherm.

Knowing the dependence of $|R_\theta|$ on p_u allows choosing a proper pair of feed pressures for the recovery C'_H/S and b using the proposed method based the ratio of the upstream and downstream time lags. More specifically, for a system with a highly nonlinear isotherm, the two feed pressures should be as low as possible, because of a strong dependence of $|R_\theta|$ on p_u at low feed pressures. On the other hand, for the cases for which the product of C'_H/S and b is relatively small, the two feed pressures should be significantly different. The selection of the pairs of feed pressures to recover the sorption parameters is illustrated in Table 6.1, which validates using the proposed time-lag ratio method for the complete characterization of membranes that follow dual-mode sorption with complete immobilization in Langmuir's sites and instantaneous equilibrium between Henry's and Langmuir's sites. In real situations, however, C'_H/S and b are not known *a priori*, and more importantly, the ideal boundary conditions do not exist. The effect of the latter on the proposed method is discussed next.

6.3.2 Application of the proposed method under real boundary conditions.

The preceding analysis was based on the assumption of the ideal boundary conditions at both the upstream and downstream interfaces of the membrane. More specifically, it is assumed that the gas concentration at the permeate interface is zero and the gas concentration at the feed interface is constant during the entire experiment. However, in reality as the gas permeates into the membrane, the feed pressure in the upstream compartment decreases whereas, as the gas permeates from the membrane, the pressure in the permeate compartment increases. As a result, the concentrations at the feed and permeate interfaces of the membrane vary with time. The actual boundary conditions at the feed and permeate interfaces in a discretized form are given by Eqs. (6.27–6.28). The implication of the real boundary conditions is that a gas permeation experiment never reaches steady state. Instead, only a pseudo-steady state can be attained. Consequently, the ratio of the upstream and downstream time lags is not a unique value.

Figure 6.2 presents the variation of $|R_\theta|$ with time for three low feed pressure experiments (1 atm) corresponding to Cases 3, 4 and 7 in Table 6.1. The respective variation of the upstream and downstream pressures with time was simulated by solving numerically the governing PDE subject to the real boundary conditions. In addition to the parameters specified in Table 6.1, the

other parameters used to simulate the pressure responses were: A = 0.00125 m^2, L = 2.35×10^{-5} m, D = 4.52×10^{-12} m^2/s, T = 298 K, V_u = V_d = 100 cm^3. The numerically-generated pressure data were used to determine the upstream and downstream time lags. For a given time t, the pressure data in a 10 s window (t – 5s, t + 5s) were used to obtain a linear trend line, which was extrapolated to the time axis. The resulting time-axis intercepts, the simulated time lags, were used to evaluate $|R_\theta|$ as a function of time. The dashed lines in Figure 6.2 correspond to the respective time-lag ratios that would be obtained with the ideal boundary conditions.

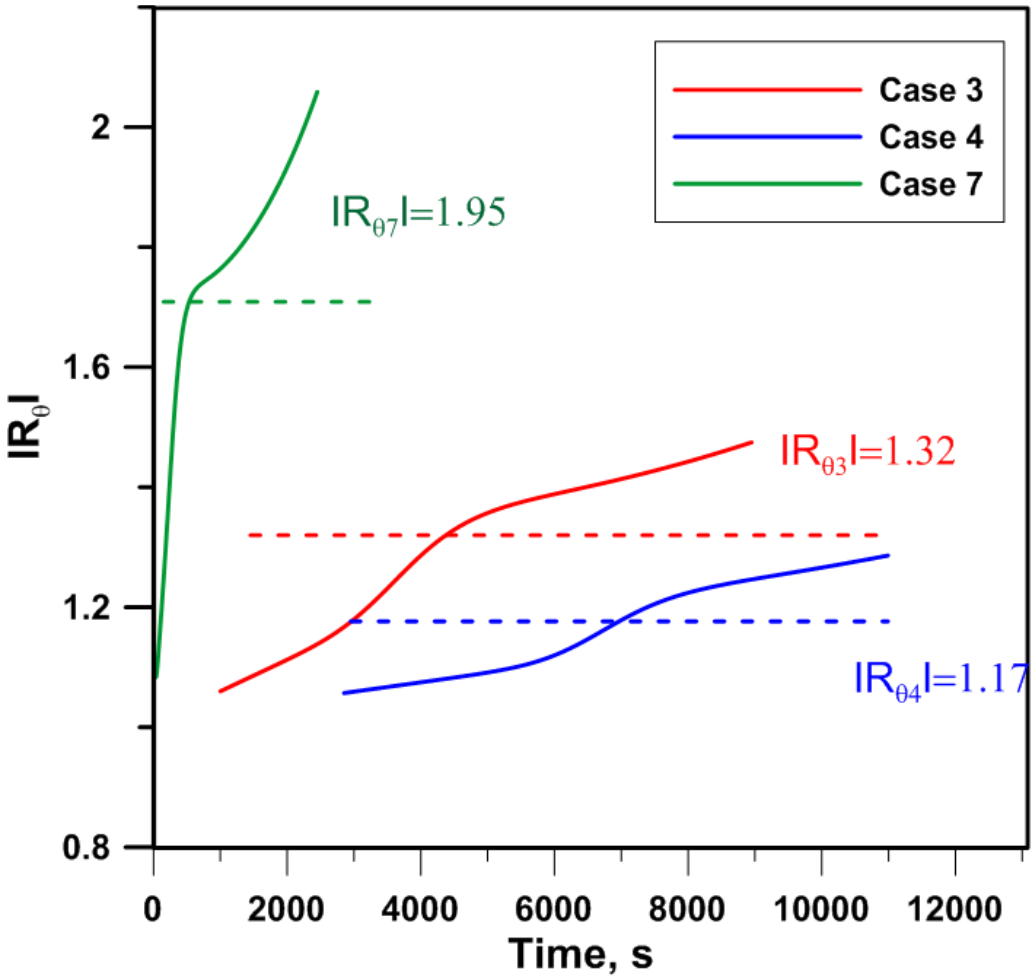

Figure 6.2: Variation of the ratio of the upstream and downstream time lags with time for Cases 3, 4 and 7 shown in Table 6.1 at 1 atm under real boundary conditions. Dashed lines indicate the corresponding $|R_\theta|$ obtained under ideal boundary conditions. Other simulation parameters: A = 0.00125 m^2, L = 2.35×10^{-5} m, D = 4.52×10^{-12} m^2/s, T = 298 K, V_u = V_d = 100 cm^3.

It can be observed that for each curve in Figure 6.2 there are two distinct regions, when $|R_\theta|$ is smaller and when $|R_\theta|$ is larger than the value corresponding to the ideal boundary conditions. The former region corresponds to transient permeation during which $|R_\theta|$ rapidly increases with time, and the latter region, in which $|R_\theta|$ continues to increase with time, but not as rapidly as before, corresponds to pseudo-steady state. The rationale for the shapes of the $|R_\theta|$ is discussed next.

Considering the upstream pressure decay due to gas permeation, it has the highest rate immediately upon initiating a permeation experiment; this is because initially the membrane is free from permeating species. As the membrane becomes more saturated with the permeant, the rate of the upstream pressure decay decreases and the intercept of the linearized portion of the pressure response curve with the time axis (apparent time lag) becomes more negative. If it were possible to reach steady state, the rate of pressure decay and the upstream time lag would approach respective constant values. However, in reality as time progresses the pressure in the upstream compartment decreases and the apparent time lag becomes more negative. In other words, the apparent upstream time lag is always negative, and its absolute value, first rapidly increases in the transient state and then continues to gradually increase at the pseudo-steady state.

On the other hand, it takes some time from the initiation of an experiment for the permeating species to reach the permeate interface of the membrane. Once that happens, gas molecules start to emerge from the membrane into the permeate compartment. As a result, the rate of gas emerging from the membrane gradually increases leading to an increase of the apparent downstream time lag in the transient state. If it were possible to reach steady state, the rate of pressure rise and the downstream time lag would approach respective constant values. In reality, as the experiment continues, because of a pressure decay in the feed compartment and a pressure rise in the permeate compartment, the driving force for gas permeation decreases leading to a gradual decrease in the rate of pressure rise and hence a gradual decrease in the apparent downstream time lag at pseudo-steady state. An example of variation of the downstream time lag with time is shown in Figure 6.3.

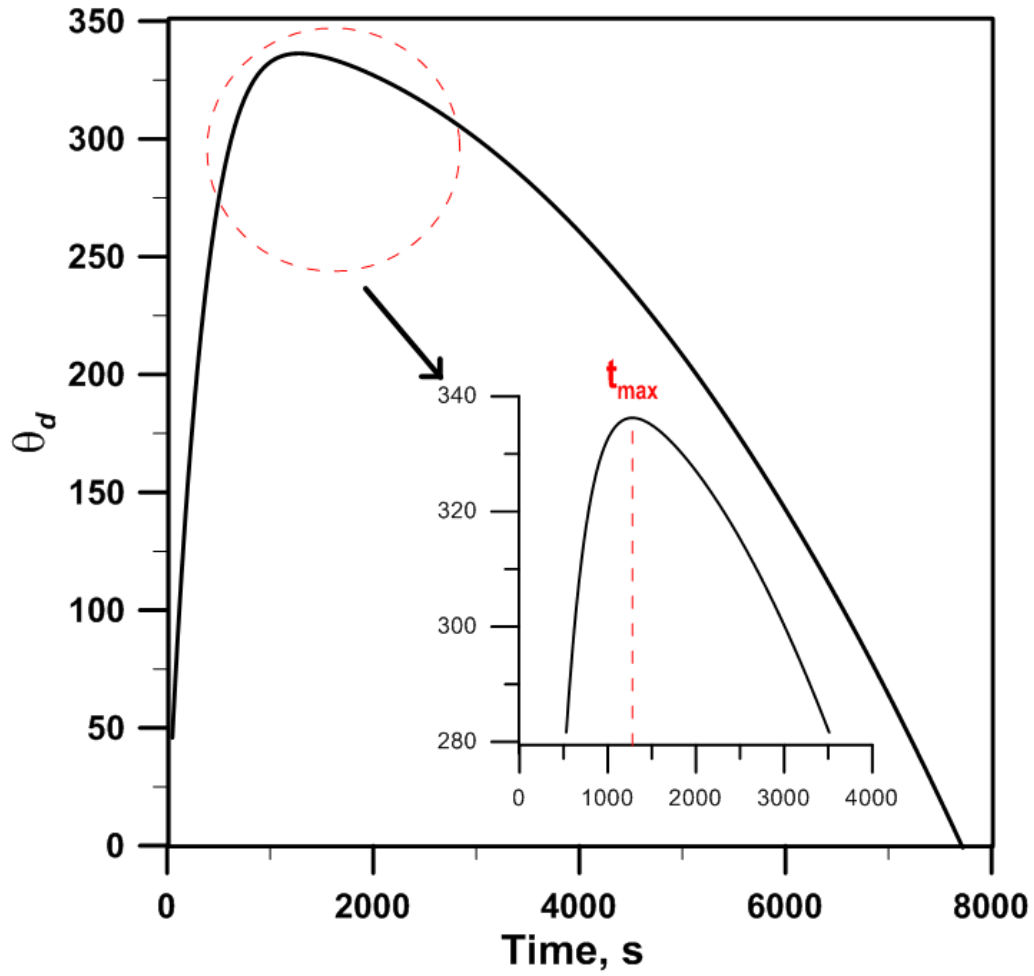

Figure 6.3: Example of variation of downstream time lag with time. Simulation parameters: A = 0.00125 m^2, L = 2.35×10^{-5} m, D = 4.52×10^{-12} m^2/s, T = 298 K, V_u = V_d = 100 cm^3, S = 2.35 cm^3(STP)/cm^3.atm ,C'_H = 107 cm^3(STP)/cm^3 , b =0.42 atm^{-1}, values corresponding to Case 1 in Table 6.1 at 1 atm.

The fact that $|R_\theta|$ rapidly increases with time at the transient permeation indicates that the rate at which the upstream time lag increases is greater than the rate of the downstream time lag increase. As pseudo-steady state is approached, the rate of $|R_\theta|$ increase with time slows down considerably. This is particularly evident for Cases 3 and 4 in Figure 6.2. Moreover, a relatively stable period of $|R_\theta|$ curve coincides with crossing of the ideal $|R_\theta|$. After that relatively stable period, the downstream time lag starts to decrease while the absolute value of the upstream time lag continues to increase leading to another period of a more rapid increase in $|R_\theta|$ with time (Case 7).

The shape of $|R_\theta|$ curves in Figure 6.2 strongly depends on the linearity of the sorption isotherm. Keeping in mind that the closer the $|R_\theta|$ ideal to 2, the more linear the sorption isotherm, and vice versa. It is evident that as the degree of nonlinearity of the sorption isotherm increases, the time to cross R_θ ideal and hence the time to reach pseudo-steady state increases. In addition, a more nonlinear sorption isotherm leads to a smaller deviation from ideal $|R_\theta|$ at pseudo-steady state. This implies a more linear pressure response curves at pseudo-steady state for membranes with nonlinear sorption isotherms, which is consistent with our previous study [22].

Although the point at which the curves cross the respective $|R_\theta|$ ideal appears to be quite distinctive, in particular for Cases 7, it would be rather difficult to decide on the value of $|R_\theta|$ to be used for the recovery of C'_H/S and b. As a result, the proposed method for the characterization of membranes would be rather useless. Therefore, it is important to find a criterion for the estimation of the time at which $|R_\theta|$ should be taken for an accurate recovery of the sorption parameters.

As already mentioned, there is a maximum downstream time lag under real boundary conditions, as shown in Figure 6.3. A question arises whether there exists a relationship between the time at which the maximum downstream time lag is observed ($t_{\max}$) and the time at which $|R_\theta|$ crosses the ideal value (t_c)? Figure 6.4 shows the plot of t_c versus $t_{\max}$ for a large number of simulated gas permeation experiments under real boundary conditions with the same volumes of the upstream and downstream compartments ($V_u = V_d = 100$ cm^3). In general, as seen in Figure 6.4, there is an approximately linear relationship between $t_{\max}$ and t_c given by:

$$t_c = 0.61\, t_{\max} \tag{6.36}$$

The corresponding coefficient of regression R^2 for Eq. (6.36) is 0.985. The slope of less than unity in Eq. (6.36) implies that t_c occurs before $t_{\max}$. Although the coefficient of regression of Eq. (6.36) is close to unity, it is evident that points in Figure 6.4 do not form a unique straight line. However, a further analysis of the data reveals that it can be grouped according to the ideal $|R_\theta|$. When the data is split into five groups for different ranges of the ideal $|R_\theta|$, it is evident that unique straight lines can be drawn for the data from each range (see the table incorporated in Figure 6.4).

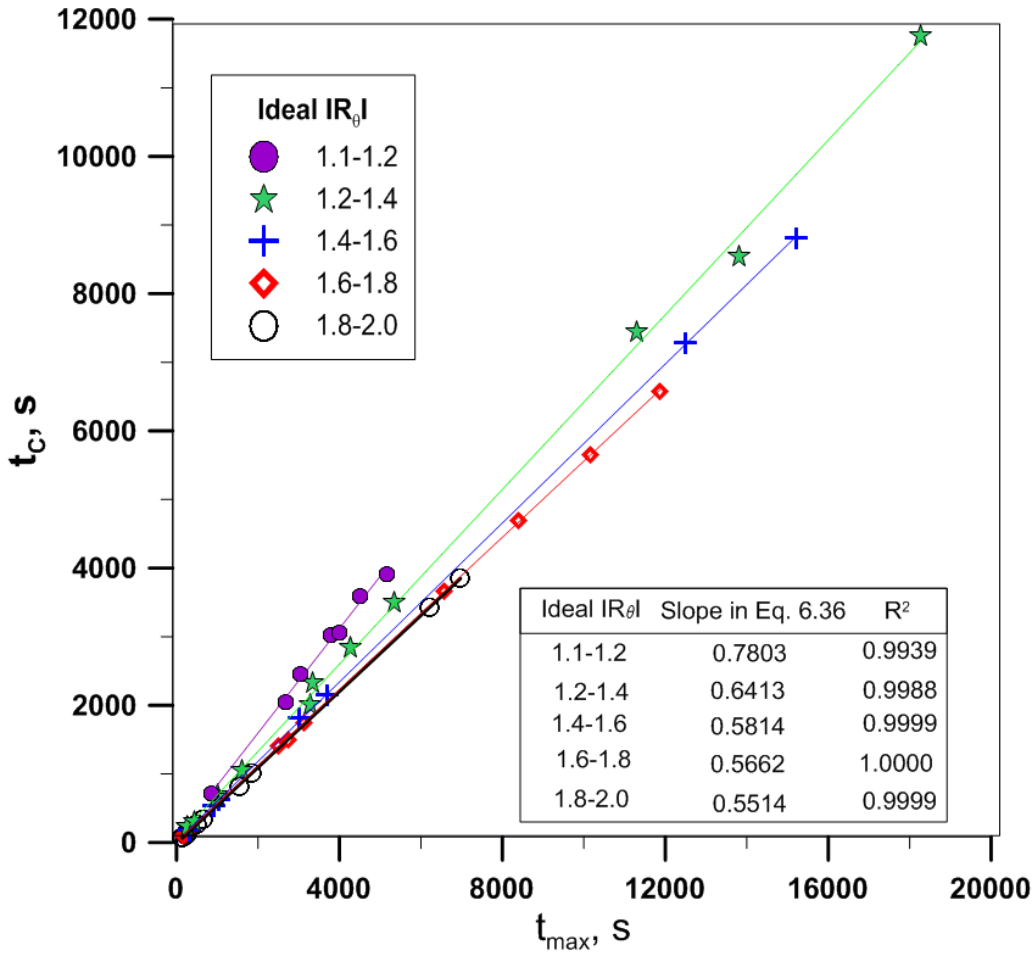

Figure 6.4: The relationships between the time at which the maximum downstream time lag is observed and the time $|R_\theta|$ curve crosses the ideal value. The simulated data is categorized according to the range of the ideal $|R_\theta|$.

The Table imbedded in Figure 6.4 presents a summary of the relationships between t_c and t_{max}; the corresponding coefficient of regression (R^2) for each relation is also provided. It is evident that the slope of the linear relationship between t_c and t_{max} increases with a decrease of the range of the ideal $|R_\theta|$. It is worth noting that the corresponding R^2 values are all greater than 0.99 indicting excellent linear relationship in each range.

The existence of almost perfectly linear relationships between t_c and t_{max} should allow the determination of membrane properties using the concept of the ratio of the upstream and downstream time lags determined simultaneously in a single gas permeation experiment. Considering that under realistic boundary conditions, the upstream and downstream time lags vary continuously with time even at pseudo-steady state, it will be important to monitor them

continuously and hence to generate $|R_\theta|$ vs. t curve similar to that shown in Figure 6.2. In our numerical simulations, we have used an arbitrarily selected time window of 10 s (t – 5 s to t + 5) to evaluate the trend lines that allow determining the two time lags. Decreasing the time window would increase the sharpness of the generated $|R_\theta|$ vs t and θ_d vs t curves. On the other hand, it would generate a higher level of noise in the determination of the θ_d and θ_u and hence $|R_\theta|$. The effect of noise, which would be an important aspect to be considered in the practical application of the proposed method, is not taken into account in this investigation.

Once the time at which the maximum downstream time lag (t_{max}) is observed, one can roughly evaluate t_c using Eq. (6.36) and check $|R_\theta|$ corresponding to t_c. Knowing such an estimated $|R_\theta|$ will allow selecting a more accurate relationship between t_c and t_{max} from the Table embedded in Figure 6.4 and to obtain a new t_c along with the corresponding new $|R_\theta|$, which should be close to $|R_\theta|$ for the ideal boundary conditions. Repeating the above analysis protocol for the experimental data obtained at another feed pressure will generate another $|R_\theta|$. With two $|R_\theta|$ values obtained independently at two different feed pressures, the method for the ideal boundary conditions described in the previous section can be used for the complete characterization of the tested membrane.

Table 6.2 summarizes the application of the method described above for the recovery of C'_H/S and b in 7 case studies listed in Table 6.1 under real boundary conditions. Along with the recovered values of C'_H/S and b, the respective errors relative to the actual values listed in Table 6.1 are also provided. As shown in Figure 6.1 and previously discussed, the optimum pair of feed pressures for the generation of $|R_\theta|$ depends on the shape of the ratio of the upstream and downstream time lags at the ideal boundary conditions, $|R_\theta|_i$, vs pressure. In real situations, this information is not known *a priori*. Consequently, the following approach was used in Table 6.2 to decide on the pair of the upstream feed pressures for the recovery of C'_H/S and b. First, for a given case study the simulation was carried at p_u = 1 atm and the method described above was used to recover $|R_\theta|$ based on the observed t_{max}. Depending on the recovered ratio of the time lags, $|R_\theta|_r$, the second p_u was selected. For $|R_\theta|_r$ close to 2, which corresponds to the linear sorption isotherm, the second simulation was carried out at high upstream pressure (15 or 30 atm). On the other hand, for the $|R_\theta|_r$ much smaller than 2, which corresponds to highly non-

linear sorption isotherm, the second simulation was carried out at p_u < 1 atm. The smaller the $|R_\theta|_r$, the lower p_u for the second simulation.

Table 6.2: Recovery of C'_H/S and b using the recovered ratio of the upstream and downstream time lags, $|R_\theta|_r$, based on the time for the maximum downstream time lag (t_{max}) under real boundary conditions.

Case, Gas &Material		p_u [atm]	$\|R_\theta\|_i$ [-]	$\|R_\theta\|_r$ [1] [-]	Recovered values and error			
					C'_H/S [atm]	ε [2]	b [atm^{-1}]	ε [2]
1	CO_2 & PIM-1[25]	1	1.846	1.845	43.9	-3.52%	0.42	-0.00%
		5	1.591	1.591				
2	C_3H_6 & PIM-1[25]	0.5	1.671	1.665	8.07	-7.78%	2.71	4.07%
		1	1.548	1.548				
3	CO_2 & Silicon Rubber filled with 5A [7]	1	1.320	1.325	106	13.6%	6.84	-3.02%
		5	1.138	1.139				
4	CO_2 & Silicon Rubber filled with 5A [26]	0.05	1.700	1.700	84.9	-38.6%	19.85	0.05%
		1	1.176	1.216				
5	CH_4 & PPOBr (36%) [27]	1	1.954	1.955	81.3	12.3%	0.108	-4.42%
		15	1.666	1.668				
6	N_2 & PPO [27]	1	1.987	1.989	26.7	1.91%	0.047	-2.08%
		30	1.839	1.802				
7	CH_4 & Glassy oriented polystyrene [28]	1	1.947	1.986	17.0	1.19%	0.614	0.00%
		30	1.706	1.702				

(1) $|R_\theta|_r$ estimated using Eq. (6.36) and then fine-tuned using the appropriate slope from the Table imbedded in Figure 6.4

(2) Error in recovered value: $\varepsilon = \left(\text{recovered} - \text{actual}\right)/\text{actual} \times 100\%$; the actual values of C'_H/S and b are listed in Table 6.1

As it could be expected, the recovery of sorption parameters in Table 6.2 for the real boundary conditions is not as good as for the ideal boundary conditions shown in Table 6.1. As observed for the ideal boundary conditions, Table 6.1, C'_H/S and b had been recovered with an error of less than 1% for most of the cases. When recovering C'_H/S and b under the realistic conditions, the operating pressures of the two experiments has to be chosen precisely for optimum parameter estimation.

For all cases presented in Table 6.2, the recovery of the C'_H/S parameter is always harder than b parameter. Solving the two-system of equations (Eq. 6.26 at two different $|R_\theta|$ obtained at

different operating pressures) was performed using the least square method. Therefore, the summation of the squares of the errors is used to determine the best solution. This difficulty of solving such system of equations is illustrated in the contour plot Figure 6.5. The error obtained on each recovered parameter C'_H/S and b shows almost parallel lines to the C'_H/S axis indicating that there is a wide range of values of C'_H/S that will lead to a minimum error. This explains the higher error obtained on recovering the C'_H/S compared to b parameters for both ideal and real boundary conditions.

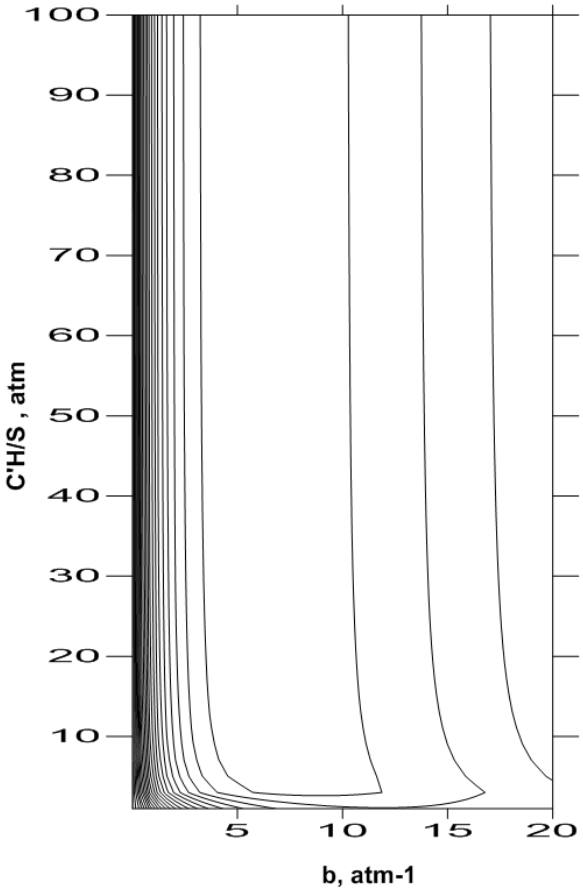

Figure 6.5: The contour plot for Case 3 in Table **6.**1

Table 6.2 presents the best results using the different operating pressures used to recover C'_H/S and b for each. The same procedure of the choice of the operating pressure was followed here except for Case 3, although it is considered a highly nonlinear case, using a second

operating pressure of 5 atm gave better results compared to a pressure lower than 1 atm. For the more linear cases (Cases 5-7), higher operating pressure was used for the second experiment and the errors presented in Table 6.2 on both parameters were the best obtained results. In Table 6.2 the results for Case 1 were presented for pressures 1 and 5 atm, however a combination of 1 atm and other operating pressure also showed a comparable error indicating more flexibility on the choices of operating pressures for this case. This flexibility is a result of the shape of the $|R_\theta|$ - pressure curve shown in Figure 6.1, where it is not as steep as for Cases 3 and 4 and not as flat as for Cases 6 and 7.

Using the recovered parameters of C'_H/S and b obtained previously (Table 6.2), the other membrane parameters, D, P, S, and C'_H are evaluated according to the previously described procedures. Table 6.3 shows the percentage error on the recovery of each parameter for the seven cases.

Table 6.3: The recovered membrane properties using the procedures described earlier under the realistic boundary conditions.

Case, Gas &Material		***p* , atm**	**Error % (ε) on the obtained parameters**				
			C'_H	***b***	***S***	***D***	***P***
1	CO_2 & PIM-1[25]	5	2.74	0.48	0.544	0.85	1.39
2	C_3H_6 & PIM-1[25]	1	9.65	3.69	1.98	3.375	5.285
3	CO_2 & Silicon Rubber filled with 5A [7]	5	1.15	2.95	13.14	12.9	1.93
4	CO_2 & Silicon Rubber filled with 5A [26]	2	4.09	0.05	49.5	36.2	4.68
5	CH_4 & PPOBr (36%) [27]	15	2.29	1.22	4.94	4.96	0.261
6	N_2 & PPO [27]	15	0.399	0.97	0.235	0.079	0.157
7	CH_4 & Glassy oriented polystyrene [28]	30	0.47	0.243	0.63	0.54	0.0977

The permeability has to be obtained from the slope of either upstream or downstream pressure curve (Eq. 6.35) using one of the experiments. Usually there are two experiments: one at high and one at low pressure. Results obtained in Table 6.3 were all calculated using the permeability obtained from the slope of the pressure response obtained at higher operating pressure and therefore the maximum time lag was recorded for this higher pressure experiment. It should be kept in mind that under the real boundary conditions steady state is never reached; therefore, the slope of the pressure response has to be evaluated in the range at which the maximum time lag occurs to ensure the most accurate evaluation of the permeability. The numerical analysis for the full characterization of the membrane showed that generally using the experiment operated at higher pressure gives better recovery accuracy in all parameters. An exception only occurred for the highly nonlinear case (Case 4). For this case, a clear trade-off occurred in the recovery accuracy of the parameters with operating pressure. Errors on some parameters were decreasing with increasing pressure while other parameters were showing higher errors with higher operating pressure. Likewise to ensure the most accurate evaluation of the apparent diffusivity from the experimental data, the maximum time lag value should be used in Eq. (6.8) to calculate the apparent diffusivity for the experiment operated at the higher pressure.

The results presented in Table 6.3 indicate that only the highly nonlinear cases (Case 3 & 4) gave higher errors on some parameters. The worse results were for Case 4, where an error of about 50% on the solubility and an error of around 36% was obtained on diffusivity although the error on *b* parameter is the lowest among all cases (0.05%). This clearly shows the limitation of this method, and only moderately to slightly linear isotherms can be characterized with an error on all recovered parameters that varies between 5 to 1%.

The seven cases considered in Table 6.3 might not be enough to objectively assess the proposed method. It would be worthwhile to apply the method for all cases used to generate Figure 6.4. It is important to emphasize the data in Figure 6.4 are applicable to any pressure. On the other hand, in all simulations the volumes of the upstream and downstream compartments were the same and equal to 100 cm^3. A question arises whether the linear relationships reported are dependent on the selected volumes of the compartments? It is safe to speculate that regardless of the actual volumes of the compartments, as long as they are the same, the same

linear relationships should be obtained for the selected ranges of the ideal $|R_\theta|$. The effect of using different volumes for the upstream and downstream compartments should be investigated. At the same time, it is expected that regardless of the combination of the upstream and downstream volumes, unique linear relationships should be observed at different ranges of the ideal $|R_\theta|$.

6.4 Conclusions

A new method to completely characterise a membrane with a nonlinear sorption isotherm that follows the complete immobilization in Langmuir's sites and instantaneous equilibrium model is proposed in this work. The new technique requires monitoring both upstream and downstream time lags. The advantage of the upstream measurements and therefore the upstream time lag relies in obtaining the theta ratio $|R_\theta|$. The theta ratio parameter is a quick check for the degree of nonlinearity of the isotherm under study. The ratio between the upstream and downstream time lags is -2 only for a linear isotherm. The utilization of both downstream and upstream asymptotic solutions assessed in reducing the number of experiments required to fully characterize the kinetic and sorption parameters of the membrane. Two permeation experiments at two operating pressures are sufficient to fully characterise the membrane. The results obtained with this method are promising and the preliminary results show that this method is capable of characterizing the category of moderately and slightly nonlinear membranes, where most of the actual membranes used in literature fall in.

6.5 Nomenclature

Symbols	Description
b:	Affinity factor, atm^{-1}
C:	Total concentration (dual-mode sorption) inside the membrane, mol/m^3
C_D:	Dissolved concentration by Henry's law, mol/m^3
C_H :	Concentration of the immobilized species adsorbed on Langmuir's sites, mol/m^3
C'_H:	Capacity parameter, cm^3STP/cm^3
D:	Diffusivity, m^2/s
D_L:	Downstream apparent diffusivity, m^2/s
D_0:	Upstream apparent diffusivity, m^2/s
L:	Membrane thickness, m
P:	Permeability, mol/m s Pa
p:	Pressure, Pa
p_0:	Upstream initial pressure, Pa
p_d:	Downstream pressure, Pa

p_u: Upstream pressure, Pa
$Q_{x=0}$: Gas accumulating upstream of the membrane, moles
$|R_\theta|_i$: The ideal absolute value of theta ratio
$|R_\theta|_r$: The estimated absolute value of theta ratio
S: Solubility, mole/Pa m^3
t_c: Critical time (time corresponding to R_θ that is closest to the ideal R_θ)
t_{max}: The time corresponding to the maximum downstream time lag
V_L: Downstream volume, m^3
V_0: Upstream volume, m^3
x: Membrane coordinate, m
z: A certain depth x in the membrane, m

Greek symbols

ε: Error percentage
Δx_1: Backward mesh size, m
Δx_2: Forward mesh size, m
θ_d: Downstream time lag, s
θ_u: Upstream time lag, s

6.6 References:

[1] H. A. Daynes, The Process of Diffusion through a Rubber Membrane, R. Soc. Proc. A97 (1920), 286-307.

[2] P. Meares, The diffusion of Gases through Polyvinyl Acetate, Journal of American Society, 76 (1954), 3415-3422.

[3] D. Bhatia, W. Vieth, The Penetrant Time-Lag for the Dual Sorption Case With Langmuir Isotherms, Journal of Membrane Science, 6 (1980), 351-357.

[4] G. H. Weiss, J. T. Bendler, M. F., Schlesinger, Continuous site Model for Langmuir Gas Sorption in Glassy Polymers, Macromolecules, 25 (1992), 990-992.

[5] W. R. Vieth and K. J. Sladek, A model for diffusion in a glassy polymer, Journal of colloid Science, 20 (1965), 1014-1033.

[6] J. H. Petropoulos, Quantitative Analysis of Gaseous Diffusion in Glassy Polymers, Part A-2, 8 (1970), 1797-1701.

[7] D. R. Paul and D. R. Kemp, The Diffusion Time Lag in Polymer Membranes Containing Adsorptive Fillers, Journal of Polymer Science: Symposium No. 41 (1973) 79-93

[8] D. R. Paul, and W. J. Koros, Effect of partially immobilizing sorption on permeability and the diffusion time-lag, Journal of Polymer science: Polymer physics edition, 14 (1976), 675-685.

[9] W. J. Koros, D. R. Paul, and A. A. Rocha, Carbon Dioxide Sorption and Transport in Polycaronate, Journal of Polymer Science: Polymer Physics Edition, 14 (1976), 687-702.

[10] W. J. Koros, A. H. Chan, and D. R. Paul, Sorption and transport of various gases in polycarbonate, Journal of Membrane Science, 2 (1977), 165-190.

[11] W. J. Koros, and D. R. Paul, Transient and Steady-State Permeation in Poly(ethylene Terephthalate) above and below the glass transition, Journal of Polymer Science, Polymer Physics Edition, 16 (1978), 2171-2187.

[12] K. Toi, K. Saito, Y. Suganuma, T. Ito, I. Ikemoto, " Numerical Examination of the Dual-Mode Model for Permeation, Sorption and Desorption Rate cures", Journal of Applied Polymer Science, 46 (1992), 1939-1944.

[13] J. A. Tshudy, C. V. Frankenberg, A model Incorporating Reversible Immobilization for Sorption and Diffusion in Glassy Polymers, Journal of Polymer Science: Polymer Physics Edition, 11 (1973), 2027-2037.

[14] E. Favre, N. Morliere, D. Roizard, Experimental Evidence and Implications of an Imperfect Upstream Pressure Step for the Time-lag Technique, Journal of Membrane Science, 207 (2002), 59–72.

[15] Y.K. Zhang, N. M. Kocherginsky, Time lag for Transmembrane Transport without Interface Equilibrium, Journal of Membrane Science, 225 (2003), 105-114.

[16] J. Guo, T. A. Barbari, A Dual Mode, Local Equilibrium Relaxation Model for Small Molecule Diffusion in a Glassy Polymer, Macromolecules, 41 (2008), 238-245.

[17] H. L., Frisch, The time-lag in diffusion, The Journal of Physical Chemistry, 61 (1957), 93-95.

18] D. R. Paul, Effect of Immobilizing Adsorption on the diffusion time-lag, Journal of membrane science: Part A-2, 7(1969), 1811-1818.

[19] N. Al-Qasas, B. Kruczek, J. Thibaut, Analysis of Gas Transport in Laminated Semi-Infinite Solid: Novel Method for Complete Membrane Characterization During Highly Transient State, Journal of Membrane Science, 460 (2014) 25–33.

[20] N. Al-Qasas, B. Kruczek, J. Thibaut, Membrane Characterization Based on the Upstream Pressure Decay in a Dynamic Gas Permeation Test, Journal of Fluid flow, Heat and Mass Transfer, 1 (2014), 57-64.

[21] M. Al-Ismaily, J.G., Wijmans, B., Kruczek, "A shortcut method for faster determination of permeability coefficient from time-lag experiments", J. Membrane Sci., 234-424 (2012), 165-174.

[22] N. Al-Qasas, B. Kruczek, J. Thibaut, The Effect of the Downstream Pressure Accumulation on the Time-Lag Accuracy for Membranes with Non-Linear Isotherms, Journal of membrane Science, 511, (2016), 119-129.

[23] B. Carnahan, H.A. Luther and J.O. Wilkes, Applied Numerical Methods, (1969), John Wiley & Sons, New York, NY.

[24] H. Wu, N. Al-Qasas, B. Kruczek, J. Thibault, Simulation of Time-Lag Experiment Using Finite Differences, Journal of Fluid flow, Heat and Mass Transfer, 2 (2015), 14-25.

[25] P. Li, T. S. Chung, D. R. Paul, Gas Sorption and Permeation in PIM-1, Journal of Membrane Science, 432 (2013), 50-57.

[26] D. R. Kemp, D. R. Paul, Gas sorption in Polymer Membranes containing Adsorptive fillers, Journal of Polymer Science: Polymer Physics Edition, 12 (1974), 485-500.

[27] J. Lianda, F. R. Sheu, R. R. Chern, H. B. Hopfenberg, Gas Sorption and Transport in Poly (phenylene oxide) (PPO) and Aryl-Brominated PPO Membranes, Chines Journal of Polymer Science, 7 No.4, (1989), 306-314.

[28] W. R. Vieth, C. S. Frangoulis, J. A. Rionda, Kinetics of sorption of Methane in Glassy polystyrene, Journal of Colloid and interface science, 22 (1966), 454-491.

Chapter 7

Conclusions

7.1 Conclusion

Three novel gas membrane characterization methods have been proposed in the current study. Each of the methods has a favorable applicability depending on the type of membranes under investigation. The first two methods (relative slope method and the deviation method) are concerned with characterizing gas membranes that exhibit a linear isotherm via monitoring the changes in the upstream pressure only and keeping the downstream compartment continuously evacuated. The major advantage of basing the membrane characterization upon the upstream pressure measurements is the satisfaction of the downstream boundary condition thereby eliminating errors associated with the downstream boundary condition. The third method proposed for gas membrane characterization, known as the theta ratio method, can be used advantageously for glassy polymers where the dual mode sorption model is applicable and for realistic experimental boundary conditions.

The relative slope method that is based on a two-membrane system, shows enviable advantages when the membrane to be characterized is a barrier material. This method makes advantage of the fact that all membranes initially behave as a semi-infinite solid and a straight line relationship prevails between the upstream pressure and the square root of time where the slope of this linear relation is a function of both diffusivity and solubility of the membrane. The combination of the tested membrane with a lower resistance layer with known properties allows the full characterization of the membrane under investigation via monitoring the early slope and the rate at which this early slope changes once the penetrant enters the second layer. Since this method is based on lamination of two membranes, the thickness of the tested membrane can be minimized. The industrial membranes known as the integrally skinned and thin film composite asymmetric membranes could be easily characterized using this technique. Moreover, if the properties of the two layers are known, the relative slope method can be used to estimate the thickness of the skin membrane which is usually difficult to be measured. The relative slope method does not require achieving steady state and does not require the gas molecules to leave

the membrane to enter the downstream compartment. As a result, this characterization method is relatively rapid; this is especially important for barrier materials.

The second proposed characterization method is also based on monitoring the upstream pressure change only and keeping the downstream compartment under evacuation thereby obeying the ideal downstream boundary condition. This method requires observing the linear slope of the initial pressure decay when the membrane is still behaving as a semi-infinite solid and clearly observing the deviation from this initial straight line slope. Experimental results indicate that membrane properties can be extracted using this method despite the uncertainty in actual feed pressure measurements. Both the relative slope method and the deviation method require an accurate monitoring of the upstream pressure variation. The two methods guarantee the complete satisfaction of the downstream boundary condition which is not possible with the conventional time-lag method.

The numerical investigation conducted in Chapter 4 showed that in order to get the most accurate time lag estimation using finite difference numerical modeling of a permeation experiment, it is highly recommended to use variable mesh size at the membrane interfaces, especially for the upstream calculations since the concentration gradient is initially extremely high. The optimal numerical scheme was determined using the analytical solution of a permeation experiment under ideal boundary conditions as a benchmark to assess the accuracy of the various numerical schemes. The optimal scheme was a compromise between accuracy and computation time. The optimal numerical parameters were then used throughout this thesis for a comprehensive investigation on the accuracy of the time-lag methods for linear and nonlinear systems under realistic boundary conditions.

The comprehensive study on the effect of the nonlinearity of the isotherm on the downstream time-lag method confirmed the increase in the time lag as a result of the presence of the Langmuir's sites. It was assumed that membranes followed dual mode sorption with complete immobilization in Langmuir's sites and instantaneous equilibrium between Henry's and Langmuir's sorption sites. Numerical simulations of gas permeation experiments using the schemes developed in Chapter 4 revealed important information about the transient period prior to reaching the pseudo steady state. The delay in achieving steady state increases with the increase in the nonlinearity of the isotherm. Under realistic boundary conditions, the steady state

is never reached, it is only approached. The larger the nonlinearity of the system, the greater the error in the apparent time lag, but at the same time the slower the rate of deviation of the downstream pressure profile from the expected asymptote curve. Since the error in the apparent time lag, even for membranes with highly nonlinear isotherms does not exceed 1%, and because of a stable response at pseudo steady-state, the possibility of having accurate downstream time-lag measurements was confirmed. At the same time, to completely characterize membranes considered in this study, it would be necessary to carry out four gas permeation experiments at four different feed pressures to obtain four independent apparent downstream time lags.

The third characterization method proposed in this work is applicable to glassy polymer membranes that follow the dual mode sorption model considered in Chapter 5. The goal was to develop a method that would reduce the number of gas permeation experiments required to completely characterize the membrane. The proposed new method relies on simultaneous monitoring of the upstream pressure decay and the downstream pressure rise to determine the ratio of the upstream and downstream time lags (R_θ) as a function of time. Assuming applicability of the ideal boundary conditions at the upstream and downstream interfaces of the membrane, R_θ reaches a constant value at steady state, which depends on the ratio of the capacity of Langmuir's sites to the solubility in Henry's sites, the affinity constant, and the feed pressure, which is known. Consequently, performing just two gas permeation experiments at two different feed pressures (instead of four experiments at four different feed pressures) could allow complete characterization of a membrane. The validity of the proposed method under real boundary conditions was investigated numerically. Under real boundary conditions there is no unique value of R_θ; however, the analysis of the generated data revealed a linear relationship between the maximum downstream time-lag, which can be observed experimentally, and the time at which R_θ is equal to the value that would be obtained under the ideal boundary conditions. Consequently, the possibility of using the proposed method under the real boundary conditions was confirmed.

7.2 Recommendations

The three proposed characterization methods are very promising for gas membrane characterization as they overcome many of the accuracy problems associated with the conventional time-lag methods. However, since the three proposed methods rely on the upstream

pressure change measurements, an efficient upstream permeation compartment design is essential for accurate upstream pressure measurements to ensure achieving high efficacy of membrane characterization. Therefore, with an accurate and properly-designed upstream experimental set up, real experiments need to be performed to truly demonstrate and justify the applicability of these proposed membrane characterization methods. The first version of such a system already exists in our laboratory and it was used to verify experimentally the proposed difference method. However, to test the other two proposed methods, an improved version of the existing system must be developed. In particular the problems associated with so-called "compression effect" must be resolved and the system must allow carrying out experiments pressures greater than just 20 kPa (3 psia).

All the numerical simulations of permeation experiments performed in this study were done assuming that the molecules in the Langmuir's site were immobilized and did not contribute to gas diffusion across the membrane. It is therefore recommended to study the effect of various degree of immobilization from no immobilization to total immobilization on the Langmuir's sites on the accuracy of the time-lag method. Similarly, it is recommended to investigate the effect of having non-instantaneous equilibrium between the molecules associated with Henry's sites and those associated to Langmuir's site on the accuracy of the time-lag method.

Appendix

VBA computer code

```
Option Base 1
Option Explicit

Sub SolveSlab()
Dim A(20000) As Double, AA As Double, AA1 As Double, ACCUMDOWN As Double, ACCUMUP As Double,
ALPHA(5000) As Double
Dim ALPMAX As Double, ALPMIN As Double, AREA As Double
Dim B(20000) As Double, BA As Double, BA1 As Double, BB As Double, BP As Double
Dim C(20000) As Double, C0 As Double, C01 As Double, C1(20000) As Double, C1ANAL(20000) As Double, C1ANALR As
Double
Dim C1NEW(20000) As Double, CC As Double, CF As Double, CFU As Double
Dim CHM As Double, CHM1 As Double, CON As Double, CON1 As Double Dim D(20000) As Double, DD As Double,
DDOW As Double, DDOWC As Double, DELTAP As Double, DIF1 As Double, DPANAL As Double, DPU As Double
Dim DTAU As Double, DPDT As Double, DTANAL As Double, DTIM As Double, DTIMSELECT As Double, DUP As
Double, DUPC As Double, DX1(20000) As Double
Dim E(20000) As Double, EE As Double, ERFC As Double, ERROR2 As Double, ERRORDOW As Double, ERRORDOWB
As Double, ERRORUP As Double, ERRORUPB As Double
Dim FACTIME1 As Double, FACTIME2 As Double, FACTOR As Double, FF As Double, FO As Double, FR As Double, FY
As Double
Dim G1 As Double, G1A As Double, G1TANAL(1000) As Double, G2 As Double, G2A As Double, G2TANAL(1000) As
Double, GG As Double
Dim H As Double, HH As Double
Dim I As Integer, ICNOISE As Integer, ICOL As Integer, IM As Integer, IMPLICIT As Integer, INOISE As Integer
Dim INTER As Double, INTERU As Double, IROW3 As Integer
Dim J As Integer, JJ As Integer
Dim K As Long, KD As Double, KD1 As Double, KK As Double
Dim LINEAR As Integer, LL As Double, LNY As Double
Dim MEANERROR As Double, MESH As Integer
Dim N As Integer, NANAL As Integer, NBC1 As Integer, NBC2 As Integer, NFACTOR As Integer, NOISE As Integer,
NOISETYPE As Integer
Dim NP As Integer, NT As Long, NSUMDIF As Double, NX1 As Integer, NX10 As Integer
Dim P As Double, P0 As Double, PATM As Double, PATMin As Double, PD As Double, PDANAL As Double, PDANALR As
Double, PDNEW As Double
Dim PI As Double, PNEW As Double, PRESD(1000) As Double, PRESU(1000) As Double
Dim R As Double, RATIO As Double, RR As Double
Dim S As Double, SEMILINE As Double, SLOPE As Double, SLOPEU As Double, SOL1 As Double, SQRTTANAL As
Double, SQRTTIM As Double
Dim SS As Double, SUM As Double, SUM1 As Double, SUM2 As Double, SUM3 As Double, SUM4 As Double
Dim SUMA As Double, SUMAN As Double, SUMC As Double, SUMD As Double, SUMDIF As Double, SUMG1 As Double,
SUMG2 As Double
Dim SUMU1 As Double, SUMU2 As Double, SUMU3 As Double, SUMU4 As Double
Dim T As Double, T1 As Double, T2 As Double, T3 As Double, T4 As Double, T5 As Double, TANAL As Double, TERM1 As
Double, TERM2 As Double
Dim TERM3 As Double, TERM4 As Double, TERM5 As Double, TERM6 As Double, TERM7 As Double, TERM8 As Double,
TERM9 As Double, THETA As Double
Dim THETAU As Double, TIM As Double, TIME As Double, TIME1 As Double, TIME2 As Double, TIMED(1000) As
Double, TIMEU(1000) As Double
Dim TINTEGRATE As Double, TOVERTHETAA As Double, TPRINT As Double, TPRINT3 As Double, TS As Double, TT
As Double, TT1 As Double, TWINDOW As Double
Dim X1 As Double, XL1 As Double, XN10 As Double
Dim VOLD As Double, VOLU As Double
Dim Y As Double
Dim Z As Double

' XL1     SLAB THICKNESS OF FIRST MEMBRANE
```

```
' C01     INITIAL CONCENTRATION OF FIRST MEMBRANE
' NX1     NUMBER OF GRID POINTS FOR FIRST MEMBRANE
' DIF1    MASS DIFFUSIVITY OF FIRST MEMBRANE
' IMPLICIT MODE OF SOLUTION - 0: EXPLICIT ; 1: IMPLICIT
' NBC1    UPSTREAM BOUNDARY CONDITIONS
' NBC2    TYPE OF BOUNDARY CONDITION FOR DOWNSTREAM SIDE OF MEMBRANE -2: Ideal BC ; 1; Real BCs,  0 when C1(L)=0; = 1 when C1(L) in equilibrium with downstream gas; 2: when C1(L)=0 but still calculating pressures

Application.ScreenUpdating = False
Randomize
Cells(15, 2) = Date
Cells(15, 3) = Timer
 ' IMPORT KNOWN VALUES
Sheets("Sheet1").Select
  TIME = Range("B1").Value
  DIF1 = Range("B5").Value
  SOL1 = Range("B6").Value
  XL1 = Range("B8").Value
  P0 = Range("B9").Value
  PATMin = Range("C4").Value
  C01 = Range("B10").Value
  NX1 = Range("B13").Value
  VOLD = Range("B20").Value
  VOLU = Range("B21").Value
  AREA = Range("B22").Value
  NP = Range("B25").Value
  TWINDOW = Range("B26").Value
  FR = Range("B27").Value
  NOISE = Range("B28").Value
  DTIMSELECT = Range("B29").Value
  TINTEGRATE = Range("B30").Value
  PD = 0#
  TANAL = TINTEGRATE
  NANAL = 1
  DTANAL = TWINDOW / (NP - 1)
  IM = 2
  R = Range("F6").Value
  T = 298#
  TS = Range("F7").Value
  PATM = Range("F8").Value
  CHM1 = Range("F2").Value ' m3(STP)/m3
  CHM = CHM1 * PATM / (R * TS) ' mol/m3
  BA1 = Range("F3").Value ' in units of 1/atm
  BA = BA1 / PATM ' in units of 1/pa
  KD1 = Range("F1").Value ' in units of m3(STP)/m3 atm
  KD = (KD1 * PATM / (R * TS)) / PATM ' in units of mol/m3 Pa
  KK = CHM1 * BA1 / KD1
  Z = (BA / KD) ' m3/mol
  PI = 3.14159265358979
  C0 = P0 / (R * T)
  S = P0 * KD / C0
  H = AREA * XL1 * S / VOLD
  BP = BA1 * PATMin
  RATIO = BP / (1 + BP)

' ****CALCULATIONS OF THE ROOTS OF THE EQUATION ALPHATNA(ALPHA)=H****

  For I = 1 To 5000
    ALPMIN = (I - 1) * PI
    ALPMAX = ALPMIN + PI / 2
    For J = 1 To 1000
```

```
      ALPHA(I) = 0.5 * ALPMIN + 0.5 * ALPMAX
      AA = ALPHA(I) * Tan(ALPHA(I)) - H
      If Abs(AA) < 0.000000000000001 Then
        Exit For
      Else
        If AA < 0 Then
          ALPMIN = ALPHA(I)
        Else
          ALPMAX = ALPHA(I)
        End If
      End If
    Next J
  Next I

' Parameters to fix: IMPLICIT, TWO BCs, LINEAR, MESH, NFACTOR, NOISETYPE
  IMPLICIT = 1   'Explicit = 0; Implicit = 1
 NBC1 = 1                '= 0 when C1(L)=0; = 1 when C1(L) in equilibrium with downstream gas; 2: when
                         C1(L)=0 but still calculating pressures
 NBC2 = 1
 LINEAR = 1              '= 0 when linear; = 1 when nonlinear isotherm
 MESH = 1                '= 0 for uniform mesh; = 1 for adjustable mesh
 NFACTOR = 2             '1: transfer 1 uniform mesh to 10 variable meshes; = 2: 3 to 10; 3: 5 to 10; 4: 2 to 10
 ICNOISE = 1

  If MESH = 0 Then
    X1 = 0#
    For I = 1 To NX1 - 1
      DX1(I) = XL1 / (NX1 - 1)
      X1 = X1 + DX1(I)
    Next I
  ElseIf MESH = 1 Then
'From     5          3         2           1
'To      10         10         10          10
'Factor  1.150984101 1.311129915 1.490777275  1.999018133
    NX10 = NX1
    If NFACTOR = 1 Then
      NX1 = NX10 + 18
      FACTOR = 1.999018133
    ElseIf NFACTOR = 2 Then
      NX1 = NX10 + 14
      FACTOR = 1.311129915
    ElseIf NFACTOR = 3 Then
      NX1 = NX10 + 10
      FACTOR = 1.15098410103701
    ElseIf NFACTOR = 4 Then
      NX1 = NX10 + 16
      FACTOR = 1.490777275
    Else
    End If
    X1 = 0#
    For I = 1 To NX1 - 1
      If I = 1 Then
        DX1(I) = (XL1 / (NX10 - 1)) / (FACTOR ^ 10)
      ElseIf I >= 2 And I <= 10 Then
        DX1(I) = DX1(I - 1) * FACTOR
      ElseIf I >= NX1 - 10 Then
        DX1(I) = DX1(I - 1) / FACTOR
      Else
        DX1(I) = XL1 / (NX10 - 1)
      End If
      X1 = X1 + DX1(I)
    Next I
```

```
  Else
  End If
  If (Abs(X1 - XL1) > 0.0000001 * XL1) Then Stop
  DTAU = DTIMSELECT * DIF1 / DX1(Int(NX1 / 2)) ^ 2

  Sheets("Sheet2").Select
  Sheet2.Cells.Clear
  Cells(1, 1) = "X(m)"
  X1 = 0#
  For I = 1 To NX1
    Cells(I + 1, 1) = X1
    X1 = X1 + DX1(I)
  Next I

  Sheets("Sheet3").Select
  ActiveSheet.Range("A2:AJ40000").Select
  Selection.Clear

'**** INITIAL CONCENTRATION DISTRIBUTION****
  P = P0
  For I = 1 To NX1
    C1(I) = C01
  Next I
  C1(1) = P * KD

  TIM = 0#
  ICOL = 2
  IROW3 = 1
  TIME1 = 1#: FACTIME1 = 100#
  TIME2 = 10#: FACTIME2 = 10#
  NT = Int((TIME - TIME2) / DTIMSELECT + 0.5) + Int(TIME1 * FACTIME1 / DTIMSELECT + 0.5) + Int((TIME2 - TIME1)
* FACTIME2 / DTIMSELECT + 0.5)
  AA = DIF1 * DTIMSELECT / DX1(1) ^ 2
  If (IMPLICIT = 0) And (AA >= 0.5) Then Stop
  If (IMPLICIT = 1) And (AA >= 0.5) Then Stop

  TPRINT = 0#
  TPRINT3 = 0#
  SUMDIF = 0#
  NSUMDIF = 0

  For K = 1 To NT
    If TIM <= TIME1 Then
      DTIM = DTIMSELECT / FACTIME1
    ElseIf TIM > TIME1 And TIM <= TIME2 Then
      DTIM = DTIMSELECT / FACTIME2
    Else
      DTIM = DTIMSELECT
    End If
    TIM = TIM + DTIM

    If IMPLICIT = 0 Then    'EXPLICIT SCHEME
      For I = 1 To NX1
        If I = 1 Then
          If NBC1 = 0 Or NBC1 = 2 Then
            C1NEW(I) = P0 * KD
          Else
            C1NEW(I) = P * KD
          End If
        ElseIf (I = NX1) Then
          If NBC2 = 0 Or NBC2 = 2 Then
            C1NEW(I) = 0#
```

```
        Else
          C1NEW(I) = PD * KD
        End If
      Else
        RR = 1 + ((KK / (1 + Z * C1(I)) ^ 2)) * LINEAR
        EE = 2 * DTIM * DIF1 / ((DX1(I - 1) + DX1(I)) * RR)
        C1NEW(I) = C1(I) + EE * ((C1(I - 1) - C1(I)) / DX1(I - 1) + (C1(I + 1) - C1(I)) / DX1(I))
      End If
    Next I

  Else    'IMPLICIT = 1
    For I = 1 To NX1
      If (I = 1) Then
        A(I) = 0#
        B(I) = 1#
        C(I) = 0#
        If NBC1 = 0 Or NBC1 = 2 Then
          D(I) = P0 * KD
        Else
          D(I) = P * KD
        End If
      ElseIf (I = NX1) Then
        A(I) = 0#
        B(I) = 1#
        C(I) = 0#
        If NBC2 = 0 Or NBC2 = 2 Then
          D(I) = 0#
        Else
          D(I) = PD * KD
        End If
      Else
        RR = 1 + ((KK / (1 + Z * C1(I)) ^ 2)) * LINEAR
        A(I) = -2# * (DIF1 / RR) * DTIM / ((DX1(I - 1) + DX1(I)) * DX1(I - 1))
        B(I) = 1# + 2# * (DIF1 / RR) * DTIM / ((DX1(I - 1) + DX1(I))) * (1# / DX1(I - 1) + 1# / DX1(I))
        C(I) = -2# * (DIF1 / RR) * DTIM / ((DX1(I - 1) + DX1(I)) * DX1(I))
        D(I) = C1(I)
      End If
    Next I
    Call TRIDAG(NX1, A, B, C, D, E)
    For I = 1 To NX1
      C1NEW(I) = E(I)
    Next I
  End If

  For I = 1 To NX1
    C1(I) = C1NEW(I)
  Next I

' *** WRITING TO SHEET 2 ****

  TPRINT = TPRINT - DTIM
  If (TPRINT <= 0#) Or (K = NT) Then
    TPRINT = 50#

' ****THE ANALYTICAL CONCENTRATION PROFILE****

    Sheets("Sheet2").Select
    Cells(1, ICOL) = TIM

    If NBC2 = 0 Or NBC2 = 2 Then 'Ideal boundary conditions
      X1 = 0#
      For I = 1 To NX1
```

```
        SUMC = 0#
        For J = 1 To 5000
          N = J - 1
          BB = Application.WorksheetFunction.ERFC((2 * N * XL1 + X1) / (2 * Sqr(DIF1 * TIM)))
          CC = Application.WorksheetFunction.ERFC((2 * XL1 * (N + 1) - X1) / (2 * Sqr(DIF1 * TIM)))
          DD = BB - CC
          SUMC = SUMC + DD
          If (Abs(DD) < 10 ^ (-50)) And J > 10 Then Exit For
        Next J
        X1 = X1 + DX1(I)
        C1ANAL(I) = P0 * KD * SUMC
        Cells(I + 1, ICOL) = C1(I)
        Cells(I + 1, ICOL + 1) = C1ANAL(I)
        SUMDIF = SUMDIF + Abs(C1(I) - C1ANAL(I))
      Next I
      ICOL = ICOL + 2
      NSUMDIF = NSUMDIF + 1

    Else   ' THE ANALYTICAL CONCENTRATION PROFILE (REAL BC)
      X1 = 0#
      For I = 1 To NX1
        SUMC = 0#
        For J = 1 To 5000
          N = J
          BB = Exp(-1 * DIF1 * ALPHA(N) ^ 2 * TIM / XL1 ^ 2)
          CC = Sin(ALPHA(N) * X1 / XL1) / (ALPHA(N))
          DD = (H ^ 2 + ALPHA(N) ^ 2) / (H * (H + 1) + ALPHA(N) ^ 2)
          EE = DD * CC * BB
          SUMC = SUMC + EE
          If (Abs(EE) < 10 ^ (-50)) And J > 10 Then Exit For
        Next J
        X1 = X1 + DX1(I)
        C1ANAL(I) = P0 * KD * (1 - 2 * SUMC)
        Cells(I + 1, ICOL) = C1(I)
        Cells(I + 1, ICOL + 1) = C1ANAL(I)
        SUMDIF = SUMDIF + Abs(C1(I) - C1ANAL(I))
      Next I
      ICOL = ICOL + 2
      NSUMDIF = NSUMDIF + 1
    End If
  End If

' *** CALCULATING NEW UPSTREAM AND DOWNSTREAM PRESSURES ***
  G1 = (C1(2) - C1(1)) / DX1(1)
  PNEW = P + DTIM * ((DIF1 * AREA * R * T) / VOLU) * G1
  DPDT = (PNEW - P) / DTIM
  If NBC1 = 0 Then
    P = P0
  Else
    P = PNEW
  End If
  SUMG1 = SUMG1 - G1 * DIF1 * AREA * DTIM

  G2 = (C1(NX1) - C1(NX1 - 1)) / DX1(NX1 - 1)
  PDNEW = PD - DTIM * ((DIF1 * AREA * R * T) / VOLD) * G2
  If NBC2 = 0 Then
    PD = 0#
  Else
    PD = PDNEW
  End If
  SUMG2 = SUMG2 - G2 * DIF1 * AREA * DTIM
```

```
' **** CALCULATING SLOPE AND INTERCEPT AND THEN THETA ****

   SEMILINE = 2 * P0 * KD * AREA * R * T * Sqr(DIF1 * TANAL) / (VOLU * Sqr(PI))
   FO = DIF1 * TANAL / XL1 ^ 2
   If (TANAL - (Int(NP / 2) - (NANAL - 1)) * DTANAL) <= TIM Then
    If NANAL = 1 Then
      SUM1 = 0#
      SUM2 = 0#
      SUM3 = 0#
      SUM4 = 0#
      SUMU1 = 0#
      SUMU2 = 0#
      SUMU3 = 0#
      SUMU4 = 0#
    End If
    DELTAP = P0 - P
    PRESD(NANAL) = PD     'Downstream pressure
    PRESU(NANAL) = DELTAP    'Upstream pressure
    TIMED(NANAL) = TIM
    TIMEU(NANAL) = TIM
    SUM1 = SUM1 + PRESD(NANAL)
    SUM2 = SUM2 + TIMED(NANAL)
    SUM3 = SUM3 + PRESD(NANAL) * TIMED(NANAL)
    SUM4 = SUM4 + TIMED(NANAL) ^ 2
    SUMU1 = SUMU1 + PRESU(NANAL)
    SUMU2 = SUMU2 + TIMEU(NANAL)
    SUMU3 = SUMU3 + PRESU(NANAL) * TIMEU(NANAL)
    SUMU4 = SUMU4 + TIMEU(NANAL) ^ 2
    G1TANAL(NANAL) = G1
    G2TANAL(NANAL) = G2
  NANAL = NANAL + 1

  '****WHEN THE VECTOR HAS BEEN FILLED, THE TIME LAG CAN BE ESTIMATED****
    If NANAL > NP Then
      If NOISE = 1 Then
        ' Writing to Sheet 6 for raw data (i.e. no noise) which could be analysed later
        ' Writing to Sheet4 (different noise levels) and Sheet5 (Summary table) - MonteCarlo if NOISE = 1
        Call MonteCarlo(NP, ICNOISE, TIMEU, TIMED, PRESU, PRESD)
        ICNOISE = ICNOISE + 1
      End If

' ****THE DOWNSTREAM PRESSURE ANALYTICALLY REAL BC***

      Sheets("Sheet3").Select
      If NBC2 = 1 Then
        X1 = 0#
        For I = 1 To NX1
          SUMD = 0#
          For J = 1 To 5000
            N = J
            LL = 2 * ((-1) ^ (N - 1)) * (H ^ 2 + ALPHA(N) ^ 2) / (H * (H + 1) + ALPHA(N) ^ 2)
            EE = Sin(ALPHA(N)) / ALPHA(N)
            FF = Exp(-1 * DIF1 * ALPHA(N) ^ 2 * TANAL / XL1 ^ 2)
            DD = (-1) ^ N * LL * EE * FF
            SUMD = SUMD + DD
            If (Abs(DD) < 10 ^ (-50)) And J > 10 Then Exit For
          Next J
          X1 = X1 + DX1(I)
          PDANAL = (1 + SUMD) * P0
        Next I
  Else
```

```
' ****THE DOWNSTREAM PRESSURE ANALYTICALLY (IDEAL BC)****

        X1 = 0#
        For I = 1 To NX1
          SUMD = 0#
          For J = 1 To 5000
            N = J - 1
            LL = 2 * P0 * KD * R * T * AREA * Sqr(DIF1) / (VOLD * Sqr(PI))
            EE = Application.WorksheetFunction.Erf((2 * N + 1) * XL1 / (2 * Sqr(DIF1 * TANAL)))
            FF = Exp(-1 * (2 * N + 1) ^ 2 * XL1 ^ 2 / (4 * DIF1 * TANAL))
            GG = (2 * N + 1) * Sqr(PI) * XL1 / (Sqr(DIF1))
            DD = GG * (EE - 1) + 2 * Sqr(TANAL) * FF
            SUMD = SUMD + DD
            If (Abs(DD) < 10 ^ (-50)) And J > 10 Then Exit For
          Next J
          X1 = X1 + DX1(I)
          PDANAL = LL * SUMD
        Next I
      End If

'**** THE UPSTREAM PRESSURE ANALYTICAL (LINEAR ISOTHERM)****

      SUMA = 0#
      For N = 0 To 5000
        CON1 = Sqr(DIF1 * TANAL) / (XL1 * Sqr(PI))
        T1 = (N + 1) * Application.WorksheetFunction.Erf(XL1 * (N + 1) / Sqr(DIF1 * TANAL))
        T2 = N * Application.WorksheetFunction.Erf((XL1 * N) / Sqr(DIF1 * TANAL))
        T3 = 2 * N + 1
        T4 = Exp((-1 * (XL1 * N) ^ 2) / (DIF1 * TANAL))
        T5 = Exp(-1 * XL1 ^ 2 * (N + 1) ^ 2 / (DIF1 * TANAL))
        TT = T1 + T2 - T3 + CON1 * (T4 + T5)
        SUMA = SUMA + TT
        If (Abs(T) < 1E-50 And N > 25) Then Exit For
      Next N
      SS = (2 * AREA * T * R * XL1 * P0 * KD) / VOLU
      DPU = SS * SUMA

' *** ANALYTICAL GRADIENT DOWNSTREAM G2A ***

      SUM = 0#
      CON = -2 * P0 * KD / (Sqr(PI * TANAL * DIF1))
      For N = 0 To 5000
        AA = Exp((-4 * XL1 ^ 2 * N ^ 2 - 4 * XL1 ^ 2 * N - XL1 ^ 2) / (4 * DIF1 * TANAL))
        SUM = SUM + AA
        If (Abs(AA) < 1E-50) And N > 20 Then Exit For
      Next N
      G2A = SUM * CON

' **** ANALYTICAL GRATIENT UPSTREAM G1A ****
      SUM = 0#
      For N = 0 To 5000
        AA = Exp(-(N + 1) ^ 2 * XL1 ^ 2 / (DIF1 * TANAL)) + Exp(-XL1 ^ 2 * N ^ 2 / (DIF1 * TANAL))
        SUM = SUM + AA
        If (Abs(AA) < 1E-50) And N > 20 Then Exit For
      Next N
      G1A = -SUM * (KD * P0 / Sqr(PI * TANAL * DIF1))

'*** steady state equation for DOWN stream (analytical)-non linear isotherm
      TERM1 = (XL1 * C1(1) / 6) + (2 * XL1 * C1(NX1) / 6) - C01 * XL1 / 2
      TERM2 = Application.WorksheetFunction.Ln(Z * C1(NX1) + 1)
      TERM3 = Application.WorksheetFunction.Ln(Z * C1(1) + 1)
      TERM4 = KK * XL1 * (Z * C1(NX1) - Z * C1(1) - (Z * C01 + 1) * TERM2) / (Z ^ 2 * (C1(NX1) - C1(1)) * (1 + Z * C01))
```

```
TERM5 = -1 * KK * XL1 / (2 * Z * (1 + Z * C01))
TERM6 = (KK * XL1) / (Z ^ 3 * (C1(NX1) - C1(1)) ^ 2)
TERM7 = ((Z * C1(NX1) + 1) * TERM2 - Z * C1(NX1) + Z * C1(1) - (Z * C1(1) + 1) * TERM3)
TERM8 = TERM6 * TERM7
TERM9 = TANAL * DIF1 * (C1(NX1) - C1(1)) / XL1
ACCUMDOWN = (TERM1 + TERM4 + TERM5 + TERM8 + TERM9) * AREA

' **** STEADY STATE EQUATION FOR UPSTREAM (ANALYTICAL)-NON LINEAR ISOTHERM***

TERM1 = -1 * TANAL * DIF1 * (C1(NX1) - C1(1)) / XL1 ^ 2
TERM2 = 1 * (2 * C1(1) / 6) + (C1(NX1) / 6) - C01 / 2
TERM3 = KK / (2 * Z * (1 + Z * C01))
TERM4 = Application.WorksheetFunction.Ln(Z * C1(1) + 1)
TERM5 = Application.WorksheetFunction.Ln(Z * C1(NX1) + 1)
TERM6 = -1 * (KK / (Z ^ 3 * (C1(NX1) - C1(1)) ^ 2))
TERM7 = ((Z * C1(NX1) + 1) * TERM5 - Z * C1(NX1) + Z * C1(1) - (Z * C1(1) + 1) * TERM4)
TERM8 = TERM6 * TERM7
TERM9 = 1 * (KK * TERM4) / (Z ^ 2 * (C1(NX1) - C1(1)))
ACCUMUP = (TERM1 + TERM2 + TERM3 + TERM8 + TERM9) * XL1 * AREA

' ****CALCULATING SLOPE AND INTERCEPT***

SLOPE = (NP * SUM3 - SUM1 * SUM2) / (NP * SUM4 - SUM2 ^ 2)
INTER = (SUM1 - SLOPE * SUM2) / NP
If NBC2 = 0 Then
  THETA = 0.00001
Else
  If SLOPE < 0.0000001 Then
    THETA = 0.000001
  Else
    THETA = -INTER / SLOPE
  End If
End If
SQRTTANAL = Sqr(TANAL)
DELTAP = P0 - P
DDOW = XL1 ^ 2 / (6 * THETA)

If LINEAR = 0 Or BA1 < 0.000001 Then
  CF = 1#
Else
  Y = Z * C1(1)
  LNY = (1 + Y) * Application.WorksheetFunction.Ln(1 + Y)
  FY = 6 * (1 / Y ^ 3) * (0.5 * Y ^ 2 + Y - LNY)
  CF = (1 + KK * FY)
End If

If LINEAR = 0 Or BA1 < 0.000001 Then
  CFU = 1#
Else
  Y = Z * C1(1)
  LNY = (1 + Y) * Application.WorksheetFunction.Ln(1 + Y)
  FY = 3 * (1 / Y ^ 3) * (0.5 * Y ^ 2 - Y + LNY - Y * Application.WorksheetFunction.Ln(Y + 1))
  CFU = (1 + KK * FY)
End If

DDOWC = CF * DDOW
ERRORDOW = (((DDOWC - DIF1) / DIF1) * 100)
ERRORDOWB = (((DDOW - DIF1) / DIF1) * 100)

SLOPEU = (NP * SUMU3 - SUMU1 * SUMU2) / (NP * SUMU4 - SUMU2 ^ 2)
INTERU = (SUMU1 - SLOPEU * SUMU2) / NP
If SLOPEU = 0 Then
```

```
  THETAU = 0#
Else
  THETAU = -INTERU / SLOPEU
End If
If NBC1 = 0 Then
  DUP = 0#
Else
  DUP = -XL1 ^ 2 / (3 * THETAU)
  DUPC = CFU * DUP
  ERRORUP = (((DUPC - DIF1) / DIF1) * 100)
  ERRORUPB = (((DUP - DIF1) / DIF1) * 100)
End If
TOVERTHETAA = TANAL / (XL1 ^ 2 / (6 * DIF1))

Cells(IM, 1) = TANAL
Cells(IM, 2) = TOVERTHETAA
Cells(IM, 3) = SQRTTANAL
Cells(IM, 4) = SLOPE
Cells(IM, 5) = INTER
Cells(IM, 6) = SLOPEU
Cells(IM, 7) = INTERU
Cells(IM, 8) = FO
Cells(IM, 9) = DELTAP
Cells(IM, 10) = PRESD(Int(NP / 2 + 0.5))
Cells(IM, 11) = DPU
Cells(IM, 12) = PDANAL
Cells(IM, 13) = SEMILINE
Cells(IM, 14) = DDOW
Cells(IM, 15) = CF
Cells(IM, 16) = DDOWC
Cells(IM, 17) = ERRORDOW
Cells(IM, 18) = ERRORDOWB
Cells(IM, 19) = DUP
Cells(IM, 20) = CFU
Cells(IM, 21) = DUPC
Cells(IM, 22) = ERRORUP
Cells(IM, 23) = ERRORUPB
Cells(IM, 24) = THETAU
Cells(IM, 25) = THETA
Cells(IM, 26) = G1A
Cells(IM, 27) = G2A
Cells(IM, 28) = G1TANAL(Int(NP / 2 + 0.5))
Cells(IM, 29) = G2TANAL(Int(NP / 2 + 0.5))
Cells(IM, 30) = ACCUMUP
Cells(IM, 31) = ACCUMDOWN
Cells(IM, 32) = SUMG1
Cells(IM, 33) = SUMG2

IM = IM + 1
If (TANAL + TWINDOW) <= (TANAL + FR) Then
  TANAL = TANAL + FR
  NANAL = 1
Else
  NANAL = NP - Int(NP * FR / TWINDOW) + 1
  TANAL = TANAL + FR
  SUM1 = 0#
  SUM2 = 0#
  SUM3 = 0#
  SUM4 = 0#
  SUMU1 = 0#
  SUMU2 = 0#
  SUMU3 = 0#
```

```
        SUMU4 = 0#
        For I = 1 To NANAL - 1
          PRESD(I) = PRESD(NP - NANAL + I + 1)
          PRESU(I) = PRESU(NP - NANAL + I + 1)
          TIMED(I) = TIMED(NP - NANAL + I + 1)
          TIMEU(I) = TIMEU(NP - NANAL + I + 1)
          G1TANAL(I) = G1TANAL(NP - NANAL + I + 1)
          G2TANAL(I) = G2TANAL(NP - NANAL + I + 1)
          SUM1 = SUM1 + PRESD(I)
          SUM2 = SUM2 + TIMED(I)
          SUM3 = SUM3 + PRESD(I) * TIMED(I)
          SUM4 = SUM4 + TIMED(I) ^ 2
          SUMU1 = SUMU1 + PRESU(I)
          SUMU2 = SUMU2 + TIMEU(I)
          SUMU3 = SUMU3 + PRESU(I) * TIMEU(I)
          SUMU4 = SUMU4 + TIMEU(I) ^ 2
        Next I
      End If
    End If
   Else
  End If
 Next K

 Sheets("Sheet1").Select
 Cells(16, 2) = Date
 Cells(16, 3) = Timer
 MEANERROR = SUMDIF / (NX1 * NSUMDIF)
 Cells(17, 2) = MEANERROR
 Cells(17, 4) = DTAU
 ERROR2 = MEANERROR / (P0 * KD)
 Cells(17, 6) = ERROR2

 Application.ScreenUpdating = True
End Sub
================================================================================
Sub TRIDAG(L As Integer, A() As Double, B() As Double, C() As Double, D() As Double, E() As Double)
 Dim BETA(20000) As Double, GAMMA(20000) As Double
 Dim I As Integer, K As Integer
 BETA(1) = B(1)
 GAMMA(1) = D(1) / BETA(1)
 For I = 2 To L
  BETA(I) = B(I) - A(I) * C(I - 1) / BETA(I - 1)
  GAMMA(I) = (D(I) - A(I) * GAMMA(I - 1)) / BETA(I)
 Next I
 E(L) = GAMMA(L)
 For K = 1 To L - 1
  I = L - K
  E(I) = GAMMA(I) - C(I) * E(I + 1) / BETA(I)
 Next K
End Sub
```